Stress driven changes in the kinetics of bilayer embedded proteins: a membrane spandex and a voltage-gated sodium channel

Pierre-Alexandre Boucher
B.Sc. Université d'Ottawa 2004
M.Sc. Université d'Ottawa 2006

Thèse soumise à la
Faculté des études supérieures et postdoctorales
dans le cadre des exigences
du programme de doctorat en physique

uOttawa

SOMMAIRE

Les protéines membranaires sont affectées par la contrainte présente dans la double couche lipidique. Cette affirmation générale est, dans cette thèse, concrétisée par deux types de protéines: le spandex membranaire et les canaux sodium voltage-dépendants. Dans ce travail, nous explorons en utilisant des méthodes de la physique théorique, les conséquences d'idées tirées de la biologie expérimentale.

Le spandex membranaire a été postulé il y a quelques années et nous étudions les implications théoriques et les bénéfices possibles de la présence de telles protéines dans la membrane d'une cellule. Il n'y a pas de protéines étant spécifiquement du spandex membranaire; n'importe quelle protéine ayant un changement de surface entre deux états non-conducteurs peut agir comme spandex. Les bactéries ont des valves osmotiques s'ouvrant à des tensions quasi-lytiques pour se protéger contre la rupture membranaire. Un spandex s'étirant à des tensions juste au-dessous de celle d'ouverture des valves osmotiques pourrait relâcher la tension assez pour permettre d'éviter une coûteuse ouverture accidentelle d'une valve lors d'une fluctuation de tension. Un autre rôle possible pour le spandex serait en tant qu'amortisseur de tension: le spandex pourrait être utilisé pour maintenir un niveau de tension fixe dans la membrane. Ceci serait utile car plusieurs canaux membranaires sont modulés par la tension.

Le cisaillement/contrainte subie lors de traumatisme crâniens cause immédiatement (< 2 min) et irréversiblement une augmentation de calcium axonal sensible au TTX. In situ, ceci entraîne des lésions axonales diffuses. La sensibilité au TTX indique que des canaux sodium voltage-dépendants (Nav) devenus "suintants" facilitent cette augmentation de calcium. Wang *et al.* ont montré que l'isoforme Nav du système nerveux central adulte des mammifères, Nav1.6, exprimé dans des ovocytes de *Xenopus* devient "suintant" lorsque soumis à une aspiration par pipette causant des blebs. Cette condition "suintante" est causée par un déplacement en direction hyperpolarizée (à gauche, ou vers une baisse de potentiel, typiquement de 20 mV) des processus cinétiquement couplés d'activation et d'inactivation dégradant ainsi une fenêtre de conductance bien confinée en une fuite de sodium sensible au TTX. Nous proposons un protocole expérimental permettant de déterminer si ce glissement vers la gauche est le résultat d'un processus tout-ou-rien ou graduel et si les courants sodium persistants glissent aussi vers la gauche lorsque traumatisés. Nous utilisons aussi la modélisation pour étudier l'excitabilité de noeuds de Ranvier traumatisés.

SUMMARY

Bilayer embedded proteins are affected by stress. This general affirmation is, in this thesis, embodied by two types of proteins: membrane spandex and voltage-gated sodium channels. In this work, we essentially explore, using methods from physics, the theoretical consequences of ideas drawn from experimental biology.

Membrane spandex was postulated to exist and we study the theoretical implications and possible benefits for a cell to have such proteins embedded in its bilayer. There are no specific membrane spandex proteins, rather any protein with a transition involving a large enough area change between two non-conducting states could act as spandex. Bacterial cells have osmovalve channels which open at near-lytic tensions to protect themselves against rupture. Spandex expanding at tensions just below the osmovalves' opening tension could relieve tension enough as to avoid costly accidental osmovalve opening due to transient bilayer tension excursions. Another possible role for spandex is a tension-damper: spandex could be used to maintain bilayer tension at a fixed level. This would be useful as many bilayer embedded channels are known to be modulated by tension.

The Stress/shear experienced in traumatic brain injury cause an immediate (< 2 min) and irreversible TTX-sensitive rise in axonal calcium. In situ, this underlies an untreatable condition, diffuse axonal injury. TTX sensitivity indicates that leaky voltage-gated sodium (Nav) channels mediate the calcium increase. Wang *et al.* showed that the mammalian adult CNS Nav isoform, Nav1.6, expressed in *Xenopus* oocytes becomes "leaky" when subjected to bleb-inducing pipette aspiration. This "leaky" condition is caused by a hyperpolarized-shift (left-shift or towards lower potentials, typically 20 mV) of the kinetically coupled processes of activation and inactivation thus effectively degrading a well-confined window conductance into a TTX-sensitive Na leak. We propose experimental protocols to determine whether this left-shift is the result of an all-or-none or graded process and whether persistent Na currents are also left-shifted by trauma. We also use modeling to assess whether left-shifted Nav channel kinetics could lead to Na^+ (and hence Ca^{2+}) loading of axons and to study saltatory propagation after traumatizing a single node of Ranvier.

DÉCLARATION D'ORIGINALITÉ

The work presented in this thesis is, to the best of my knowledge new and original. I am the first author of all three papers presented in this thesis. They were written in collaboration with my supervisors Béla Joós and Catherine Morris. All the results presented in the articles were obtained using my own code (programmed in Fortran).

REMERCIEMENTS

Merci tout d'abord à Béla Joós pour m'avoir enseigné la physique. Merci aussi de m'avoir fait confiance en me confiant des charges de cours; je me suis découvert une passion pour l'enseignement grâce à toi.

Thanks to Cathy Morris for teaching me biology and English. The language barrier was difficult (and there was a barrier along more than one axis), but we eventually got across.

Merci aussi aux multiples locataires du 338*b* : Martin Bertrand, Jean-François Joly, Martin Forget et Daniel O'Keeffe. Les heures de discussions hors-sujet que nous avons eues ont été très appréciées.

Merci à Antoine Dubé pour de l'aide avec LaTeX.

Merci à Vladimir pour m'avoir sorti et changé les idées durant la rédaction de cette thèse.

Merci à ma famille pour m'avoir toujours encouragé à étudier.

Finalement, merci à Josianne, pour tout.

Contents

List of Figures

List of Tables

Chapter 1

Introduction to Membrane Spandex

The idea of "Spandex" proteins came from a review article by Dr. Catherine Morris published in the Anatomical Record in 2002[1]. The review was titled "How Did Cells Get Their Size?" and explained evolution mechanisms leading to cells the size we know them today. The review especially concentrated on the importance of membrane tension in protocells (or early cells) and how that tension could be relieved by the opening of mechanosensitive channels. Then came the suggestion that there might be some added value for a mechanosensitive channel to act as a membrane spandex. The idea didn't seem to raise much interest until Dr. Morris convinced Dr. Béla Joós (and me) to study the topic, mechanosensitive channels acting as membrane spandex, from a theoretical perspective. This work resulted in an article published in the Biophysical Journal[2] which will be presented after the subject has been properly introduced.

What is meant by "mechanosensitivity" in this work, is the modulation of a membrane protein's function by mechanical forces, especially those arising from the interaction between the protein and the cell membrane. Mechanosensitivity does not necessarily mean that a protein is activated mechanically, but simply that its function is affected by membrane mechanics.

1.1 Cells and membranes

The cell is the most basic functional unit of life[3]. It is not the smallest structure and can be divided in many different parts and can have substructures, but the cell is the smallest component considered to be alive. Organisms made of single cells, such as bacteria, are named unicellular. Others, such as humans, made of a composition of cells, are multicellular. Cell size can vary from the micrometer to the millimeter range.

Although cell structure can be quite complex, the main feature of interest in this work is the cell membrane, also known as the plasma membrane, responsible for isolating the interior of the cell from the exterior. This membrane draws its mechanical properties from the properties of its main constituents: phospholipids (see Fig. 1.1).

Phospholipids combine two very different properties: they are made of a hydrophilic ("water loving") head and two hydrophobic ("water hating") tails. This type of molecule combining both properties is referred to as amphipathic. The most common membrane forming lipid is phosphatidylcholine, whose choline molecule, attached to the phosphate group, forms the hydrophilic head. The phosphate group is linked to a glycerol group on which two hydrocarbon chains, forming the hydrophobic tails, are attached. The hydrocarbon chains can have "kinks", unsaturated double bonds between two hydrocarbons. These double bonds are stiffer than single bonds as they limit the flexibility of the chain, thus affecting membrane properties. The chains can also vary in length simply by having a different number of hydrocarbons, and again this will affect membrane properties.

The amphipathic property of phospholipids is the basis of membrane structure. Hydrophilic heads easily dissolve in water whereas hydrophobic tails do not: in solution water rearranges around hydrophobic compounds in a cage structure thus reducing entropy (by maintaining a structure). The free-energy cost of exposing hydrophobic tails to water is thus quite high and to avoid it phospholipids auto-assemble in structures where only the hydrophilic heads are exposed to water (for a more complete discussion of possible structures see e.g., [4]). One such structure is the bilayer: phospholipids arranges in a "sandwhich" structure with their head to the outside thus shielding their hydrophobic tails from water. This structure closes on itself, to protect the edges of the bilayer from water, forming the cell membrane, which is about 5 nm thick. This arrangement renders the membrane impermeable to polar solutes, including amino acids, ions, nucleic acids (DNA and RNA)

and proteins. Any movement of such solute must hence be mediated by gates or channels embedded in the bilayer.

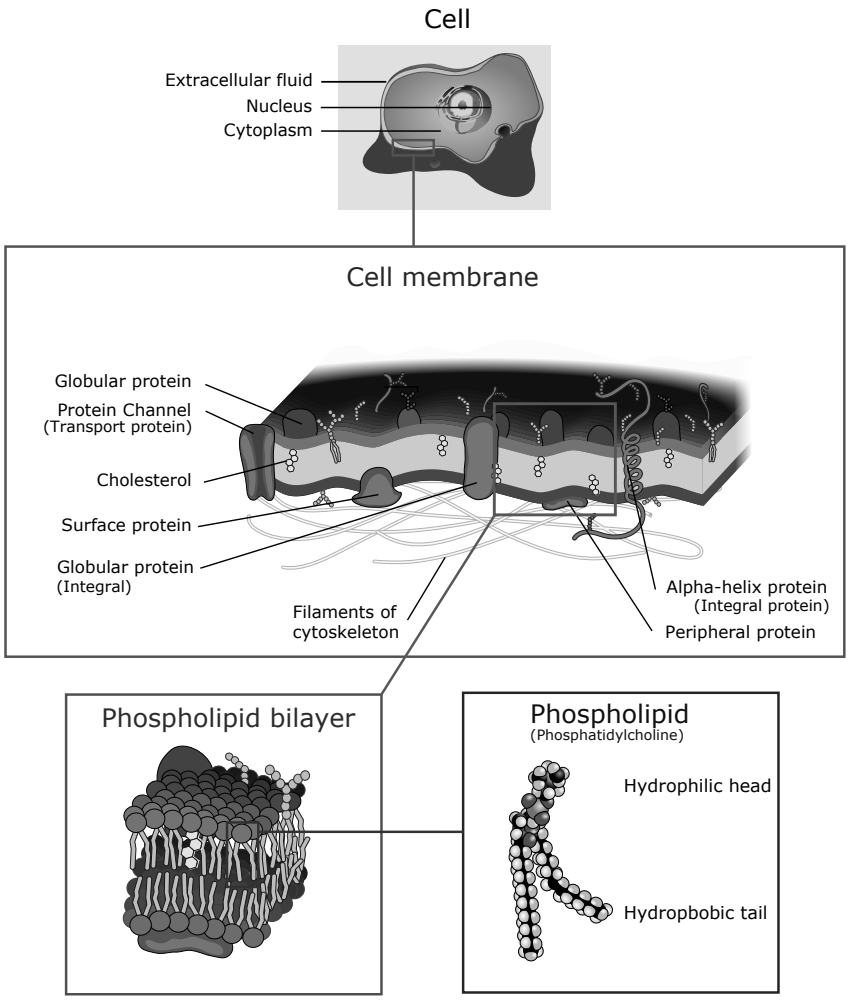

Figure 1.1 Cartoon of different levels of cell structure: a cell, a cellular membrane, a lipid bilayer and a phospholipid. Modified from [5].

Lipid bilayers are essentially two-dimensional fluids: the lipids are practically free to diffuse in the membrane's plane but they must remain in that plane. This image of lipids freely diffusing naturally leads to the fluid mosaic model[6]. In this model membrane constituents diffuse freely in the membrane. A uniform distribution of proteins and different lipids would hence be expected. Although the fluid mosaic is possible, it is really a special case and a more complex model is required to explain lateral distribution of cell membrane constituents. Imagine a membrane composed of two types of lipids, one dramatically longer than the other. There would be an energetic cost to placing one of the long lipids next to a

short one as the short lipid would be unable to completely shield the hydrophobic tails of the long lipid from water. Hence the system would adopt a conformation minimizing contact between the two lipid populations, leading to segregation of lipid types. Such reasoning applies for a large height difference; for a smaller one (i.e., leading to an interaction energy of the order of thermal energy) there would be fluctuations in the segregation pattern.

A similar argument can be made using intrinsic curvature instead of lipid length. Some lipids have an intrinsic curvature: they have a conical shape. Thus assembling them leads to a naturally curved leaflet. Such lipids would then segregate to the bilayer leaflet corresponding to their curvature, or to membrane areas of similar curvature thus minimizing free-energy.

The same arguments on height difference and curvature can be made for bilayer embedded proteins with only a slight difference: proteins could segregate and form clusters but there is also the possibility of proteins having specific lipid composition around them because of, say, specific spatial conformation, or charge attraction/repulsion.

A last argument that can be made against the fluid mosaic model is that there could be cellular mechanisms at play to actively segregate or position specific molecules in certain areas. For example, ankyrin proteins mediate the attachment of different membrane proteins to the spectrin cytoskeleton thus allowing for spatial segregation of membrane proteins[7]. The cytoskeleton can be thought of as a biological scaffolding of a cell: it helps maintain shape and integrity.

1.2 Mechanosensitivity

The first paper of this thesis begins with "Multiconformation membrane proteins whose states displace different areas make mechanosensitive transitions between those states". It seems like we went out of our way to express something that has been known for quite some time: mechanosensitive channels exist (See e.g., [8, 9, 10, 11, 12] and references therein). We were however careful about this first sentence to properly introduce the idea conveyed throughout the paper: "multiconformation membrane proteins whose states displace different areas" does not solely apply to the "traditional" mechanosensitive channels (e.g., MscL and MscS), but can also include proteins not traditionally considered to be mechanosensitive (e.g., Kv channels and rhodopsin). Then we insist that these proteins, since they displace different

areas in the membrane, are necessarily sensitive to bilayer mechanics. Their activation (i.e., gating) might not be driven by tension only, but it is certainly modulated by bilayer mechanics.

Since such proteins, with states displacing different areas, occur in all organisms, and since small bilayer strains are required to attain rupture (lysis), we hypothesize that cells might use proteins with large changes in area as tension buffers. In a lesser measure, any membrane protein with conformations of different areas could also be used as a tension buffer. Note that we used the word "proteins" and not "channels" as we argue that any bilayer-embedded protein, be it a channel or not, can act as membrane spandex.

The idea originates from a 2002 paper [1] where it was suggested that a high density of MscL channels would reduce the need that they ever open. The argument is based on the reported kinetic analysis of MscL channels which suggests that opening of the channel is not tightly coupled to its expansion and that expansion occurs before gate opening [13]. MscL expands about 1.5 to 2 fold when opening whereas a lipid bilayer ruptures after expanding by a factor of about 1.03. The possibility of expanding the channel without opening a permeation pathway could render the bilayer very elastic, like spandex!

1.2.1 Mechanosensitive Channel of Large conductance:

The Mechanosensitive channel of large conductance (MscL), is a non-specific channel protein which opens at near-lytic tensions (~ 12 mN/m)[14]. Its major role is generally accepted to be an emergency valve in case of osmotic downshock(see e.g., [15, 16]).

Suppose a bacterium normally operating in an isotonic environment is suddenly immersed in pure water (see Fig. 1.2). The difference in ion gradient would cause water to influx thus causing the bacterium to inflate. By inflating, any reserve membrane area would unfold and, if such unfolding is not sufficient, the lipid bilayer would stretch until the influx stops, or until the lipid bilayer ruptures. Here the MscL channels come to the rescue of the bacterium in danger of rupturing its bilayer by opening a non-specific permeation pathway: water and ions can efflux through the open MscL, leaving the bacterium in a poor condition (having lost some of its essential metabolites) but still alive and able to recuperate. Indeed MscL with its large pore allows not only water and ions to cross the membrane, but also osmolytes up to $400 - 500$ kDa.

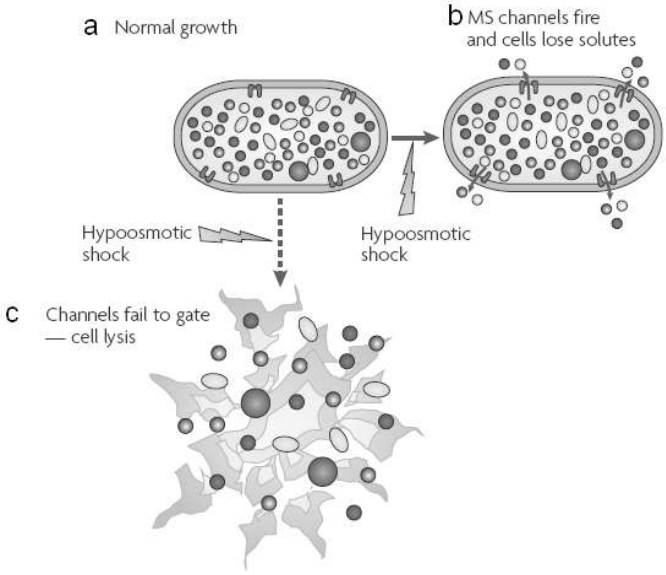

Figure 1.2 Upon Osmotic downshock a normally growing bacterium (a) will release osmolytes through emergency osmovalves (b) (i.e., mechanosensitive channels). If the channels fail to gate, the cell inflates until it lyses (c). Reprinted by permission from Macmillan Publishers Ltd: Nat. Rev. Microbiol.[17], copyright 2007.

The proposed gating scheme for MscL[13] (see Fig. 1.3) is a first transition from a closed-resting state to a closed-expanded state. This first transition is the main mechanosensitive transition and causes the protein to expand in the plane of the membrane by about 18 nm^2. From the closed-expanded state, the protein can change conformation into a sequence of subconducting states until it reaches the fully open state. Conformation changes from the closed-expanded state to the subconducting states have small changes of in-plane area (about $2-6$ nm^2) and thus are relatively tension-independent.

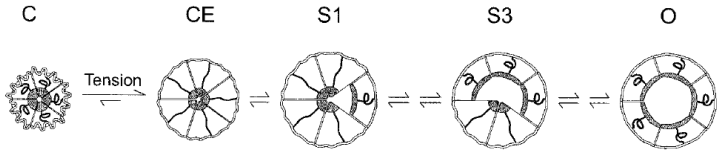

Figure 1.3 Gating scheme for MscL: under tension, a MscL in the closed (C) state changes conformation to a closed-expanded (CE) (or pre-expanded) state. From this closed-expanded state, the transition to the subconduction (S1, S3) and open (O) states is almost tension-independent. Reprinted from Publication Biophys. J., **81**(2), 917-936[13], Copyright 2001, with permission from Elsevier.

The in-plane area expansion of MscL was estimated as ~ 6 nm^2 by fitting its activation curve with a simple two-state model[14]. Modeling studies based on the crystal structure[13] gave an estimate of ~ 20 nm^2. This discrepancy has been explained with more complex models which include the stiffness of the closed and open states[18, 19]; it is also possible that slight variations in channel parameters (activation energy and area expansion) yield a shallower activation curve, corresponding to an smaller apparent area change upon opening[20].

1.2.2 Mechanosensitive Channels of Small conductance

Understanding the mechanosensitive channel of small conductance (MscS) is still a work in progress. We will try to sum up the current state of knowledge on that channel (see e.g., [21] and references therein).

MscS is thought to maintain turgor during a bacterium's normal life cycle by opening a non-selective permeation pathway across the lipid bilayer. It opens at ~ 5.5 mN/m[22]; at a lower tension than MscL and expands ~ 16 nm^2[23, 24, 25] upon opening.

The interesting difference between MscL and MscS, is the ability of MscS to change its tension response: under a prolonged subsaturating stress, MscS opens but only transiently (see e.g., [26, 27]). If additional stress is applied MscS can be activated again, but only a portion of the population will activate. MscS can hence do things which MscL cannot: inactivate and desensitize. The inactivated state is non-conducting and insensitive to tension; the desensitized state is apparently a non-conducting that can be re-activated but with a higher threshold tension (i.e., a desensitized channel has a right-shifted activation). However it has recently been reported[28] that desensitization of MscS (also termed adaptation) is an artifact of the experimental method used: in a patch clamp setting the bilayer's inner leaflet is free to slide so tension can be relaxed by rearrangement of the lipids. The same process is not possible in the outer leaflet as it is attached to the pipette to form the seal (see Sec. 3.5.1). Since MscS senses tension from the inner leaflet, it closes upon prolonged stimuli not because it adapts or desensitizes, but because the tension it feels is relaxed. This is further confirmed by the fact that no adaptation/desensitization is seen in whole spheroplast recordings. Inactivation however occurs in both patch clamp and whole cell mode, so it seems safe to assume it is a different channel state.

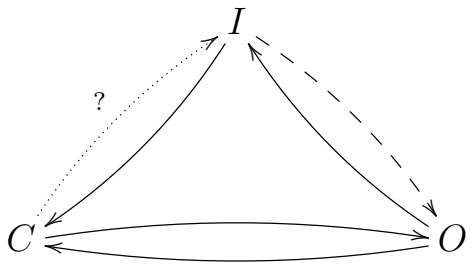

Figure 1.4 Diagram showing the transitions between the closed (C), open (O) and inactivated (I) states of MscS. The transition from the inactivated to the open state has not been characterized[26, 27] and is shown as a dashed line. Similarly the transition from closed to inactivated is shown dotted with a question mark as it may not be possible in wild type MscS; it has however been shown to be possible in some mutants (G121A, F68S and L111S).

In wild type MscS, the inactivated state cannot be reached directly from the closed state, it can however be accessed via subconducting states[27]. This is why, under a slow tension ramp, no current is seen through MscS: all the channels first activate to a subconducting state (a state with a very low conductivity) and then inactivate; for a fast ramp however, the channels open[26]. The inactivated state being thought to have a larger in-plane area than the closed state, such a transition under a slow ramp (a silent expanding transition) is reminiscent of spandex.

Interestingly a mutation, G121A (substituting a Glycine for an Alanine, a slightly bigger amino acid at position 121), renders the transition from the closed state directly to the inactivated state possible. The inactivated state having a larger in-plane area than the closed state, the G121A mutation makes a silent closed-closed expansion transition possible[27]. More mutations that render the silent closed-inactivated transition possible(F68S and L111S) have recently been identified[29].

A lot is still to be understood about MscS: why is the inactivated state insensitive to tension? How is tension sensed? What are the structures of each state (assuming the states presented here are correct)?

1.2.3 Osmoprotection by a single MscL?

In the article (see Ch. 2), we argue that a single MscL channel could be sufficient to prevent an *E. coli* sized bacterium immersed in pure water from rupturing (see Fig. 1.2). We argue

that a single MscL channel could relieve the osmotic gradient before the bacterium would rupture. Even though the results from the calculation are mentioned in the article, the calculation itself is not shown; this is what we will do here.

Ignoring any electrical driving force, the ion flux through a channel is given by[30]:

$$\phi_{channel} = -\frac{\pi a^2 D c}{l + \pi a/2}, \tag{1.1}$$

where a and l are the channel radius and length respectively, D is the ion diffusion constant and c is the difference in ion concentration between both sides of the channel. This equation is obtained through Fick's law, with a correcting factor in the denominator (the $\pi a/2$ term). This correcting factor considers the flux at the mouth of the pore, and effectively makes the pore longer. It is obtained by analogy with the electrical resistance of the pore, where including the access resistance to the pore effectively makes it longer by $\pi a/2$.

The concentration rate of change is then given by:

$$\frac{dc}{dt} = -\frac{\phi_{channel}}{V} = -\frac{\pi a^2 D}{l + \pi a/2}\frac{c}{V}, \tag{1.2}$$

with V the bacterium volume.

The assumption that the bacterium is immersed in pure water is quite extreme: this situation represents the biggest osmotic downshock possible for a cell. In such a situation, a cell, even loaded with many MscL could not survive a prolonged exposure to pure water as it would either rupture from excess osmotic stress, or lose all essential osmolytes through open osmovalves and eventually die (M. Kilfoil, personal communications). Any less extreme osmotic downshock than pure water would be easier to survive. Assuming that the external ion concentration is fixed at $c = 0$ (i.e., pure water), Eq. 1.2 has a solution:

$$c = c_0 \exp(-\frac{\pi a^2 D}{V(l + \pi a/2)}t). \tag{1.3}$$

The time constant of the concentration change, assuming $D = 1.5 \times 10^{-9}$ m^2/s [30], $a = 12.5$ Å, $l = 25$ Å[20] and $V = 10^{-18}$ m^3 is about 0.63 s. An initial internal concentration

of 1 M would then yield a safe pressure differential ($0.2 - 0.3$ osm) [15] within $0.75 - 1$ s of pore opening.

Dynamic tension spectroscopy[31] shows that rupture tension increases with loading rate. A pure lipid bilayer subjected to a moderate tension ramp (about 1 mN/m/s) is safe for about 10 s (note that in the paper, we mention 100 s, this is a typo, 10 s is the correct value). Supposing the pore opens 1 mN/m below rupture tension, then there is 1 s between pore opening and potential bilayer rupture, enough time for a single channel to efflux enough ions to save the bacterium.

Increasing the number of channels reduces the time constant of internal concentration decrease: twice as many channels reduce the time constant by a factor 2 etc. This dependance arises from Eq. 1.2, as the total flux through channels is proportional to the number of channels. Reported numbers of MscL per bacterium cover a wide range: from 5 to 60 copies[32, 33], these numbers would yield time constants of the order of 0.1 to 0.01 s, which suggests there are more MscL than a bacterium would actually need.

There are some caveats to this calculation. 1) The channel efflux is calculated using a simplistic model (i.e., diffusion through a cylinder) and does not consider the possibility that flux through the channel may be hampered by structures inside the channel, or that the mouth of the channel could be obstructed by a cytoplasmic vestibule. 2) The time constant of the efflux for many channels completely ignores channel kinetics: the stochastic aspect of channel opening is more proeminent in small populations of channels. 3) Any electrical or electrodiffusion effects are ignored.

Even with these caveats and the number of approximations made, the point remains that with only a handful of MscL channels a bacterium could survive a potentially catastrophic osmotic downshock. Thus, there are apparently too many MscL in bacteria. Moreover, we did not even consider MscS in our calculation: even though MscS has a smaller conductance, is it generally more abundant than MscL ($20 - 30$ copies of MscS per cell[33]).

1.2.4 Viability assays

Levina et al. [15] carried viability assays on *E. coli* expressing mechanosensitive channels (see Fig. 1.5), including MscL and MscS. In their experiment, the cells were grown in an

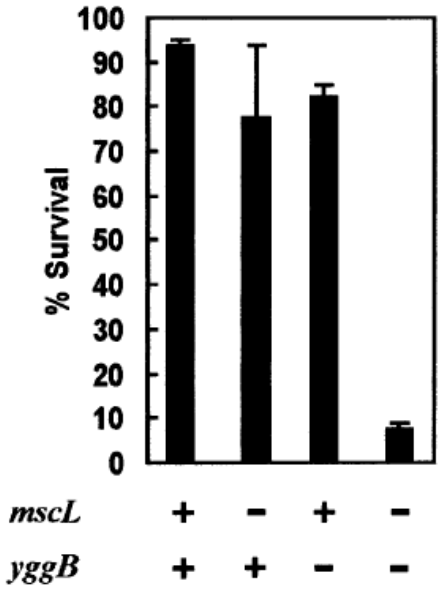

Figure 1.5 Survival rate upon a 0.5 osm hypoosmotic shock for bacterial strain with (+) and without (-) the genes encoding for MscL (gene = *mscL*) and MscS (gene = *yggB*). The presence of only MscS or only MscL is sufficient for osmoprotection. Reprinted by permission from Macmillan Publishers Ltd: EMBO journal[15], copyright 1999.

environment containing 0.5 M NaCl, and then placed in a medium with the same pH, but without the salt. The survival of the cells is measured after 30 min.

Interestingly, MscL and MscS are both, separately, sufficient for survival of the bacteria to the osmotic downshock. Deleting both of them kills practically all the cells. This experiment raises the question: if only MscL is sufficient, and if only MscS is sufficient, then why have both of them? Why would two populations of channels, which do the same job (i.e., emergency osmovalves) be produced by a cell when having only one of the populations is apparently enough? Why would a cell spend some of its resources on building channels that are not essential to its survival? Could it be that MscS and MscL also have other jobs, say as spandex?

1.2.5 Osmolyte fluctuations

There can be many sources of bilayer tension fluctuations. One of them, presented in the article (see Ch. 2), is osmo-metabolite fluctuations. We here review that calculation. For simplicity we assume a vesicle with spherical symmetry, but the basic ideas remain the same

for any vesicle shape. Consider a spherical vesicle with a bacteria-like volume (radius = 1 μm), in a 1 M isotonic solution at 300 K. A single osmolyte appearing inside the vesicle would cause an osmotic influx of water, increasing vesicle volume and hence increasing tension in the vesicle lipid bilayer.

The final volume would be such that initial and final internal concentrations are equal, we have:

$$\frac{N_{osmolytes}}{V_{initial}} = \frac{N_{osmolytes} + 1}{V_{final}}, \tag{1.4}$$

from which the final radius can be calculated:

$$r_{final} = r_{initial} \sqrt[3]{1 + \frac{1}{N_{osmolytes}}}. \tag{1.5}$$

Knowing the initial and final radii of the vesicle, and using the bilayer compressibility $K = 235$ mN/m,the area change can be calculated, which can be used to find the tension increase:

$$\Delta\gamma = K \frac{r_{final}^2 - r_{initial}^2}{r_{initial}^2}, \tag{1.6}$$

where $\Delta\gamma$ is the tension increase.

Using the numbers mentioned above gives a tension increase of approximately 0.2×10^{-6} mN/m per added osmolyte. A 4% fluctuation in osmolyte concentration (corresponding to approximately 10^8 osmolytes) would yield a tension fluctuation of about 1 mN/m.

The whole point of this calculation is that, under normal biological conditions, fluctuation in osmolyte concentration is not unexpected. If such fluctuations are large enough (and we just showed that a small fluctuation of 4% leads to a tension fluctuation of about 1 mN/m, with a lysis tension of $\sim$ 10 mN/m), they might accidentally gate osmovalves (e.g., MscS and MscL). Accidental gating of such channels would be very costly for a cell as precious osmolytes would be lost. Hence having proteins acting as membrane spandex, proteins able to damp membrane tension changes, might prevent accidental gating of osmovalve channels.

1.3 Other spandex candidates

Being the most studied mechanosensitive channels and having large area increase upon transition[13, 23], MscL and MscS were obvious choices as potential spandex proteins for our study. Three other proteins, from eukaryotic cells, are presented in the article (see Ch. 2) as spandex candidates. We briefly introduce them here and refer the reader to the article for more on these proteins' potential spandex properties.

1.3.1 Prestin

Prestin is the motor protein in outer hair cells[34] (the sensory receptor cells of the ear), allowing for rapid changes in length and stiffness which are required for proper hearing[35]. It has been described as a piezoelectric device[36]: changes in transmembrane potential causes change in protein shape and conversely change in protein shape causes a change in transmembrane potential. This ability of prestin to change the length of the outer hair in response to a change in potential would have an effect on membrane tension and hence makes prestin a spandex candidate.

1.3.2 Kv1-type channels

Kv1-type channels (or *Shaker*) are voltage-gated potassium channels which are modulated by membrane tension[37]. *Shaker* channels also have an effect on cell electromotility through their channel opening[38]. It would be surprising if such channels had no effect on membrane tension and mechanics.

1.3.3 Rhodopsin

Rhodopsin is the membrane protein of rod outer segment (photoreceptor cells in the retina) responsible for monochromatic vision in the dark[39]. Upon photoactivation, rhodopsin changes conformation to a slightly larger state. Being present in rod outer segment in high density ($\sim 25,000\ \mu\mathrm{m}^{-2}$), photoactivation of a significant portion of the rhodopsin would probably have an effect on the bilayer membrane. There might even be a negative feedback mechanism whereby photoactivated rhodopsins would expand and relax membrane tension thus preventing other rhodopsin from changing conformation because of a lowered tension.

1.4 Budded membrane microdomains as tension regulators

Sens and Turner[40] established a theoretical model of membrane tension regulation by budding microdomains. Although not directly related to spandex proteins, their work is still relevant as they deal with tension regulation. It turns out that their modeling shares some features with ours, and some of their results are also reminiscent of ours. For this reason, we present a brief overview of their modeling and results.

Their work considers the response to tension of membrane microdomains, which tend to be invaginated under low tension and flat under high tension. This flattening of a budded membrane domain delivers extra area to the main membrane thus relaxing tension.

The model membrane consists of the main membrane (modeled as a linear spring) and the budded microdomains, acting as membrane reservoirs. Strain is applied to the system by pulling on a bilayer embedded tether, thus increasing the area by the value A_T (see Fig. 1.6).

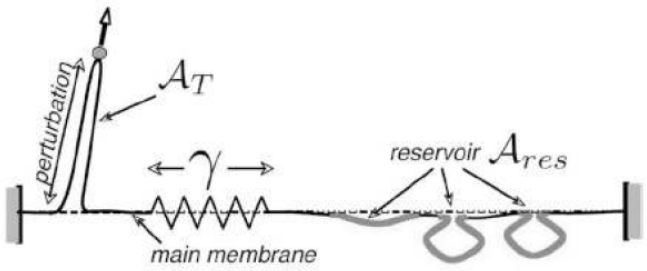

Figure 1.6 Schematic representation of the model. The tension in the bilayer membrane (γ, shown as a spring) increases upon movement of the tether (which increases total area by A_T). The reservoir budded microdomains of total area A_{res} flatten in response to the increased tension. Reprinted figure with permission from P Sens, MS Turner. *Budded membrane microdomains as tension regulators*, **Phys. Rev. E 73**, 31918 (2006)[40]. Copyright 2006 by the American Physical Society.

The membrane tension, under an area increase A_T reads:

$$\gamma = \gamma_0 + K_s(A_T + A_{res} - A^0_{res}), \tag{1.7}$$

where γ_0 is the membrane tension when no strain is applied, K_s is the stretching modulus (or area compressibility), A_{res} is the membrane area in the buds and A^0_{res} is the membrane area

in the buds at zero strain. Flattening of budded domains reduces A_{res} and hence reduces membrane tension. This equation is similar to the equation for membrane tension used in Ch. 2 and in Ref. [41].

For a fixed level of membrane tension, the state (budded or flat) of a microdomain is the result of the competition between two energies: the line energy of contact between the microdomain and the bilayer, and the bending energy of the bud. This line energy could come from e.g., different height of the lipids forming the microdomain and the bilayer. This energy is proportional to the length (perimeter) of the neck of a bud.

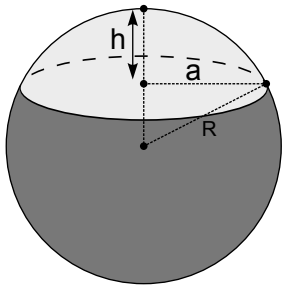

Figure 1.7 A spherical cap (the budded domain) (light gray) of a sphere (dark gray) showing the parameters: sphere radius (R), radius of the base of the spherical cap (a) and spherical cap height (h).

Assuming budded domains to be spherical caps of fixed surface S and of radius R, the line energy can be calculated from "simple" geometry. Using Pythagoras' theorem (see Fig. 1.7), we have:

$$h = R - \sqrt{R^2 - a^2}, \tag{1.8}$$

where h is the height of the spherical cap and a is the radius of the base of the cap. Solving for a gives:

$$a = \sqrt{2Rh - h^2} = \sqrt{2Rh(1 - \frac{h}{2R})}. \tag{1.9}$$

But the surface of a spherical cap is $S = 2Rh\pi$, and we can substitute $\beta = h/2R$ so that we have:

$$a = \sqrt{\frac{S}{\pi}}\sqrt{(1-\beta)}. \tag{1.10}$$

Now, as mentioned above, the line energy is proportional to the length of the edge of the spherical cap:

$$f_\sigma = 2\pi\sigma\sqrt{\frac{S}{\pi}}\sqrt{(1-\beta)} = 2\sigma\sqrt{\pi S}\sqrt{(1-\beta)}, \tag{1.11}$$

where σ is the line energy per unit length. Note that in the paper[40] there is a typo as the factor 2 in the line energy was omitted. The rest of the calculations are correct and take into account that missing factor.

The parameter beta can be rewritten:

$$\beta = \frac{h}{2R} = \frac{2\pi Rh}{4\pi R^2} = \frac{S}{4\pi R^2} = \frac{4S}{16\pi R^2} = \frac{SC^2}{16\pi}, \tag{1.12}$$

with the curvature $C = 2/R$. β solely defines the shape of the bud with $\beta = 0$ corresponding to a flat microdomain and $\beta = 1$ to a fully budded one. In their modeling Sens and Turner assign an upper limit to β as $\beta = 1$ would mean a bud separated from the membrane with no contact whatsoever with the lipid bilayer (i.e., the line energy would be zero).

The bending energy of the bud is obtained through the integral:

$$f_\kappa = \oint \frac{\kappa}{2}\left(\frac{1}{R_1^2} + \frac{1}{R_2^2}\right) dA, \tag{1.13}$$

where κ is the bending energy, and R_1 and R_2 are the principal radii of curvature. Since it is assumed that the bud is spherical, we have $R_1 = R_2 = R$, and the integral becomes:

$$f_\kappa = \frac{\kappa}{2}\oint\left(\frac{2}{R}\right)^2 dA = \frac{\kappa}{2}C^2\oint dA = \frac{\kappa}{2}C^2 S, \tag{1.14}$$

$$f_\kappa = 8\pi\kappa\beta, \tag{1.15}$$

with $\beta = SC^2/16\pi$, as in Eq. 1.12. Note that R is expected to take values in the range of a few hundred nanometers[40].

Including membrane tension, the flat state is favored by high tension as tension should unfold reserve membrane area. The surface energy cost of forming a bud is hence linked to the change in membrane area between a flat and a budded state:

$$f_\gamma = \gamma S - \gamma \pi a^2. \tag{1.16}$$

This equation considers the energetic cost of reducing an initial area of S (corresponding to a flat microdomain) to an area of πa^2 (corresponding to the area of the neck of a bud). Using the value of a found in Eq. 1.10, we get:

$$f_\gamma = \gamma S - \gamma \pi \frac{S}{\pi}(1-\beta) = \gamma S \beta. \tag{1.17}$$

The total energy of a microdomain then reads:

$$f_{\sigma,\kappa,\gamma}(\beta) = 2\sigma\sqrt{S\pi}\sqrt{(1-\beta)} + 8\pi\kappa\beta + \gamma S\beta. \tag{1.18}$$

Assuming the microdomain is large enough that at zero tension the budded state is favored, then increasing tension favors the flat state. For a critical tension γ^*, both states have the same energy (see Fig. 1.8):

$$\gamma^* = \frac{2\sigma\sqrt{\pi S} - 8\pi\kappa}{S}. \tag{1.19}$$

For tensions larger than γ^*, the flat state is favored, for smaller tensions, the budded state is favored. However, the transition from budded to flat (or flat to budded) must go through an energy barrier. The position of this barrier can be found analytically by taking the derivative of the energy of a domain with respect to its shape parameter β (and remembering that the bud surface, S, is taken as constant):

$$\beta_{barrier} = 1 - \left(\frac{\sqrt{\pi S}\sigma}{8\pi\kappa + \gamma S}\right)^2. \tag{1.20}$$

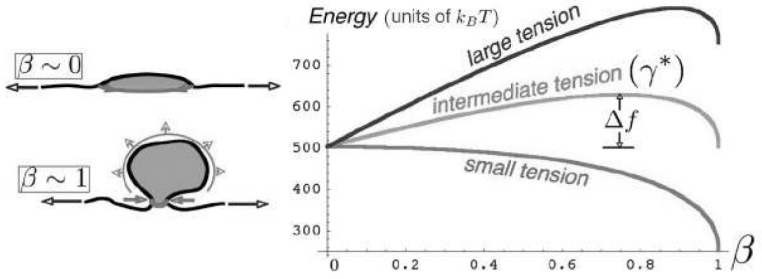

Figure 1.8 Left: $\beta \sim 0$ corresponds to the flat state; $\beta \sim 1$ corresponds to the budded state. The neck region (the region of the bud which remains in contact with the bilayer) is shown with arrows. Right: energy of the system as a function of microdomain state (β). For small tensions, the budded state is favored; for large tensions, the flat state is favored; for intermediate tensions ($\gamma = \gamma^*$) the flat and budded states have the same energy. In this case, the energy barrier for changing shape is given by $\Delta f = f_{max} - f(\beta_{bud}) = f_{max} - f(0)$. Reprinted figure with permission from [40]. Copyright 2006 by the American Physical Society.

Considering a collection of N microdomains, with total area $NS\beta_{bud}$, (β_{bud} is the maximal value of β that can be reached, $\beta = 1$ being impossible as there would be no contact between the domain and the membrane), we have a fraction ϵ of domains in the budded state (and accordingly a fraction $1 - \epsilon$ of domains in the flat state). The rate of change of ϵ is given by:

$$\tau_0 \frac{d\epsilon}{dt} = -\epsilon \exp\left[-(f_{max} - f(\beta_{bud}))/kT\right] + (1-\epsilon)\exp\left[-(f_{max} - f(\beta = 0))/kT\right], \qquad (1.21)$$

where τ_0 is the characteristic time for domain shape change, f_{max} is the energy barrier, i.e., the energy of the least favorable domain shape given by Eq. 1.20. The time-dependence of the right-hand side of the equation arises from tension as membrane tension is also changing with time (more presicely with ϵ) according to:

$$\gamma = \gamma_0 + K_S(A_T + \epsilon NS - \epsilon_0 NS), \qquad (1.22)$$

where ϵ_0 is the fraction of domains in the budded state at the tension γ_0. If the increase in membrane area A_T is matched by the decrease in budded membrane area, then membrane tension can be kept at a fixed level.

Under a strain ramp, the results are quite similar to the membrane spandex results: membrane tension increases linearly with strain until domains start flattening (or spandex proteins start expanding); in the flattening (expansion) region, membrane tension remains practically constant, until all domains are flat (all spandex are expanded); membrane tension is then once again linear with strain (see Fig. 1.9).

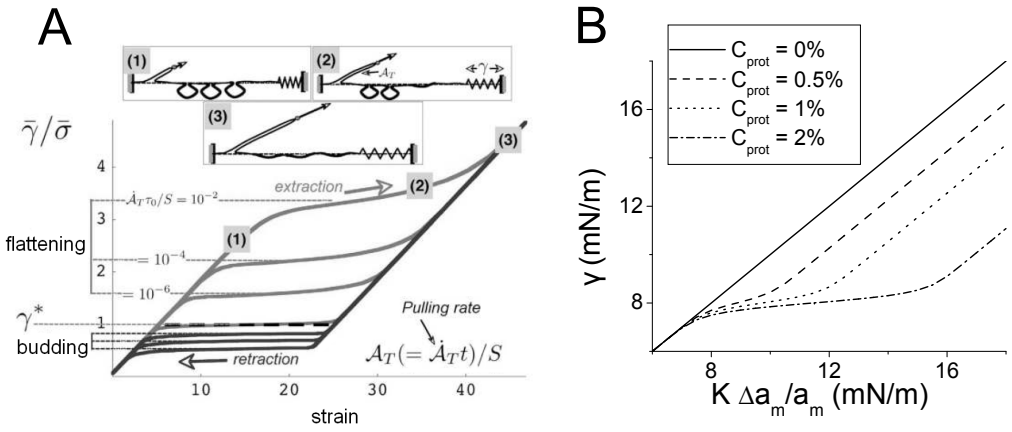

Figure 1.9 A) Simulation of membrane tension as a function of area increase for different tether pulling rates ($\dot{A}_T$). In the domain flattening region, membrane tension is kept at a relatively fixed level; this is reminiscent of spandex proteins which can also damp membrane tension increase. Reprinted figure with permission from [40]. Copyright 2006 by the American Physical Society. B) Membrane tension as a function of strain for different concentrations of spandex proteins; spandex proteins can regulate tension increase in a similar fashion as budding microdomains. Reprinted figure with permission from [2].

Although the system is quite different from the one we aim to study (membrane microdomains vs spandex proteins), one of the basic modeling ideas remains the same: membrane tension is regulated by a two-state mechanical process.

Moreover the results share some similarities: budding microdomains are able, just like membrane spandex, to regulate membrane tension. The kinetic modeling used here is also similar to what is used in the spandex paper.

It would be interesting to study a membrane comprising both budding microdomains and spandex proteins. For example, a mechanosensitive protein could be embedded in a budded domain. If the curvature of the budded state favored the closed/contracted state of the protein and a flat domain favored the open/expanded state, a system oscillating between budded+closed and flat+open could be possible. If the domain was flattened by a tension

increase, this flattening could then cause the mechanosensitive membrane protein to gate which would in turn cause an increase in domain size. If the tension increase was just sufficient to cause the domain flattening, an increase in domain size would cause it to return to the budded state. This cycle could repeat itself indefinitely. Although such a contraption is interesting, it might not be of biological interest.

1.5 Articles review

The area of mechanosensitive channels and proteins is wide and very active, so a complete literature review is practically impossible. Below is a short (and incomplete) overview of the literature pertaining to mechanosensitive channels and some related topics.

1987 Martinac, Buechner, Delcour, Adler and Kung[42] reported the first experimental observation of channels gated by pipette suction in E. coli spheroplast, in a patch clamp setting. Although they reported the channels detected as pressure-activated, they are stretch-activated channels, a confusion that still lasts because of the widespread use of patch clamp experiments. They also postulated that such tension-sensitive channel could have osmoprotective properties.

1997 Häse, Minchin, Kloda and Martinac[32] radio-labelled MscL from *E. coli* and were able to determine that MscL is located in the inner cytoplasmic membrane. They also determined the number of MscL to be approximately 50 per bacterium.

1999 Levina, Totemeyer, Stokes, Louis, Jones and Booth[15] performed viability assays on E.coli cells lacking certain genes and identified two genes (yggB and kefA) to be responsible for MscS activity. They also showed that having the genes that regulate only for MscS or only for MscL is sufficient for osmoprotection (but do not show explicitly channel activity upon osmotic downshock). Some of their results are reproduced in Fig. 1.2.4.

Sukharev, Sigurdson, Kung and Sachs[14] used patch clamp technique along with video microscopy to monitor pressure, tension and current in a single channel liposome with reconstituted MscL. This allowed the measurement of the tension midpoint of activation of MscL as 11.8 mN/m. MscL's area change upon expansion was also calculated as 6.8 nm^2 by using the equation:

$$P_{open} = \frac{1}{1 + \exp\left((\Delta E - \gamma \Delta A)/kT\right)}, \tag{1.23}$$

which assumes that MscL has only two states (open and closed). It was later shown [19, 13, 18] that 6.8 nm^2 is an underestimate of the real area change upon expansion which is actually closer to 20 nm^2. In this paper, they also identified multiple subconducting states for MscL and calculated the transitions rates between those states. MscL undergoes a (silent closed-closed) pre-expansion before opening, and this transition carries the bulk of the mechanosensitivity.

2001 Sukharev, Durell and Guy[13] used the crystal structure of *M. tuberculosis* MscL to propose a gating mechanism for MscL. In this mechanism, MscL expands by about 20 nm^2. This model is also consistent with MscL having a closed-closed silent pre-expansion occurring before channel opening. This pre-expansion carries the bulk of the tension dependence and consists of about $\sim 80\%$ the total area change (leaving the remaining $\sim 20\%$ to the opening transition itself).

Sukharev and Markin[18] present a model considering MscL as an elastic rim surrounding the inner gate. They give the free-energy difference between the closed and open states as:

$$\begin{aligned} \Delta G_{min} &= -\left(\Delta A_{op} + \frac{\gamma_{0.5}}{B_{op}} - \frac{\gamma_{0.5} + B_{core}\Delta A_{core}}{B_{rim} + B_{core}}\right)\Delta\gamma + \\ &\quad \frac{1}{2}\left(\frac{1}{B_{rim} + B_{core}} - \frac{1}{B_{op}}\right)\Delta\gamma^2, \end{aligned} \tag{1.24}$$

where $\Delta\gamma = \gamma - \gamma_{0.5}$, is the difference between membrane tension and midpoint tension, B_{core}, B_{rim} and B_{op} are the stiffness of the core, the stiffness of the rim in the closed state and the stiffness of the rim in the open state respectively. ΔA_{core} is the area difference between the rim and the core and ΔA_{op} is the area

difference between the area of the rim under tension and the area of the rim at zero tension. The model is fitted to experimentally obtained data and predicts a very stiff (120 MPa) open state, and a soft (6 MPa) closed state. The model is consistent with the fact that simple two-state Boltzmann fit of experimental data yields a change of area upon expansion of only $\Delta A = 6$ nm^2[14], for a channel with $\Delta A = 20$ nm^2[13].

2002 Batiza, Kuo, Yoshimura and Kung[43] showed that having only MscS or MscL is sufficient for osmoprotection. Moreover they showed that MscS buffers the opening of MscL: an osmotic downshock just sufficient to gate MscL (in a bacterium without MscS) would not be sufficient to gate MscL in the presence of MscS: a larger downshock is required. The method used in this paper is quite interesting: they used a mutant form of MscL (L19C) to which another agent could bind, but only if the mutant MscL is open (residue 19 is located inside the gate region of MscL, thereby only accessible from the open state). This agent, upon binding, renders the channel toxic (leaky), thus allowing the determination of the minimal downshock necessary to gate (a mutant form of) MscL in the presence of MscS. In the spandex paper, we proposed an experiment similar to this one to study the effect of spandex proteins. A cysteine normally shielded inside the protein which became exposed by expansion (not opening) of a spandex protein could be used to detect their expansion (as current cannot be used).

Perozo, Kloda, Cortes and Martinac[44] showed by reconstituting MscL in synthetic phosphatidylcholine bilayers containing chains of different length that hydrophobic mismatch alone cannot gate MscL. Short lipid chains however lower the threshold of activation. They also showed that the bilayer's intrinsic curvature can trap MscL in the open state.

Sukharev[22] showed that MscS has a midpoint tension of ~ 5.5 mN/m and the opening of its pore is accompanied by an area change of ~ 8.4 nm^2 (when fitted with a two-state Boltzmann model). MscS opens at a lower tension than MscL (which opens at 11.8 mN/m[14].

2003 Stokes *et al.*[33] showed that MscS and MscL expression is increased from a basal level by growth in high osmolarity environment, possibly to prepare for an eventual osmotic downshock. They also showed that entry into the stationary phase triggers an increase in expression of MscS and MscL.

2004 Laitko and Morris[37] used macroscopic patch currents of the 5aa mutant of Shaker channels to show that the stretch sensitive activation of this channel is not through a different pathway (or different conformations) but is really an acceleration of the transitions by stretch. Moreover their results show that activation and inactivation of the channel are affected to the same extent by stretch.

Chiang, Anishkin and Sukharev[20] used statistical modeling to show that slight variations in channel parameters (ΔE and ΔA) of MscL could reduce the apparent slope of the activation curve. This could possibly explain the discrepancy between estimated channel area change[13] and experimentally obtained values from two-state fitting[14]. By using only the initial part of the activation curves, they obtain values of $\Delta A = 20.4$ nm^2, which is consistent with structural modeling which predicts ~ 20 nm^2. Interestingly they used the midpoint of activation of MscS (at 5.5 mN/m) to extrapolate the pressure-tension relationship in each patch (i.e., they used the activation midpoint of MscS as a calibrating tension).

Wiggins, Phillips and coworkers[45, 46, 47] established a theoretical framework for the calculation of the energetics of membrane-protein interactions for mechanosensitive channels. They considered many effects: areal deformation by the expanding channel, Gaussian curvature and spontaneous curvature of the lipid bilayer, interface interaction at the protein-lipid boundary, bilayer midplane deformation and bilayer thickness deformation, with the midplane deformation and Gaussian curvature terms being about an order of magnitude smaller than the others, which are in the range of 10 kT (as estimated for MscL). These estimates are of the same order of magnitude as the free energy difference between protein states obtained experimentally, hinting that bilayer mechanics play an essential role in mechanosensitive protein energetics.

Markin and Sachs[19] established a theoretical model for the thermodynamics of mechanosensitivity, including the stiffness of the different protein states. They included factors such as membrane stiffness, thickness, spontaneous curvature and changes in channel shape and length. The model predicts that the midpoint tension and the slope of the gating curve are generally not independent. The different stiffnesses of the closed and open states of MscL is used to explain the discrepancy between its predicted[13] and observed[14] area change upon expansion. The model is also adapted to explain the observed switch between tension-activated to tension-inactivated of gramicidin A[48] as a function of lipid bilayer thickness.

2005 Norman, Liu, Rigby, Raso, Petrov and Martinac[49] present a method to visualize MscL channels in living bacteria using confocal microscopy. They created a fusion gene between mscl (the gene for MscL) and the gene encoding for a fluorescent protein (GFP). The MscL-GFP channel has the same parameters as MscL, but requires more tension to open (this paper refers to pressure as the activation stimulus of MscL). Visualization reveals that MscL does not segregate at the bacterial poles like other membrane proteins, but is rather dispersed evenly.

Akitake, Anishkin and Sukharev[26] studied MscS in a patch clamp setting. They found that the opening of MscS is voltage-independent, but inactivation from the open state is voltage-dependent in depolarized conditions. The area change upon expansion is estimated as 18 nm^2. They also found that under a slow ramp, channel activity (current) is smaller than a under fast ramp. They hypothesized that MscS is not only sensitive to tension, but also sensitive to the rate of tension change.

2007 Akitake, Anishkin, Liu and Sukharev[27] studied experimentally the adaptive behavior of the MscS channel. Their focus was on the conformation changes between states: by applying point mutations to the channel, they were able to modify its kinetics, thus identifying key elements responsible for closure and

desensitization. Although not the main point of the paper, they found a mutation (G121A) which activates a pathway from the closed state to the inactivated state, i.e., a closed-closed expanding transition. This mutation is however highly toxic as once the channel is open it cannot close upon tension release.

Booth *et al.*[16] provide a thorough review of mechanosensitive channels as osmoprotectors tested with viability assays. They provide an experimental protocol with a list of ways to improve sensitivity or automation of the process. Mutants providing a gain or loss of function may prove to be toxic. A gain of function can be toxic because the channels open up at too low a tension, and a loss of function results evidently because the channel cannot release osmolytes upon osmotic downshock.

Booth, Edwards, Black, Schumann and Miller[17] give an excellent review of current knowledge on mechanosensitive channels. They suggest that expression of MscS channels is regulated by the osmolarity of the environment in which the bacterium grows. Moreover, some channels appear to be silent under patch-clamp experiment. They also suggest that the function of mechanosensitive channels is not solely osmoprotection: mechanosensitive channels could also be involved in maintaining structural integrity. An argument on interplay of cell wall and membrane being poorly understood is also provided.

Boucher, Joós, Zuckermann and Fournier[41] studied a theoretical model for the rupture kinetics of lipid bilayers subjected to a strain ramp in the absence and in the presence of antimicrobial peptides. The rupture is driven by the nucleation of pores. Although the effect is minimal, insertion of peptides in the model bilayer relieves tension, providing a theoretical framework (along with the work by Sens[40]) for relaxation of bilayer tension. It is to be noted however that peptides make lipid bilayers more susceptible to rupture.

Ursell, Huang, Peterson and Phillips[50] studied from a theoretical point of view the bilayer-mediated interaction between two membrane proteins. They found that interaction between neighboring channels leads to a left-shift of midpoint tension (i.e., the channels open at lower tensions). Additionally, the slope of the

activation curve increases when the channels are separated by small distances (compared to infinite separation).

2008 Reeves, Ursell, Sens, Kondev and Phillips[51] present a theoretical model of lipid bilayer deformation in the context of voltage-gated channels, arguing that such deformations play an important role not only in mechanosensitive channels, but in essentially any membrane protein with different conformations. They divide conformation changes in three major classes: midplane bending (uneven changes in radius from top to bottom), compression (change in height) and footprint dilation (change in area). Expected shifts in activation potential as a function of bilayer tension and thickness are calculated.

Powl, East and Lee [52] studied the effect of anionic lipids (=negatively charged) on MscL. They determined that anionic lipids accelerate the transition from the closed state to the open state, and slow the transition from the open state to a subconducting state. The open state is thus favored in the presence of anionic lipids.

Anishkin, Kamaraju and Sukharev[24] used molecular dynamics simulation to study the closed-open transition of MscS. They predicted the area change upon expansion to be ~ 16 nm^2. They also found that flux through the pore is correctly approximated by macroscopic electrodiffusion.

2009 Beyder and Sachs[38] studied the electromotility of Shaker K^+ transfected HEK-293 cells using atomic force microscopy. Electromotility in wild type HEK is linear with transmembrane potential[53] but transfected HEK cell's electromotility saturates at a potential corresponding to channel opening. They showed, using mutant forms of the channel that the gating mechanism is not involved, but really the activation (i.e., the change of shape) of the channel drives the change in electromotility. They put forward a few hypotheses: charge movement due to voltage sensor movement, local tension decrease due to channel opening and change in channel height pushing the cantilever, but none of these are completely

satisfying. The most probable solution is local buckling of the lipid bilayer due to uneven channel expansion (Shaker expands mostly in the interior leaflet of the bilayer). This experiment is quite promising for the main idea behind spandex proteins: that membrane protein conformation changes have an effect on lipid bilayer mechanics. The conjugate use of whole-cell recording with atomic force microscopy could be an ideal tool to study spandex proteins.

2010 Belyy, Kamaraju, Akitake, Anishkin and Sukharev[28] studied the adaptative behavior of MscS and MscL channels in excised patches and whole spheroplast mode. Adaptation is a reversible channel activity decline upon prolonged stimulus. They showed that adaptation is the result of the relaxation of the inner lipid leaflet, leading to asymmetric tension distribution which is less favorable to channel opening. In the patch clamp setting, the inner leaflet is not attached to the glass pipette and is thus able to slide against the fixed exterior leaflet to relax. In whole spheroplast mode the inner leaflet has no loose ends and is hence unable to relax, explaining why adaptation can be seen in patch clamp but not in whole spheroplast mode. They also report that even though the spandex effect of opening channels could have an effect on adaptation they could not detect any.

Belyy, Anishkin, Kamaraju, Liu and Sukharev[29] studied the structure of MscS both in patch clamp experiments and in molecular dynamics simulations. Their focus was on the structure of MscS states, and they identified two mutants (F68S and L111S) which can silently inactivate directly from the closed state. Interestingly, both these mutations, contrary to G121A (which once opened cannot close or inactivate), do not seem to be toxic and hence provide for even more possibility of silent spandex mutants of MscS.

Not mentioned in this (short) list are some very good reviews on mechanosensitive channels[9, 10, 11, 12, 54]. Having briefly introduced the topic of mechanosensation and tension relaxation, we now present our work.

Chapter 2

Mechanosensitive Closed-Closed Transitions in Large Membrane Proteins: Osmoprotection and Tension Damping

P-A Boucher, CE Morris and B Joós

Reprinted from Biophysical Journal,
97(10) 2761-2770, Copyright (2009),
with permission from Elsevier.

Mechanosensitive Closed-Closed Transitions in Large Membrane Proteins: Osmoprotection and Tension Damping

Pierre-Alexandre Boucher,[†] Catherine E. Morris,[‡] and Béla Joós[†*]
[†]Institut de Physique, Ottawa-Carleton Campus de l'Université d'Ottawa, Ottawa, Ontario, Canada; and [‡]Neurosciences, Ottawa Health Research Institute, Ottawa, Ontario, Canada

ABSTRACT Multiconformation membrane proteins are mechanosensitive (MS) if their conformations displace different bilayer areas. Might MS closed-closed transitions serve as tension buffers, that is, as membrane "spandex"? While bilayer expansion is effectively instantaneous, transitions of bilayer-embedded MS proteins are stochastic (thermally activated) so spandex kinetics would be critical. Here we model generic two-state (contracted/expanded) stochastic spandexes inspired by known bacterial osmovalves (MscL, MscS) then suggest experimental approaches to test for spandex-like behaviors in these proteins. Modeling shows: 1), spandex kinetics depend on the transition state location along an area reaction coordinate; 2), increasing membrane concentration of a spandex right-shifts its midpoint (= tension-Boltzmann); 3), spandexes with midpoints below the activating tension of an osmovalve could optimize osmovalve deployment (required: large midpoint, barrier near the expanded state); 4), spandexes could damp bilayer tension excursions (required: midpoint at target tension, and for speed, barrier halfway between the contracted and expanded states; the larger the spandex Δ-area, the more precise the maintenance of target tension; higher spandex concentrations damp larger amplitude strain fluctuations). One spandex species could not excel as both first line of defense for osmovalve partners and tension damper. Possible interactions among MS closed-closed and closed-open transitions are discussed for MscS- and MscL-like proteins.

INTRODUCTION

Multiconformation membrane proteins whose states displace different bilayer areas make mechanosensitive (MS) transitions between those states (1). Not surprisingly, such proteins occur in all organisms (1–4). Since bilayer strain >3–4% quickly leads to rupture (5), cells might use large Δ-area MS membrane proteins as tension buffers (Fig. 1, *A* and *B*). Large Δ-area (>100% range) membrane proteins occur in high-turgor walled prokaryotes and are osmoprotective (3). Here we consider, on theoretical grounds, direct tension buffering by MS membrane proteins. Theory developed for eukaryotic cells suggests how irreversible (plastic) tension buffering could be achieved from folded membrane (e.g., caveolae, filopodia) (6), but there is no equivalent theory for reversible (elastic) membrane tension buffering by tension-gated membrane proteins. Inspired by the characteristics and expression levels of bacterial osmovalves, we have postulated (7) that populations of membrane proteins with MS closed-closed transitions could operate as stochastic membrane spandex—i.e., as stretch-gated tension buffers. Specifically, it was MscL with its MS preopening expansion transition (8) and its apparent overexpression of ~60/cell (B. Martinac, personal communication, 2009; and reported in 1997 as ~50 channels/cell (10)) that inspired the idea. MscS family proteins too may have MS closed-closed transitions. Here we generate a simple energetic and dynamical theory for membrane spandex, and suggest several ways to investigate whether MS bacterial membrane proteins operate as tension buffers.

Bacterial osmotic valve proteins

The best-characterized MS membrane proteins are bacterial MscL, MscS, and their homologs (3,4). Both multimers expand to form nonselective channels that serve as emergency osmovalves (3). Valve opening at slightly sublytic tensions (e.g., (11, 12)) releases osmolytes and water, reducing cell volume, wall distension, and bilayer tension (3,13). Although the benefits of valve opening are clear, so are the costs: loss of expensive osmolytes and, at low pH, exposure of cytoplasm to potentially lethal acidification (14). MscL, e.g., releases osmolytes up to 400–500 kDa. However, recognizing acceptable tension noise, saving valve opening for truly catastrophic perturbations, would seem a desirable general strategy.

Why do bacteria express multiple copies of MscL and MscS per cell? MscS expands at tensions substantially lower than MscL. Why? Estimates of MscL channels/cell differ by an order of magnitude (i.e., ~5–~50) (10,15), but even at the low end, the entire MscL/MscS collection would seem excessive for emergency osmolyte release. A single stretch-activated MscL (~1 nS unitary conductance, P_{open} ~1 at near-lytic tensions (16)) should suffice. With its large pore size (a 25 Å cylinder of radius 12.5 Å (17)), one open MscL could relieve tension in a bacterium exposed to pure water, yielding a safe pressure differential (<0.4 Osm (15)) within ~0.55 s. This time course assumes exponential decrease of cytoplasmic osmolytes via a channel with efflux characteristics as per

Submitted June 1, 2009, and accepted for publication August 31, 2009.

*Correspondence: bjoos@science.uottawa.ca

Editor: Reinhard Lipowsky.

0006-3495/09/11/2761/10 $2.00

doi: 10.1016/j.bpj.2009.08.054

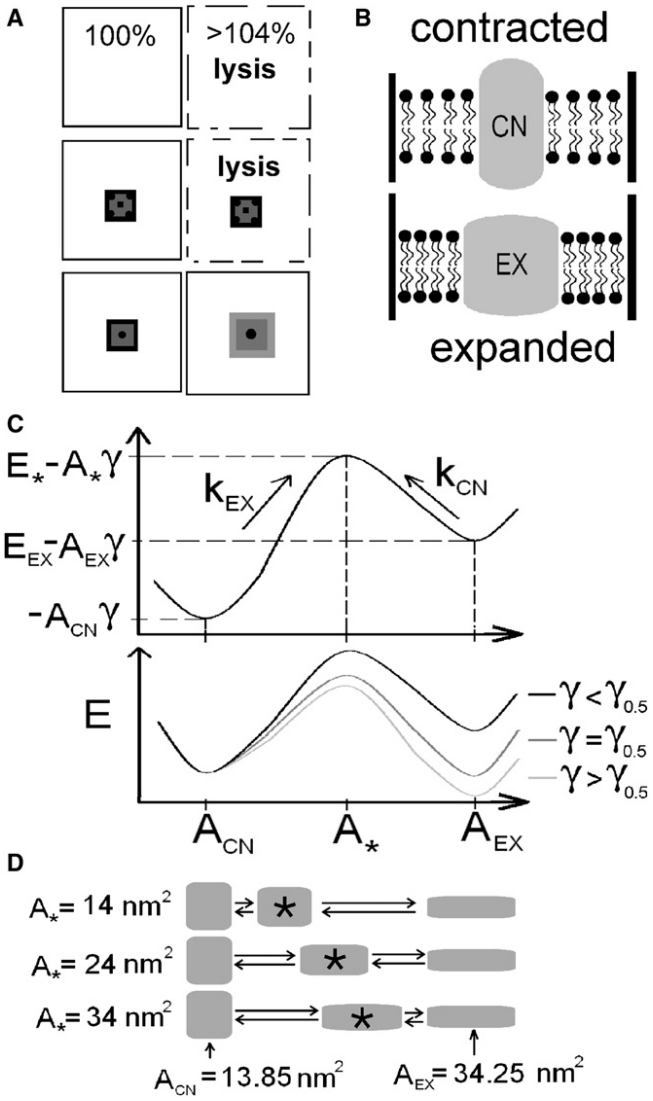

FIGURE 1 (*A*) Pure lipid bilayers (*top*), or ones with nonexpansible proteins (*middle*), rupture (i.e., lyse) under strain ~4%, whereas expanding proteins (*bottom*) could prevent lysis by relief of tension. (*B*) The spandex model states (contracted, CN; expanded, EX). For a given strain, bilayer tension ($= \gamma$) is higher with CN than with EX. (*C*) Spandex energy landscapes (reaction coordinate: protein area). (*Top*) A landscape for $\gamma < \gamma_{0.5}$, the spandex midpoint tension, illustrates the model's parameters: A_{CN}, A_*, and A_{EX} are the areas associated with the CN, transition (barrier) and EX states. With CN taken as the reference state, E_* and E_{EX} are the energies of the barrier state and of EX. k_{EX} and k_{CN} are the transition rates. (*Bottom*) As bilayer tension increases, the energy of the EX and barrier states decrease linearly, relative to CN. At $\gamma = \gamma_{0.5}$ CN and EX have the same energy and the probabilities of being expanded and contracted (P_{EX}, P_{CN}) are equal. (*D*) Three spandex proteins with different values for A_* (the transition energy maximum's position) and with A_{CN} and A_{EX} fixed at values reported for MscL (17).

Eq. 11-6 in Hille (18) (cytoplasmic [osmolyte] = 1 M, bacterial volume = 10^{-15} l, diffusion constant = 1.5×10^{-9} m^2/s). Bacterial protoplasts rupture at ~10 mN/m. Dynamic tension spectroscopy (5) shows that bilayers rupturing in that range (8–9 mN/m) are safe for ~100 s under low-to-moderate bilayer strain rates (~1 mN/m/s), and that for strain rates ~100-fold faster, the same bilayer ruptures at tensions twofold higher. This suggests that during turgor upsurges, a population of MscL with a closed-closed expansion en route to opening could obviate the need to use the valve.

In addition to multiple copies of MscL and MscS, bacteria express MscS homologs whose expression increases when conditions demand osmoprotection (3). Viability assays plus electrophysiological and biochemical analysis reveal that in exponential and stationary phase growth, *Escherichia coli* deploys 10–15 and 20–30 copies, respectively, of MscS/cell, with growth at high osmolarity further increasing MscS density (15). Could the excess have nonvalve mechanoprotective roles? MscS channels can enter a nonconducting expanded state (19); in vitro, this occurs from the open state, but in vivo conditions might favor direct transition from closed (CN) to inactivated (EX) as seen in vitro for an MscS point mutant (20). A fast open-inactivated transition (<1 ms range) in vivo might achieve almost the same effect, while also providing minor osmotic relief. The notion of MscS having an EX state with little or no associated flux seems especially plausible, given that a handful of MscS homologs (3), by patch clamp, are electrically silent. Such silent EX states in either osmovalve proteins or in coexpressed proteins might serve as a first line of defense to relax bilayer tension while retaining valuable osmolytes.

We develop a two-state model directly comparable to stochastic two-state models for ligand-, voltage-, and mechanically gated channels: spandex transitions occur across energy barriers small enough to be surmounted by thermal energy, with the gating free energy linearly dependent on membrane tension (21). Within that context, we ask what design features of spandex proteins might allow them to act as tension relievers.

Bilayer tension fluctuations in walled cells

Surprisingly little information is available on the mechanical interplay of cell wall and lipid bilayer, an interaction highly relevant to bilayer tension and hence to MS gating of bilayer-embedded bacterial proteins. Area compressibility can be directly assessed for unsupported bilayers (22), but not for complex bilayers supported by cell walls. Nevertheless, when turgor presses bacterial bilayers against the mechanically supportive peptidoglycan cell wall (23), bilayer tension must change in concert with any wall compressibility changes such as those due to exterior and interior environment pH variations (24).

Osmo-metabolite fluctuations will also generate bilayer tension fluctuations. Consider bacteria-sized spherical vesicle of radius = 1 μm in a 1 M isotonic solution at 300 K and suppose a single additional osmolyte (plus osmotically obliged water) appears inside the vesicle. At a typical bilayer compressibility of 235 mN/m (22), the resulting tension increase is 0.235×10^{-6} mN/m per osmolyte. A $\pm 4\%$ fluctuation in [osmolyte] would correspond at 1 M (~10^8 osmolytes)

to a ± 1 mN/m tension fluctuation (= 1/8 times the osmovalve midpoint tension); depending on load-sharing between bilayer and wall under the prevailing conditions, this might gate an osmovalve.

In walled (i.e., elevated turgor pressure) nanomechanical motions, as measured in yeast (25), may also be relevant there. The ATP- and temperature-dependent periodic nanomechanical motions (~3 nm, 0.8–1.6 kHz), thermodynamic characteristics, and force magnitude (~10 nN) suggest concerted myosin-type action. If force associated with the motion distributed itself over the entire plasma membrane, bilayer tension (assuming spherical geometry) would be 2×10^{-4} mN/m (= 0.25×10^{-4} times the osmovalve midpoint tension). Several simultaneous motions might generate tension noise (above the turgor background) sufficient to mistrigger an osmotic valve. It is worth noting that bacteria, too, possess dynamic (proto)cytoskeletons (26).

MS closed-closed transitions in various proteins

As noted above, electrophysiological and structural indications for MscS (20) and MscL (27) (and mutants) point to MS closed-closed transitions, preopen EX states in the activation path, or to closed-inactivated EX states. Its preopening transition may expand MscL to ~80% of its open area, the remaining 20% occurring on pore opening (8). MscS opens directly from the closed state, but under sustained tension, inactivates, possibly enlarging further (20). Additionally, if, in situ, some MscL and MscS multimers were occluded when open (both possess elaborate cytoplasmic filters), this would let them act as spandexes.

Eukaryotic cells also have spandex candidates. Prestin, described as a piezoelectric device (e.g., (28)) would be a ''voltage-activated spandex''. Changes of the in-plane area of this outer hair cell membrane proteins (99 nm^2 (29) when contracted), which occupies ~60% of the membrane (30), alter the cell's dimensions (28,31). Its MS transition would need to be described along at least two reaction coordinates (i.e., area and charge displacement) (32). The length-scale of prestin's piezoelectric transition is of the same order as for other MS proteins (8.4 nm^2 for MscS (19), 4 nm^2 for prestin (30)). In Kv1-type (*Shaker*) channels, atomic-force microscopy (AFM) evidence shows that voltage sensor transitions affect membrane electromotility (33), likely reflecting lateral interactions between protein and lipid bilayer, a not-unexpected finding given the MS activation kinetics of *Shaker* (e.g., (34)). Kinetic interplay between two species of piezoelectric MS proteins may develop when fast-gating Kv channels optimize prestin mechanics (35). Photodetecting rhodopsin occurs at 25,000 μm^{-2} in rod outer segment membrane (36), i.e., ~35% surface occupancy given its in-plane area (15 nm^2 (37)). Since photoactivation causes an estimated 1.3 nm^2 (38) area change, simultaneous photoactivation of all the rhodopsins must perturb bilayer tension; coembedded membrane proteins would ''feel'' the event.

Here, using MscL-like and MscS-like values, we generate a prototype model for membrane proteins with expanding closed-closed transitions. Our two-state (CN/EX) protein has an activation barrier on a single reaction coordinate: spandex area in the plane of the bilayer. The barrier position along this axis proved critical to spandex transition kinetics. Modeling the transition as solely tension-dependent is a useful simplification but ignores other possible energy dependences. In reality, multiple sources of energy may contribute and accordingly, multiple reaction coordinates would pertain, with barriers to expansion along those reaction coordinates (21,32), as with voltage-gated proteins modulated by tension (39,40). In much the same way, energy arising from the height difference between a spandex and the lipid bilayer (hydrophobic mismatch) would be another reaction coordinate. The model implicitly includes this free energy in E_{EX}, the energy difference between the reference (CN) and expanded (EX) states. Wiggins and Phillips (41,42) calculated gating energetics for a MscL-like MS protein embedded in a lipid bilayer and found the major contribution to be the protein's areal deformation.

Our model differs from this and other models that focus on the individual-molecule traits of an MS protein (e.g., molecular dynamics simulations). We assign individual protein properties then explore how the MS protein behaves as part of a population; kinetics (not equilibrium energetics) is the issue of central interest. In a recent overview, Phillips et al. (43) indicated that isolated versus densely-packed MS proteins will exhibit different behaviors. They examined the pairwise energetic interactions of close-proximity MS proteins (44) but not population behaviors.

Because 1), the membrane spandex idea was inspired by the large Δ-area osmovalves (channels whose opening could trump any other MS transition); and 2), there is straightforward biological relevance and experimental potential in bacterial systems, we specified that spandex transitions are ones involving no fluxes. However, in other systems, potentially dangerous fluctuations of bilayer tension might be driven not osmotically but strictly mechanically (e.g., cells strained by erratic shear flow). There, other classes of Δ-area transitions—perhaps even MS open-open transition—might serve as spandex transitions. In circulating erythrocytes, for instance, some of the abundant transport proteins might take part-time jobs as spandex.

MODELING

Sukharev et al. (27) and Sukharev and Markin (45) described the opening (and expansion, as in our case) of a MS protein in terms of opening and closing rates. A similar method is used here. A spandex membrane protein is considered to be a two-state protein (Fig. 1 *B*). The states, neither of which supports a flux, are contracted (CN) and expanded (EX). There is a transition or barrier state where the energy of the protein is at a maximum E_* (27). A typical plot of the

variation of the enthalpy of the spandex as a function of its area is shown in Fig. 1 *C*, where γ is bilayer tension. Using this energy landscape, the expansion k_{EX} and contraction k_{CN} rates can be written as

$$\begin{aligned} k_{EX} &= k_0 \exp((-E_* + (A_* - A_{CN})\gamma)/k_B T_r) \\ k_{CN} &= k_0 \exp((-E_* + E_{EX} - (A_{EX} - A_*)\gamma)/k_B T_r), \end{aligned} \quad (1)$$

where k_0 is the attempt rate taken as equal for both transitions to preserve detailed balance, and E_* and E_{EX} are, respectively, the barrier and the EX state energy with respect to the CN state. A_{CN}, A_*, and A_{EX} are the areas of the three states. $k_B T_r$ is the room temperature energy per particle. The rate of change of occupancy of the expanded state is

$$\frac{dP_{EX}}{dt} = -k_{CN} P_{EX} + k_{EX}(1 - P_{EX}), \quad (2)$$

where P_{EX} is the probability for a protein to be in the EX state. The corresponding probability for the CN state is given by $P_{CN} = 1 - P_{EX}$. The equilibrium (i.e., infinite time) solution of Eq. 2 is

$$P_{EX} = \frac{k_{EX}}{k_{EX} + k_{CN}}, \quad (3)$$

and does not depend on E_*, k_0, or A_*.

Expanded proteins occupy more space in the plane of the bilayer, reducing both the area available for lipids and bilayer tension. Considering the stress-strain relation in a lipid bilayer ($\gamma = K\Delta a/a_0$), where $\Delta a/a_0$ is the strain on the lipid bilayer and K is the compressibility modulus of the lipid bilayer; and substituting for the relative area increase in a similar way as in the literature (6,46),

$$\gamma = K\frac{\Delta a_m}{a_m} - \frac{K\Delta A C_{prot}}{A_{CN}} P_{EX}, \quad (4)$$

where $\Delta a_m/a_m$ is the strain imposed on the whole system (i.e., lipid bilayer + spandex proteins) and ΔA is the spandex area change ($= A_{EX} - A_{CN}$). $\Delta a_m/a_m$ is independent of the proteins and should be seen as a relative area change induced, e.g., by osmotic swelling. The last term in Eq. 4 corresponds to the relaxation of the bilayer due to spandex expansion. The protein concentration, C_{prot}, is defined as the ratio of the area occupied by contracted spandexes to the total area of the system. Taking the derivative of Eq. 4 with respect to time:

$$\frac{d\gamma}{dt} = K\frac{d}{dt}\frac{\Delta a_m}{a_m} - \frac{KC_{prot}\Delta A}{A_{CN}}\frac{dP_{EX}}{dt}. \quad (5)$$

The quantity $K\Delta a_m/a_m$ is the tension felt by a pure bilayer or a bilayer with nonexpansible proteins and will be used to express strains in accessible units.

The tension at which half of the spandex proteins are in the expanded state at equilibrium is called the midpoint, $\gamma_{0.5}$ (Fig. 1 *C*, *bottom*). The relation among $\gamma_{0.5}$, ΔA, and E_{EX},

$$\gamma_{0.5} = \frac{E_{EX}}{\Delta A}, \quad (6)$$

is obtained by setting equal the rates in Eq. 1.

The spandex time constant, τ_{prot}, is the characteristic time needed to reach the P_{EX} value associated with the tension, and is given by

$$\tau_{prot} = \frac{1}{k_{EX} + k_{CN}}. \quad (7)$$

The τ_{prot} is a function of A_*, k_0, and E_* as well as of ΔA and E_{EX}.

Values for the constant parameters are $k_B T_r = 4.04$ pN nm (corresponding to 23°C) and $K = 235$ mN/m (22). $A_{CN} = 13.85$ nm^2 and ΔA to 20.4 nm^2 (similar to MscL (17)) are used unless stated otherwise. E_{EX} is set through Eq. 6 by setting the midpoint $\gamma_{0.5} = 8$ mN/m (slightly lower than the lytic tension of bacterial and spheroplast bilayers). The values k_0 and E_*, although not independent parameters, are adjusted to have a maximum value of the time constant $\tau_{max} = 5$ ms, the same order of magnitude as the time constant for the opening of MscL (16). These values are used unless stated otherwise. The parameters left to vary are A_*, C_{prot}, and $\Delta a_m/a_m$, which may be a function of time, depending on the type of simulation. The model is solved numerically: at every timestep, the values of P_{EX} and γ are computed by using Eqs. 2 and 5, respectively.

One spandex in a large bilayer (i.e., isolated protein) would not affect bilayer tension. The $C_{prot} = 0$ condition, simulating vanishingly small levels of spandex, is used here when characterizing a spandex's fundamental properties.

Except for tension relaxation, the model ignores bilayer-mediated protein-protein interactions such as those occurring at short-range due to thickness or midplane deformations (40,42). Assuming that short-range means $<3\times$ the protein's radius (43), the maximum C_{prot} our model can handle is ~10% for a protein the size of MscL.

The finite stiffnesses of spandex states would displace energy minima and maximum when bilayer tension changed; ignoring this detail makes the independent analysis of kinetically relevant parameters clearer (see Supporting Material).

PROTEIN CHARACTERISTICS

Isolated protein characteristics

To understand membrane spandex populations, we first need to characterize, for different spandexes, isolated spandex behavior under stress. An important spandex parameter is area change upon expansion, ΔA, which directly impacts spandex tension sensitivity (Fig. 2 *A*). Even proteins not considered mechanosensitive per se, but having a small ΔA (in the 1 nm^2 range, e.g., rhodopsin and some voltage-gated channels) would be tension-modulated. A large ΔA makes the transition very abrupt with tension as seen in Fig. 2 *A*.

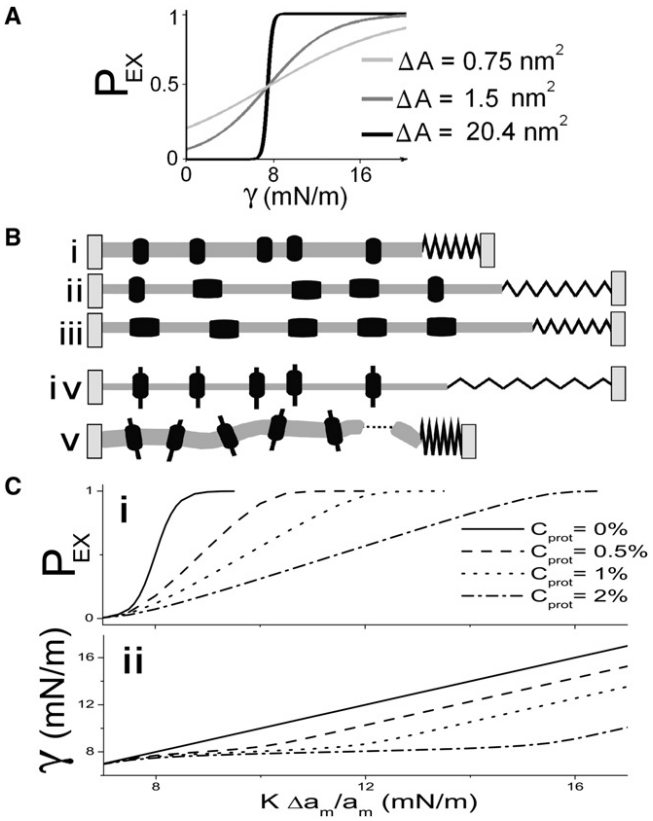

FIGURE 2 (*A*) $P_{EX}(\gamma)$ (i.e., tension-Boltzmanns) for three different ΔA spandexes with the same midpoint at 8 mN/m (i.e., slightly lower than that for MscL). $\Delta A = 0.75$ nm^2 could be any generic small ΔA protein; $\Delta A = 1.5$ nm^2 is in the range calculated for KvAP activation (38); and $\Delta A = 20.4$ nm^2 corresponds to MscL (17). (*B*) A mildly stressed membrane with contracted spandex proteins (*i*) that is suddenly exposed to a large strain (due, say, to high turgor) (*ii*) will experience elevated bilayer tension (the spring length, γ, increases) that progressively falls as more spandex proteins expand (*iii*). If the membrane contained exclusively nonexpansible proteins (*iv*) it would be more likely to rupture (*v*). (*C*) The effect of spandex concentration, C_{prot}, on P_{EX} (*i*), and on γ (*ii*), as a function of imposed strain (multiplied by bilayer compressibility: $K\Delta a_m/a_m$). (*i*) Shows the P_{EX} midpoint right-shifting and (*ii*) shows bilayer tension flattening with increasing C_{prot}.

What constitutes the optimal value of ΔA for a good anti-rupture spandex? Such a spandex needs to remain contracted, except when tension reaches values dangerous for the integrity of the lipid bilayer. A ΔA as large as feasible is called for. Very large proteins could be costly or risky to produce error-free, but the limit is set by metabolism, not by the physics of spandex. The advantage offered by a large ΔA spandex, as we show in the next subsection, can be equaled by a larger concentration of a smaller spandex (albeit not so small as to make it tension-insensitive).

Characteristics of a population of proteins

Spandex transition rates in the model depend only on bilayer tension. This tension is, however, relaxed by the expanding spandex proteins (Fig. 2 *B*). The level of strain required to expand half a spandex population is calculated by setting $P_{EX} = 1/2$ and $dP_{EX}/dt = 0$, and using Eq. 4 to obtain the relation

$$\gamma_{0.5pop} = \gamma_{0.5} + \frac{KC_{prot}\Delta A}{2A_{CN}}, \quad (8)$$

where $\gamma_{0.5pop}$ is the imposed strain (multiplied by the compressibility $= K\Delta a_m/a_m$) at which half the proteins are in the expanded state. The value $\gamma_{0.5pop}$ depends on [spandex].

In Fig. 2 *C i*, the slope of P_{EX} becomes shallower with increasing C_{prot} giving the appearance of a smaller ΔA spandex with a higher midpoint. However, this figure can be misleading because P_{EX} alone does not give a good idea of bilayer tension. Fig. 2 *C ii* plots bilayer tension versus imposed strain for several C_{prot}. Below the spandex's midpoint tension, curves superpose but approaching the midpoint (8 mN/m), they start diverging as spandex expansion stabilizes bilayer tension relative to imposed strain.

Position of the transition barrier

The value of A_* is of central importance to the kinetics of a spandex protein. When A_* is close to A_{CN}, the exponent for k_{EX} in Eq. 1 becomes small making k_{EX} a weak function of γ. At high tensions, the closing rate, k_{CN}, becomes very small due to its exponential dependence on γ leaving the time constant (Eq. 7) dominated by k_{EX}. Thus at large tensions, the time constant becomes a weak function of tension, as seen in Fig. 3 *A*. Similar reasoning applies where A_* is close to A_{EX} (Fig. 3 *C*). When A_* is midway between A_{CN} and A_{EX}, the time constant is symmetric in γ above and below the threshold (Eq. 1).

A spandex designed to prevent bilayer rupture would need to react fast when tension increased to near the bilayer's lytic value, but need not be particularly fast at lower tension. So a spandex with a large value of A_* would be appropriate (Fig. 4 *A*). To maintain a fixed bilayer tension, a spandex would need to expand fast when tension rises, and contract equally fast when tension decreases. Here, a barrier located halfway between EX and CN states would be optimal. A protein that needed to avoid interference from tension fluctuations above its midpoint could achieve that by having a small A_*.

Given the importance of A_*, it would interesting to know what controls its value. Can the transition barrier be displaced, and if so, can a spandex protein be controlled such that it would act as a good tension reliever in one set of conditions and a good tension damper in another set of conditions?

TENSION DAMPING

Cell membranes are subjected to time-varying strains due to fluctuations in osmotic and hydrostatic pressures and adhesion strengths, plus, for walled high turgor cells, to variations in cell wall elasticity. Could spandex proteins serve to maintain bilayer tension within a given range (if/when it was

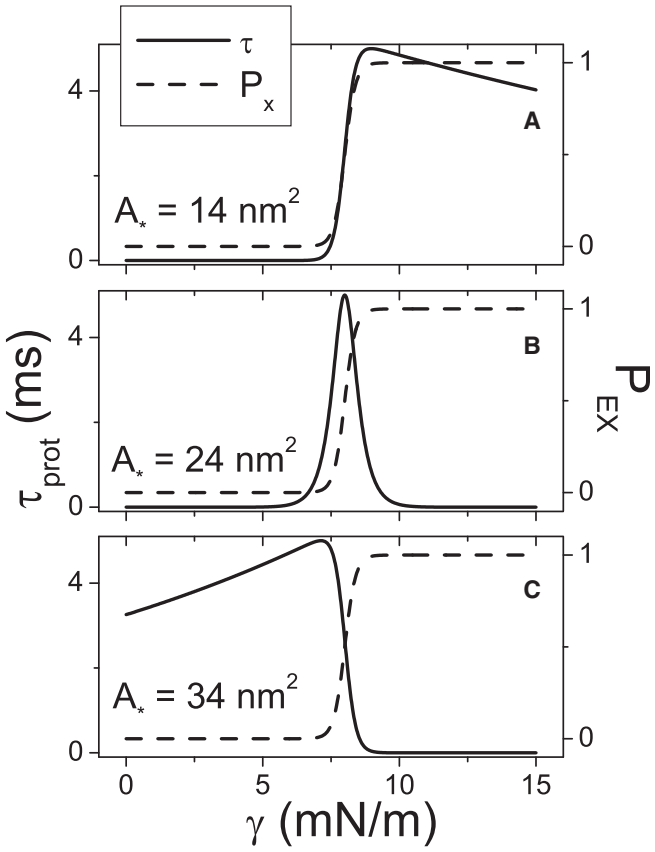

FIGURE 3 For an isolated spandex protein ($C_{prot} = 0$), varying barrier location, A_*, changes the tension-dependence of τ_{prot} (the protein time constant, from Eq. 7) (*solid lines*) without changing the tension-dependence of P_{EX} (from Eq. 3) (*dashed lines*).

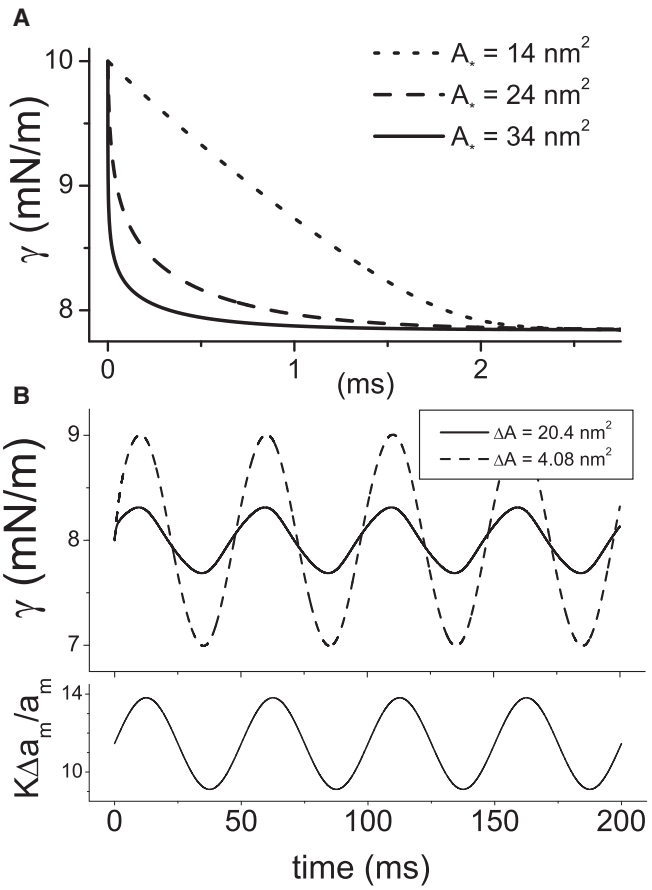

FIGURE 4 (*A*) Spandexes with different A_* values but otherwise identical parameters ($\gamma_{0.5}$, ΔA, τ_{max}, C_{prot}, etc.) relieve tension with different speeds. The time course of bilayer tension after a step strain at $t = 0$ (0–4.26%) ($K\Delta a_m/a_m$ = 0–10 mN/m) is plotted for three different A_* spandexes ($C_{prot} = 2\%$); though all three have the same τ_{max}, they have different $\tau(\gamma)$ behavior (Fig. 3). (*B*) Two different spandex proteins serve to damp bilayer stress (*top*) under oscillatory strain (*bottom*). Damping quality depends on the spandex ΔA. C_{prot} is varied to keep the product $\Delta A C_{prot}$ constant: $\Delta A = 20.4$ nm^2 and $C_{prot} = 0.02$ (*solid line*) and $\Delta A = 4.08$ nm^2 and $C_{prot} = 0.1$ (*dashed line*). The strain is initially set to $\gamma_{0.5pop} = 11.5$ mN/m, then oscillates with an amplitude of 1% (corresponding to 2.35 mN/m), with a period of $T = 50$ ms (i.e., $10 \times \tau_{max}$ for these spandexes).

advantageous for stretch-modulated membrane proteins to operate within a particular tension range)? To simulate the reaction of spandex protein to random strains, strain was varied as a sine wave. In Eq. 4, we put $\Delta a_m/a_m = \mathrm{Amp}[\sin(2\pi t/T)]$, where t is time and T is the period.

For optimal tension damping, a spandex protein must expand to relieve bilayer tension as it increases above a certain target value γ_0 and contract to increase tension as it decreases below that value. A spandex protein's midpoint ($\gamma_{0.5}$) must hence equal γ_0 (arbitrarily 8 mN/m in this work). The goal is to maintain the system in the flat section of Fig. 2 *C ii*, where strain can vary, but tension is kept almost constant. The flat region increases with the density of spandexes. This region is centered at the spandex population midpoint $\gamma_{0.5pop}$ (Eq. 8) where $P_{EX} = 0.5$ in the P_{EX} versus applied strain curve (Fig. 2 *C*, *i* and *ii*).

It would take a spandex of arbitrarily large ΔA to keep bilayer tension constant; its P_{EX} would be unity above the midpoint, and 0 below. For finite values of ΔA, tension will change around the target tension because the expansion probability on either side of the midpoint is not infinitely steep with tension (Fig. 2 *A*).

For a spandex to be a good tension damper, expansion and contraction transitions must be equally dependent on tension, i.e., equally fast, which requires a transition barrier located halfway between CN and EX (Fig. 3). In this section (and in Fig. 4 *B* and Fig. 5) we therefore use a value A_* halfway between A_{CN} and A_{EX}.

Fig. 4 *B* illustrates the effectiveness of such a spandex with a sinusoidal applied strain centered at $\gamma_{0.5pop}$. Note how a spandex with a larger ΔA damps more effectively than another with a small ΔA. However, larger C_{prot} would increase the effectiveness of any spandex population (Fig. 5 *A*). At sufficiently high C_{prot}, even proteins with very small area expansion (e.g., KvAP with ~1.5 nm^2) could serve as tension-damping spandex proteins. The maximum tension that could be relieved would, however, be small.

As seen in Fig. 5 *B* the bilayer tension oscillates with a large amplitude when strain oscillation period is short, and vice versa when it is long. The limit on the period below which

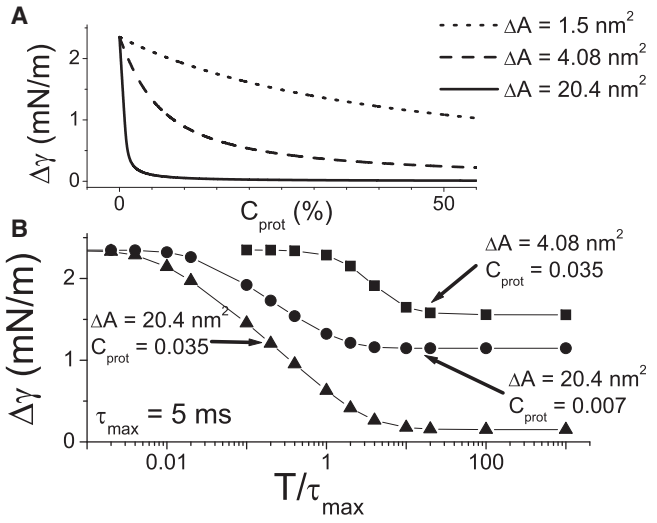

FIGURE 5 Damped tension excursions. (*A*) For a quasistatic strain oscillation, the amplitude of the tension variation, $\Delta\gamma$, for three different spandexes varies C_{prot}. (*B*) $\Delta\gamma$ varies with the period (T) of the oscillating strain (normalized to τ_{max}). For rapid oscillations (toward the *left*), tension damping is ineffective and the tension oscillation amplitude is that of the strain oscillation (multiplied by compressibility = 2.35 mN/m). For slow strain oscillations (toward the *right*), the effectiveness varies with C_{prot} and ΔA. In panels *A* and *B*, strain amplitude is 1% (corresponding to 2.35 mN/m). Plots were obtained by solving the model for different C_{prot}; ΔA and T and are not analytic functions.

the tension oscillation amplitude,$\Delta\gamma$, is no longer damped is a function of both ΔA and C_{prot}. Fig. 5 *B* also shows how a large ΔA spandex protein is more effective than a smaller ΔA.

INTERACTING POPULATIONS

Bacterial osmovalve opening is best saved for near catastrophic bilayer strain, so a mechanism whereby the valve could ignore transiently increasing tension would be useful. Two populations of MS proteins, one acting as spandex, the other as osmovalve, could help ensure the osmovalve's appropriate deployment. The two populations could be different proteins, e.g., MscS-like proteins as spandex, MscL as osmovalve. Alternately, one protein modulated two ways might serve. In a MscS/MscL pairing, the MscS would need to expand to a nonpermeant state. In vitro, MscS exhibits three states: closed, open, and inactivated (20). MscS gating models based on high-resolution structure (47) indicate that conditions that increase the separation between TM3a (transmembrane helix regions whose rotations break a vapor lock to create a permeation path) should lead to more rapid inactivation. Perhaps in vivo bilayer chemistry provides such conditions. The transit from closed to inactivated (either directly or perhaps via a very short-lived open state) would be a MS expansion (19) and could allow MscS to serve as spandex. Though not seen in vitro for wild-type MscS, it seems plausible in vivo as it does occur in vitro for mutant MscS-G121A (20). Alternatively, closed-open would be a spandex transition if, in vivo, the permeation path was occluded.

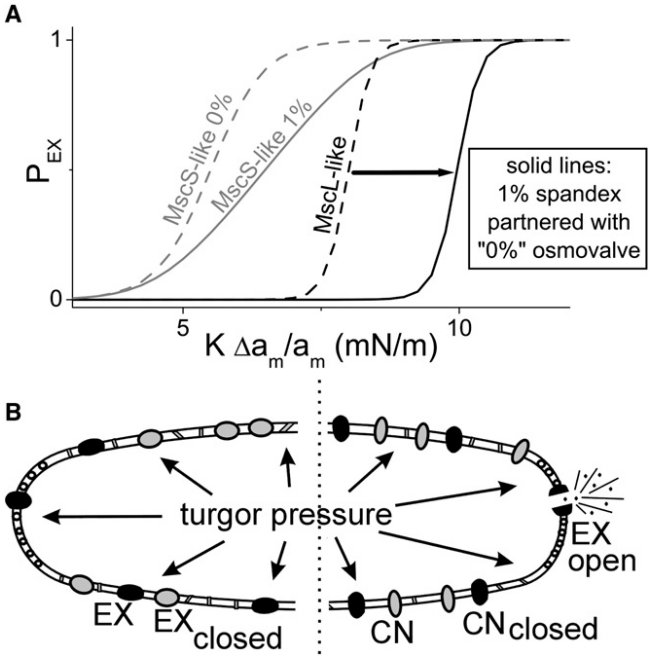

FIGURE 6 Spandex-osmovalve partnerships. (*A*) For a MscS-like spandex and a MscL-like osmovalve, dotted lines show isolated protein (C_{prot} = 0 Boltzmanns). If the membrane concentration of MscS-like spandex is increased to 1% (*gray solid*), this right-shifts (*arrow*) the Boltzmann of the single MscL-like osmovalve (*black solid*). (*B*, *left*) differential modulation of a MscL population to yield a spandex/osmovalve duo. Anionic lipids positively influence stress-induced opening of MscL (53) and cardiolipin, an anionic negative curvature lipid, segregates to the poles of cylindrical bacteria (54). MscL is ubiquitously dispersed in bacterial membranes (55) (unlike pole-preferring osmotransporter, ProP (56)). If the polar chemical environment is needed for osmovalve opening and not for the preopening expansion, then MscL along the cylindrical surface of the bacterium could exclusively operate in spandex mode. Moreover, since Laplace's law dictates that tension in the cylinder would exceed that at hemispheres, spandex would respond before the polar osmovalves, thus preventing its unnecessary deployment (i.e., effectively right-shifting the MscL-osmovalve, as in panel *A*). Two spandexes are shown black for the modulated MscL and gray for different protein species to indicate that multiple spandex species (e.g., MscS-like proteins) could participate. (*B*, *Right*) If proteins in the cylindrical region were unable to expand, the full impact of increasing turgor pressure would be borne by one, or a few, polar osmovalve(s) that would expand, open, and dump osmolytes.

Consider two populations—a MscS-like spandex and a MscL-like osmovalve—of proteins in a bilayer subjected to a slow (quasistatic) increase of imposed strain that expands the MscS-like population but not the MscL-like osmovalve. This requires that the MscS-like spandexes have a (single protein) midpoint, $\gamma_{0.5}$, below that of the osmotic valve, and that its transition be sharp enough to expand all the spandex before the valve is deployed. For the MscL-like channel we re-use parameters from the previous sections, and for the MscS-like spandex we take its midpoint to be 5.5 mN/m, $\Delta A = 8.4$ nm^2 (19), $A_{CN} = 10$ nm^2.

Assuming a bacterium has only one (or a few) MscL multimers able to act as osmovalves, the $C_{prot} = 0\%$ case would approximate its cell-population response. Fig. 6 *A* shows the

behavior of an isolated MscL-like osmovalve on an imposed strain axis (due, say, to turgor pressures of various strengths). Also plotted are the spandex behaviors, first for the isolated protein case ($C_{prot} = 0\%$) and then for an upregulated population ($C_{prot} = 1\%$) of MscS-like spandex (this result was seen in Fig. 3). The new result here is as follows: in the presence of 1% MscS, the midpoint of the (isolated) MscL-like osmovalve shifts (its slope unchanged) to higher strains (i.e., higher turgor pressures). The critical point is that the osmovalve (the MscL-like protein) still opens at the same bilayer tension, but the system strain needed to achieve the appropriate tension is larger because part of the strain is absorbed by the expanding MscS-like spandex proteins. The need for a population of spandex could explain why low MscS levels, equivalent to the basal level of expression for low osmolarity exponential phase growth, are insufficient for osmoprotection (15).

Fig. 6 *B* depicts how the spandex-dependent MscL right-shift could operate in bacteria with (at least) one MscL-like osmovalve plus a population of either functional (*left*) or nonfunctional (*right*) spandex. The spandex could be MscS-like (*gray*) and/or MscL-like multimers (*black*) that can expand, but that do not open, due to modulation by spatially segregated bilayer constituents (see caption). Note how in this scenario, the bilayer mechano-chemical confinement of osmovalve-competent MscLs at the hemispherical region, plus operation of spandex in the chemically distinctive and more highly pressure-sensitive cylindrical regions, further enhances the valve/spandex partnership.

DISCUSSION

That membrane proteins with large Δ-area transitions can reversibly control cell shape is known (31); that large Δ-area transitions could also be exploited to reversibly control membrane tension is what we explore here. Bacteria, which have MS membrane proteins with exceptionally large Δ-area transitions (3), intermittently experience moderate to extreme osmotic perturbations. Some bacterial MS proteins expand at intermediate, others at near-lytic membrane tensions. For both, it is unclear why multiple copies are deployed and how/if they interact functionally. We explored how closed-closed spandex proteins modeled on bacterial MscL and MscS (or hypothetical nonpermeable variants) might prevent tension increases or maintain bilayer tension within particular ranges. In bacteria, regulation of bilayer tension by such spandex proteins could prevent cell rupture and/or unwarranted openings of osmovalves. In effect, expressed at sufficiently high density, MscL-like multimers capable of preopening spandex transitions should reduce their own use as osmolyte dumpers. For diverse proteins whose behavior changed with fluctuating tension (e.g., the voltage-gated channels of prokaryotic as well as eukaryotic cells) (39), damping spandexes could enhance tension stability.

To explore spandex membrane tension buffering, a model for spandex expansion/contraction kinetics was presented. Although consistent with previous MS membrane protein models (27,45,40–42,48,49), it includes only the energy contribution from area relaxation due to expanding proteins, with the energy barrier position made an explicit parameter. Tension-sensitive spandex kinetics revealed how the transition barrier position (A_*) dominates kinetics, without affecting the equilibrium. The model also reveals the consequence of an inherent negative feedback: insofar as a population of spandex proteins relieves bilayer tension upon expansion, it right-shifts its own effective midpoint tension as well as that for other MS proteins like osmovalves.

For optimal tension relief versus damping, spandexes of different properties are needed. To minimize osmovalve opening or forestall transient supralytic tensions, spandexes must act below these danger zones. During slow increases, tension rise stalls, thanks to spandex expansion. If tension did rise (e.g., during abrupt osmotic shocks), a spandex population would draw tension down toward the protein midpoint value. To ensure fast responses, A_* must be close to the A_{EX}.

In real MS proteins, A_* might be influenced by the stiffness of the protein states (45). A soft CN, stiff EX spandex would be an ideal tension reliever (A_* close to A_{EX}), and a spandex with equally stiff states, an ideal tension damper (A_* midway). A membrane protein's tertiary and quaternary structure determines its stiffness and allied mechanical properties. Insofar as spandex structure changed with different bilayer lipid species, covalent modifications, ionic environments etc., a cell might, to suit different needs, regulate the relative location of A_* in a given spandex. A single gene product might, thereby, provide for both tension relief and tension damping.

Spandex, if sufficiently abundant, shifts the midpoint tension of other proteins to higher tensions, possibly preventing them from expanding/opening. The spandex ΔA need not be particularly large. The condition to be obeyed is that the entire spandex population must expand before the event to be prevented could occur. This puts a condition on both the midpoint and ΔA (directly related parameters). In real cells and membranous organelles, high density proteins whose main functions are not to act as spandex but that happen to have Δ-area transitions, albeit small ones, might help preventing lytic tension increases.

Where spandexes serve to maintain a fixed bilayer tension, their midpoint must coincide with the system's target tension. A large ΔA spandex is most effective, but small ΔA spandex can suffice if present at high density. A large ΔA spandex is more effective in maintaining a target tension precisely; smaller ΔA spandexes allow deeper fluctuations. Another characteristic tension damper requirement, equally fast reactions to tension increases or decreases, is only possible with the transition barrier located midway between CN and EX. The [spandex] required depends on the strain level to be damped and spandex ΔA.

We finish by suggesting experimental approaches to explore spandex in cells and liposomes.

A fundamental system-level functional property of a spandex is its inherent negative feedback: as [spandex] increases, the system P_{EX} (strain) relation right-shifts and its slope flattens (see 0% vs. 1% plots for a MscS-like spandex, Fig. 6). With current signaling expansion, the closed-open expansion of MscS could be used to test this. MscS channels bioengineered to be photoinactivatable would be ideal (light would then lock-in their CN state). A giant protoplast with channels at high density (say approaching 1%) would be whole-cell clamped using a slow pressure ramp to strain the bilayer and yield a P_{EX} (strain) relation. Part of the population would then be photoinactivated, a new P_{EX} (strain) relation would be obtained, and so on, until one functional channel (0%) was tested. Or, more prosaically, with protoplast volume accurately measured, one could do among-protoplast comparisons of P_{EX} (strain) for WT channels at densities from very high down to 0%; such data might already be extant.

The other class of dose-response predictions of Fig. 6 (strain right-shift of MscL activation with increasing (MscS-like) [spandex]) should, in principle, be testable in MscS-and-MscL spheroplasts under whole-cell clamp (applied pipette pressure would constitute applied strain) by monitoring the output of an exquisitely sensitive pressure servo. Existing devices are designed for speed (e.g., (50)), but redesign for sensitivity seems feasible. During a slow volume (pressure) ramp in the absence of spandex, the output of the servo as a function of time should be a straight sloped line. With spandex present, the pressure servo output would at some point increase until all the spandex was deployed (response steepness would increase with increasing ΔA, and total deflection would be proportional to [spandex]) then resume increasing linearly in parallel to the no-spandex line (Fig. 2 *C*). MscL current turn-on would occur later and later (apparent right-shift) with more and more spandex.

AFM (33) might be able to detect tension relief and tension damping due to spandex events. With bacterial spheroplasts of known diameter, whole-cell clamped (isotonic solutions, fixed voltage, known pipette pressure) current would give the time course of osmovalve openings, while cell size nano-variations were followed by AFM in constant force mode. The latter would reflect bilayer tension changes, i.e., spandex activity. The temporal relationship between tension and current fluctuations (with flux effects compensated) would give a picture of the spandex behavior of the MS proteins (e.g., MscL, MscS, or their mutants).

To test for spandex-dependent osmo-mechano-protection, liposomes or bacteria under mechanical strain (osmotic downshock, fluid turbulence) could be used. One approach: reconstitute a spandex(es) (e.g., WT-MscL, which has a preopening spandex transition; MscS-G121A, which expands from closed to inactivated) at reasonably high density into small liposomes preloaded with two fluoro-tracers (one too large to permeate open MscS or MscL and one that permeates the channel). The spandex would require a cysteine, endogenous or mutated into the protein, as inaccessible to the exterior medium except upon expansion, when a traceable sulfhydryl reagent present only in the bath would bind. Spandex should extend the strain range over which liposomes release neither of the aqueous tracers, and progressive [spandex] increases should progressively extend the strain range over which spandex-cysteine modification occurs without release of aqueous tracers. Live cell tests of bacteria overexpressing recombinant spandexes could combine cysteine-accessibility assays with viability assays (e.g., (14, 51)).

Engineered spandex proteins might be useful in the context of circulating drug delivery liposomes (52) that encounter transient, potentially lytic osmotic and shear forces.

SUPPORTING MATERIAL

An appendix with four figures is available at http://www.biophysj.org/biophysj/supplemental/S0006-3495(09)01447-7.

This work was funded by grants from the Natural Sciences and Engineering Research Council of Canada to B.J., and from the Heart and Stroke Foundation, Ontario, and the Canadian Institutes of Health Research to C.E.M.

REFERENCES

1. Hamill, O. P. 2006. Twenty odd years of stretch-sensitive channels. *Pflügers Arch. Eur. J. Phys.* 453:333–351.
2. Sukharev, S. I., and A. Anishkin. 2004. Mechanosensitive channels: what can we learn from ''simple'' model systems? *Trends Neurosci.* 27:345–351.
3. Booth, I. R., M. D. Edwards, S. Black, U. Schumann, and S. Miller. 2007. Mechanosensitive channels in bacteria: signs of closure? *Nat. Rev. Microbiol.* 5:431–440.
4. Corry, B., and B. Martinac. 2008. Bacterial mechanosensitive channels: experiment and theory. *Biochim. Biophys. Acta Biomembr.* 1778:1859–1870.
5. Evans, E., V. Heinrich, F. Ludwig, and W. Rawicz. 2003. Dynamic tension spectroscopy and strength of biomembranes. *Biophys. J.* 85: 2342–2350.
6. Sens, P., and M. S. Turner. 2006. Budded membrane microdomains as tension regulators. *Phys. Rev. E.* 73:31918.
7. Morris, C. E. 2002. How did cells get their size? *Anat. Rec.* 268: 239–251.
8. Sukharev, S. I., S. R. Durell, and H. R. Guy. 2001. Structural models of the MscL gating mechanism. *Biophys. J.* 81:917–936.
9. Reference deleted in proof.
10. Häse, C. C., R. F. Minchin, A. Kloda, and B. Martinac. 1997. Cross-linking studies and membrane localization and assembly of radiolabeled large mechanosensitive ion channel (MscL) of *Escherichia coli*. *Biochem. Biophys. Res. Commun.* 232:777–782.
11. Booth, I. R., M. D. Edwards, S. Black, U. Schumann, W. Bartlett, et al. 2007. Physiological analysis of bacterial mechanosensitive channels. *Methods Enzymol.* 428:47–61.
12. Batiza, A. F., M. M. C. Kuo, K. Yoshimura, and C. Kung. 2002. Gating the bacterial mechanosensitive channel MscL in vivo. *Proc. Natl. Acad. Sci. USA.* 99:5643–5648.
13. Perozo, E. 2006. Gating prokaryotic mechanosensitive channels. *Nat. Rev. Mol. Cell Biol.* 7:109–119.
14. Levina, N., S. Tötemeyer, N. R. Stokes, P. Louis, M. A. Jones, et al. 1999. Protection of *Escherichia coli* cells against extreme turgor by

activation of MscS and MscL mechanosensitive channels: identification of genes required for MscS activity. *EMBO J.* 18:1730–1737.

15. Stokes, N. R., H. D. Murray, C. Subramaniam, R. L. Gourse, P. Louis, et al. 2003. A role for mechanosensitive channels in survival of stationary phase: regulation of channel expression by RpoS. *Proc. Natl. Acad. Sci. USA.* 100:15959–15964.
16. Perozo, E., A. Kloda, D. M. Cortes, and B. Martinac. 2002. Physical principles underlying the transduction of bilayer deformation forces during mechanosensitive channel gating. *Nat. Struct. Mol. Biol.* 9: 696–703.
17. Chiang, C. S., A. Anishkin, and S. Sukharev. 2004. Gating of the large mechanosensitive channel in situ: estimation of the spatial scale of the transition from channel population responses. *Biophys. J.* 86: 2846–2861.
18. Hille, B. 1984. Ionic Channels of Excitable Membranes., Vol. 174. Sinauer, Sunderland, MA.
19. Sukharev, S. I. 2002. Purification of the small mechanosensitive channel of *Escherichia coli* (MscS): the subunit structure, conduction, and gating characteristics in liposomes. *Biophys. J.* 83:290–298.
20. Akitake, B., A. Anishkin, N. Liu, and S. I. Sukharev. 2007. Straightening and sequential buckling of the pore-lining helices define the gating cycle of MscS. *Nat. Struct. Mol. Biol.* 14:1141–1149.
21. Jackson, M. B. 2006. Molecular and Cellular Biophysics. Cambridge University Press, Cambridge, UK.
22. Rawicz, W., K. C. Olbrich, T. McIntosh, D. Needham, and E. Evans. 2000. Effect of chain length and unsaturation on elasticity of lipid bilayers. *Biophys. J.* 79:328–339.
23. Beveridge, T. J. 1988. The bacterial surface: general considerations towards design and function. *Can. J. Microbiol.* 34:363–372.
24. Koch, A. L., and S. Woeste. 1992. Elasticity of the sacculus of *Escherichia coli*. *J. Bacteriol.* 174:4811–4819.
25. Pelling, A. E., S. Sehati, E. B. Gralla, J. S. Valentine, and J. K. Gimzewski. 2004. Local nanomechanical motion of the cell wall of *Saccharomyces cerevisiae*. *Science.* 305:1147–1150.
26. Callaway, E. 2008. Cell biology: bacteria's new bones. *Nature.* 451: 124–126.
27. Sukharev, S. I., W. J. Sigurdson, C. Kung, and F. Sachs. 1999. Energetic and spatial parameters for gating of the bacterial large conductance mechanosensitive channel, MscL. *J. Gen. Physiol.* 113: 525–540.
28. Hudspeth, A. J. 2008. Making an effort to listen: mechanical amplification in the ear. *Neuron.* 59:530–545.
29. Mio, K., Y. Kubo, T. Ogura, T. Yamamoto, F. Arisaka, et al. 2008. The motor protein prestin is a bullet-shaped molecule with inner cavities. *J. Biol. Chem.* 283:1137–1145.
30. Adachi, M., and K. H. Iwasa. 1999. Electrically driven motor in the outer hair cell: effect of a mechanical constraint. *Proc. Natl. Acad. Sci. USA.* 96:7244–7249.
31. Zheng, J., W. Shen, D. Z. Z. He, K. B. Long, L. D. Madison, et al. 2000. Prestin is the motor protein of cochlear outer hair cells. *Nature.* 405: 149–155.
32. Lecar, H., and C. E. Morris. 1993. Biophysics of mechanotransduction. *In* Mechanoreception by the Vascular Wall.. Futura Publications, Mount Kisco, NY.
33. Beyder, A., and F. Sachs. 2009. Electromechanical coupling in the membranes of *Shaker*-transfected HEK cells. *Proc. Natl. Acad. Sci. USA.* 106:6626–6631.
34. Laitko, U., and C. E. Morris. 2004. Membrane tension accelerates rate-limiting voltage-dependent activation and slow inactivation steps in a *Shaker* channel. *J. Gen. Physiol.* 123:135–154.
35. Ospeck, M., X. Dong, and K. H. Iwasa. 2003. Limiting frequency of the cochlear amplifier based on electromotility of outer hair cells. *Biophys. J.* 84:739–749.
36. Lamb, T. D., and E. N. Pugh. 2004. Dark adaptation and the retinoid cycle of vision. *Prog. Retin. Eye Res.* 23:307–380.
37. Teller, D. C., T. Okada, C. A. Behnke, K. Palczewski, and R. E. Stenkamp. 2001. Advances in determination of a high-resolution three-dimensional structure of rhodopsin, a model of G-protein-coupled receptors (GPCRs). *Biochemistry.* 40:7761–7772.
38. Marsh, D. 2007. Lateral pressure profile, spontaneous curvature frustration, and the incorporation and conformation of proteins in membranes. *Biophys. J.* 93:3884–3899.
39. Morris, C. E., and P. F. Juranka. 2007. Lipid stress at play: mechanosensitivity of voltage-gated channels. *Curr. Top. Membr.* 59:297–337.
40. Reeves, D., T. Ursell, P. Sens, J. Kondev, and R. Phillips. 2008. Membrane mechanics as a probe of ion-channel gating mechanisms. *Phys. Rev. E.* 78:041901.
41. Wiggins, P., and R. Phillips. 2004. Analytic models for mechanotransduction: gating a mechanosensitive channel. *Proc. Natl. Acad. Sci. USA.* 101:4071–4076.
42. Wiggins, P., and R. Phillips. 2005. Membrane-protein interactions in mechanosensitive channels. *Biophys. J.* 88:880–902.
43. Phillips, R., T. Ursell, P. Wiggins, and P. Sens. 2009. Emerging roles for lipids in shaping membrane-protein function. *Nature.* 459:379–385.
44. Ursell, T., K. C. Huang, E. Peterson, and R. Phillips. 2007. Cooperative gating and spatial organization of membrane proteins through elastic interactions. *PLOS Comput. Biol.* 3:803–812.
45. Sukharev, S. I., and V. S. Markin. 2001. Kinetic model of the bacterial large conductance mechanosensitive channel. *Biologièeskie Membrany.* 18:440–445.
46. Boucher, P. A., B. Joós, M. J. Zuckermann, and L. Fournier. 2007. Pore formation in a lipid bilayer under a tension ramp: modeling the distribution of rupture tensions. *Biophys. J.* 92:4344–4355.
47. Wang, W., S. S. Black, M. D. Edwards, S. Miller, E. L. Morrison, et al. 2008. The structure of an open form of an *E. coli* mechanosensitive channel at 3.45 Å resolution. *Science.* 321:1179–1183.
48. Markin, V. S., and F. Sachs. 2004. Thermodynamics of mechanosensitivity. *Phys. Biol.* 1:110–124.
49. Hamill, O. P., and B. Martinac. 2001. Molecular basis of mechanotransduction in living cells. *Physiol. Rev.* 81:685–740.
50. Besch, S. R., T. Suchyna, and F. Sachs. 2002. High-speed pressure clamp. *Pflügers Arch. Eur. J. Phys.* 445:161–166.
51. Anishkin, A., V. Gendel, N. A. Sharifi, C. S. Chiang, L. Shirinian, et al. 2003. On the conformation of the COOH-terminal domain of the large mechanosensitive channel MscL. *J. Gen. Physiol.* 121:227–244.
52. Zhu, T. F., and J. W. Szostak. 2009. Preparation of large monodisperse vesicles. *PLoS One.* 4:e5009.
53. Powl, A. M., J. M. East, and A. G. Lee. 2008. Anionic phospholipids affect the rate and extent of flux through the mechanosensitive channel of large conductance MscL. *Biochemistry.* 47:4317–4328.
54. Mukhopadhyay, R., K. C. Huang, and N. S. Wingreen. 2008. Lipid localization in bacterial cells through curvature-mediated microphase separation. *Biophys. J.* 95:1034–1049.
55. Norman, C., Z. W. Liu, P. Rigby, A. Raso, Y. Petrov, et al. 2005. Visualization of the mechanosensitive channel of large conductance in bacteria using confocal microscopy. *Eur. Biophys. J.* 34:396–402.
56. Romantsov, T., Z. Guan, and J. M. Wood. 2009. Cardiolipin and the osmotic stress responses of bacteria. *Biochim. Biophys. Acta.* 1788:2092–2100.

Biophysical Journal, Volume 97

Supporting Material

Mechanosensitive closed-closed transitions in large membrane proteins: osmoprotection and tension damping

Pierre-Alexandre Boucher, Catherine E. Morris, and Bela Joos

Appendix A

Model including the stiffness of the proteins

Protein states can be viewed as oscillating about a minimum energy configuration. In this model, each protein can exist in either a contracted (CN) or an expanded (EX) state, and to each state corresponds a particular stiffness which is the curvature of the energy well. The stiffness is a property of the state and is independent of any external factor.

The minima of energy (i.e. the contracted and expanded states) are displaced on the area axis towards larger areas as tension increases (Fig. S1), because of the curved shape of the energy landscape around the energy minima (assumed to be parabolic). The same reasoning applies to the barrier except that since it is a maximum, the displacement upon application of tension is towards smaller areas. In this section, the work by Markin and Sachs [38] is followed.

Sukharev and Markin [35] assume that the transition occurs at the point where the energy parabolas for each state intersect. The position of the barrier thereby becomes linked to the stiffness of the closed and opened states. Although it can be valid as a first approximation, there is no a *priori* reason why the transition should occur at the intersection of the two wells. A barrier state is hence added to the model as a parameter, just like in the model without the stiffness of the states. The stiffness of the barrier, B_*, is also not a function of the stiffness of the contracted state, B_{CN}, nor of the expanded state, B_{EX}.

Modeling the precise energy landscape is not necessary. What are required are the initial positions of the minima and the maximum and the curvature around these points. These values enable the elaboration of a model for a spandex protein incorporating stiffness. Only the difference in energy between the initial state and the barrier for the transition (expansion or contraction) are relevant to the kinetics.

Generalizing Eq. 1, the rate equations are:

$$k_{EX} = k_{0EX} exp\left(-\frac{(E_* - E_{EX})}{k_B T_r}\right)$$
$$k_{CN} = k_{0CN} \exp\left(-\frac{E_* - E_{CN}}{k_B T_r}\right) \quad \text{(S1)}$$

where k_{0EX} and k_{0CN} are taken to be the same and equal to k_0.

Assuming the energy is parabolic around the minima and maximum, the energies of the states and of the barrier are now given by:

$$E_{CN} = \frac{1}{2} B_{CN}(A - A_{CN}^0)^2 - \gamma A$$
$$E_{EX} = E_0 + \frac{1}{2} B_{EX}(A - A_{EX}^0)^2 - \gamma A$$
$$E_* = E_0 + \frac{1}{2} B_{EX}(A - A_{EX}^0)^2 - \gamma A \quad \text{(S2)}$$

where ${A_{CN}}^0$, ${A_{EX}}^0$ and ${A_*}^0$ are the areas associated with each state and E_0 and ${E_*}^0$ are the energies of the expanded and barrier states at zero tension. The states are displaced by the application of tension. A is the area of the protein when oscillating around the energy extrema ${A_{CN}}^0$, ${A_{EX}}^0$ and ${A_*}^0$.

Taking the derivative of these energies as a function of the area, A, to find the area where the energy is a minimum (or a maximum in the case of the barrier) for each state:

$$A_{EX}^{min} = A_{EX}^{0} + \frac{\gamma}{B_{EX}}$$
$$A_{CN}^{min} = A_{CN}^{0} + \frac{\gamma}{B_{CN}}$$
$$A_{*} = A_{*}^{0} - \frac{\gamma}{B_{*}} \quad \text{(S3)}$$

These areas (with the superscript 'min') correspond to the areas of each state when the bilayer is under tension. The change in area between the contracted and expanded states is now given by:

$$\Delta A = A_{EX}^{0} - A_{CN}^{0} - (\frac{1}{B_{CN}} - \frac{1}{B_{EX}})\gamma \quad \text{(S4)}$$

Since the states do not necessarily have the same stiffness, the area change upon expansion is no longer a constant but a function of the bilayer tension, γ. For MscL this could allow for reconciliation of the x-ray structure which predicts an area change of about *20* nm^2 and kinetic models that give an estimate of *6* nm^2 [36].

Replacing the values from Eq. S3 into Eq. S2 to get the energies of the minima and the maximum as a function of tension only, which can then be re-written in terms of energy difference between each state and the barrier:

$$E_{*} - E_{CN} = E_{*}^{0} - (A_{*}^{0} - A_{CN}^{0})\gamma + \frac{\gamma^2}{2}(\frac{1}{B_{*}} + \frac{1}{B_{CN}})$$
$$E_{*} - E_{EX} = E_{*}^{0} - (A_{*}^{0} - A_{EX}^{0})\gamma + \frac{\gamma^2}{2}(\frac{1}{B_{*}} + \frac{1}{B_{EX}}) \quad \text{(S5)}$$

Interestingly, since the energies are second-order functions of the tension, there are mathematically two values for the midpoint, $\gamma_{0.5}$. The midpoint occurs at the tension which allows an equal occupation of the two possible states, that is, when both states have the same energy. However the larger value must be considered unphysical because it occurs when the value of A_{CN} has become larger than the value of A_{EX}. Remember that the minima not only decrease in energy when there is no bilayer tension, but are also displaced towards larger areas and the softer states are displaced towards larger areas faster than the stiffer states. The midpoint is then given by:

$$\gamma_{0.5} = \frac{(A_{CN}^{0} - A_{EX}^{0}) + \sqrt{(A_{EX}^{0} - A_{CN}^{0})^2 - 2\,E_0\left(\frac{1}{B_{EX}} - \frac{1}{B_{CN}}\right)}}{\frac{1}{B_{EX}} - \frac{1}{B_{CN}}} \quad \text{(S6)}$$

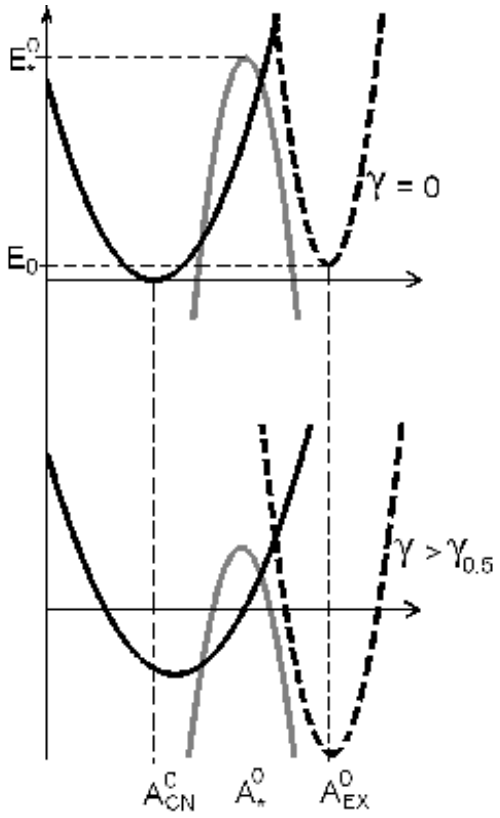

Figure S1 : Energy of the spandex protein as a function of its area, including the stiffness of the states. A: Energy of each state separately: the full line corresponds to the contracted state, the dashed line to the expanded state, the grey line to the barrier. The actual energy landscape is a composition of these three states, but the precise shape of the energy landscape is not important, only the position and height of the maximum and minima as well as the curvature around them are important for the kinetics of transition of the spandex protein. B: Energy of the three states at a tension larger than the midpoint tension. The area of the contracted and expanded states increase and the area of the barrier decreases. However the expanded state moves towards larger areas slower than the contracted state because it is stiffer (i.e. its parabolic shape is more pronounced). E_*^0 is the barrier height, E_0 the energy of the expanded state when there is no bilayer tension, A_{CN}^0, A_*^0 and A_{EX}^0 are the areas of the contracted, expanded and barrier states at zero tension. The zero of energy is set at the energy of the contracted state at zero tension.

By increasing their size, even protein that remain in the contracted state partially relieve bilayer tension. Taking this into account, the expected average tension is:

$$\gamma = K\frac{\Delta a_m}{a_m} + \frac{K\,C_{prot}}{A_{CN}}\left(\left(A_{CN}^0 - A_{EX}^{min}\right)P_{EX} + \left(A_{CN}^0 - A_{CN}^{min}\right)(1 - P_{CN})\right) \quad \text{(S7)}$$

Taking the derivative with respect to time and noting that A_{EX}^{min} and A_{CN}^{min} are functions of the tension γ from Eq. S3, Eq. S7 becomes:

$$\frac{d\gamma}{dt} = K\,\frac{d}{dt}\frac{\Delta a_m}{a_m} + \frac{K\,C_{prot}}{A_{CN}^0}\frac{\left(A_{CN}^0 - A_{EX}^{min}\right)\frac{dP_{EX}}{dt} + \left(A_{CN}^0 - A_{CN}^{min}\right)\frac{dP_{CN}}{dt}}{1 + \frac{K\,C_{prot}}{A_{CN}^0}\left(\frac{P_{EX}}{B_{EX}} + \frac{P_{CN}}{B_{CN}}\right)} \quad \text{(S8)}$$

For clarity, the values of A_{CN}^{min} and A_{EX}^{min} have not been substituted with their values from Eq. S3 (even though they have been taken into account in the derivative). Also, like in the previous section, $\Delta a_m/a_m$ is the strain imposed on the bilayer plus protein system and is independent of any protein properties.

The tension where the time constant is maximum cannot be found analytically in this model, but it can be readily obtained through simulation. Once this $\gamma_{\tau max}$ is obtained the value of τ_{max} can be set by adjusting the values of k_0 and E_*^0 (in Eq. 7).

The model including the stiffness of the protein states is solved numerically in a similar way as the model without the stiffness of the protein states. The parameters used are the same adding just the parameters: B_{CN}, B_{EX} and B_*.

Appendix B

Protein under tension including the stiffness of the proteins

Including the stiffness of the proteins, the probability of being in the contracted (CN) and expanded (EX) states and the time constant are now not only functions of tension but of the stiffness of the states and of the barrier.

The value of B_* was taken to be $5\ k_BT_r$. There are no values in the literature, but the barrier should be stiff so that when it moves to smaller area under the action of tension it does not go below the contracted state area which increases. The stiffness values given by Sukharev and Markin [35] were taken as reference values for B_{CN} and B_{EX}. As above, the value of C_{prot} was set to zero to avoid the effect of protein expansion on tension.

Our model imposes a lower limit on the stiffness of the contracted state. Under biologically relevant tensions, the contracted state must not cross the barrier nor the expanded state. Hence it must be stiff enough to avoid this.

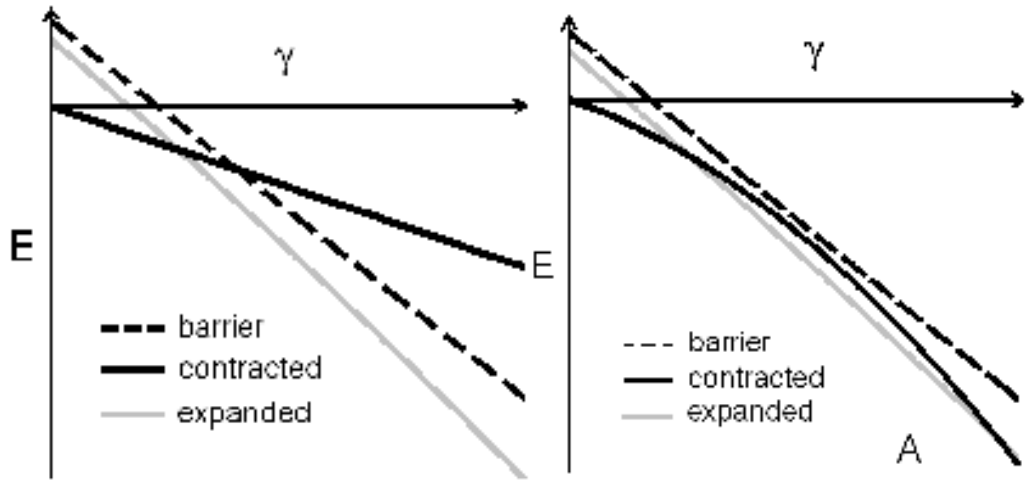

Figure S2 : Varying the stiffness of the contracted state, B_{CN}, and keeping the stiffness of the expanded state, B_{EX}, and of the barrier state, B_*, constant, the energy of the protein is shown as a function of tension, γ for the different protein states. A: The energy of the expanded and contracted states cross twice when the expanded state is stiffer than the contracted state. There are two midpoints, two tensions where the occupancy of the states is *0.5*. B: When the contracted state is stiffer than the expanded state, the energies only intersect once, at the midpoint.

Fig. S2 shows that the energies of the contracted and expanded states will intersect (on the tension scale) once or twice depending on which state is stiffer. Having the energies intersect twice means that there will be two midpoints. This situation is probably unphysical as it results from the assumption that the energy well of a state is parabolic at any tension.

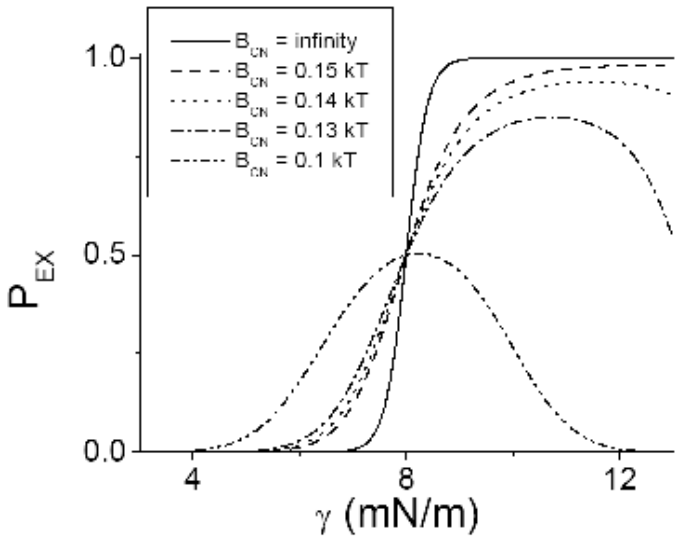

Figure S3 : Changing the stiffness of the contracted state, B_{CN}, changes the probability of being in the expanded state, P_{EX} as a function of bilayer tension,γ. The curve becoming shallower with a smaller B_{CN}, the protein appears to have a smaller expansion upon transition (ΔA). If the contracted state is softer than the expanded state, then it may, at sufficiently high tension, become bigger than the expanded state. This is shown by the curve for P_{EX} curving down with increasing tension. B_{EX} was set to infinity.

As can be seen from Fig. S3 a stiffer contracted state makes the transition less shallow (more abrupt) because as tension increases the expanded states moves to larger areas faster than the contracted state, thus increasing the effective change in area upon expansion (ΔA).

If all the states are very stiff, the model is essentially the same as the model without stiffness as the area difference between the states remains practically constant.

Now if the contracted state is made very stiff and the expanded state soft, as in Fig. S4, the results show a slope at the midpoint giving a larger area change upon expansion than that at zero tension (i.e. the curve in Fig. S4 is steeper for smaller values of B_{EX}). This is because the soft expanded state, upon tension increase, will move towards larger areas faster than the stiff contracted state thus giving a larger spandex area change.

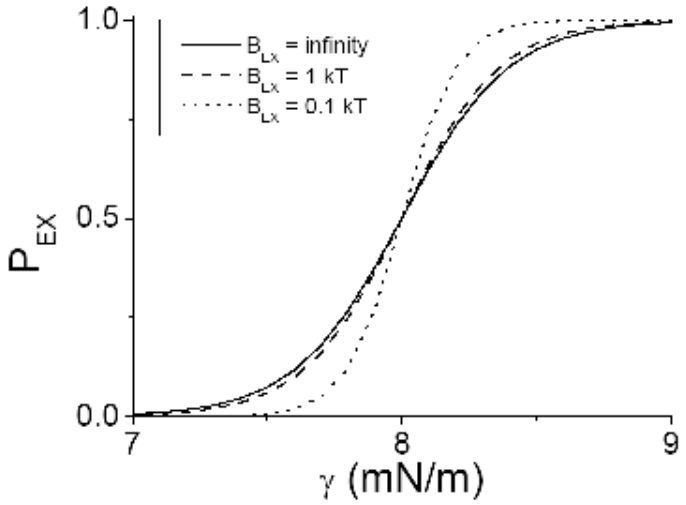

Figure S4: Changing the stiffness of the expanded state, B_{EX}, the probability of being in the expanded state, P_{EX}, varies as a function of bilayer tension. The area of the expanded state increases faster with tension than the area of the contracted state, thus making the curve for P_{EX} steeper, giving the impression of a larger change in area between states than the actual value. B_{EX} was set to infinity.

However, this picture of protein stiffness is not complete. A protein cannot expand indefinitely in the plane of the membrane, there is a maximum beyond which the protein structure would be destroyed or the chemical bonds would break. To correct this, the energies of the states should be calculated in more detail: although the parabolic approximation is accurate close to the zero-tension states, it is probably not valid at larger tensions.

Chapter 3

Introduction to traumatized voltage-gated sodium channels

In the second part of this thesis, including Ch. 3, 4, 5 and 6, we study a different topic than in the first part but also related to bilayer embedded proteins. The first part of this thesis covered interactions between membrane proteins and membrane tension and how proteins expanding in the plane of the membrane could relieve tension. The second part of this thesis studies voltage-gated sodium (Nav) channels, and how changes in their kinetics due to traumatic stress can affect a neuronal system.

In neurons, information is transmitted by the propagation of action potentials: rapid changes in membrane potential. The axon is made of a series of nodes, called nodes of Ranvier, which are excitable, and internodes, which are not excitable and are electrically insulated by a myelin sheath covering them. The myelin does not cover the nodes of Ranvier. Action potentials are transmitted along the neuron's axon by saltatory conduction: the action potential signal is transmitted by passive conduction (much like on a copper wire) in the internodes. Upon reaching a node, the action is regenerated and sent through the next internode. This process ensures both rapid and reliable transmission of action potentials across large distances.

How is the action potential regenerated at nodes of Ranvier? At steady-state, neurons

maintain a high external sodium concentration and a low internal sodium concentration, with a more negative electrical potential inside the neuron. The neuron is then said to be polarized. This concentration gradient is maintained in part by the sodium/potassium pumps: molecular machines which pump out sodium ions and pump in potassium ions. Upon depolarization (a potential change toward more positive potentials) by an incoming axon potential, voltage-gated sodium (Nav) channels located in the node open thus letting sodium in. This influx of sodium further depolarizes the node causing a cascade opening of Nav channels. Nav channels then inactivate (become non-conducting) and the node, after a brief refractory period, returns to its initial steady-state, ready to fire another action potential. This is the basic mechanism for an action potential.

In this second part of the thesis, we study the possible theoretical consequences of changes in the response of Nav channels to potential variations as a result of trauma. By trauma, we mean a physical or mechanical injury to an axon. It could occur, for instance, as a result of a blow to the head which produces strong shear forces on the axons. Experimentally, it is simulated by using pipette aspiration to stretch the cell membrane and cause bleb formation[55]. The presence of bleb is the first histopathological sign of trauma[56]. Whether stretch induced by pipette aspiration properly mimics the type of trauma which causes traumatic brain injuries and diffuse axonal injury has not yet been established. The similarities in the environments make the conjecture very plausible. Nonetheless, our study focuses on the electrophysiological consequences of changes in Nav channel kinetics, leaving aside the clinical aspect.

Wang *et al.*[55] showed that the kinetics of Nav1.6 channels (the voltage-gated sodium channel of adult myelinated axons) expressed in Human Embryonic Kydney (HEK) cells and in *Xenopus* oocytes are modified irreversibly in traumatized membrane patches. The fact that Nav channel kinetics are affected by stretch is not surprising, other channels have already been reported to be stretch sensitive (see e.g., Ref. [37]), but irreversible changes were unexpected. The changes in Nav1.6 kinetics are a displacement of the dependence of both activation and inactivation in the hyperpolarized direction. This is what we call "left-shift". The channel, when its kinetics are left-shifted, becomes active at more hyperpolarized potentials. Even though the channel might very well not have undergone any structural changes, we say, by extension, that a channel is "left-shifted" when its kinetics are left-shifted.

What causes this left-shift is still unknown, it could be that Nav channels are attached to some other cellular structure (e.g., ankyrin) and detachment from this structure causes the left-shift. Such a scenario would result in all channels in a system being either intact or left-shifted, with no intermediate possible. Another possibility is that the environment around Nav channels is disturbed in a continuous manner by trauma, causing all the channels to left-shift together in arbitrarily small steps. These ideas are further explored in Ch. 4 where we suggest experimental protocols yielding maximally useful data and more precisely, experimental protocols to test the mechanism of left-shift.

Whether Nav channels in native systems also become left-shifted is unknown. Experiments to establish this are especially difficult to perform (M. Martina, G. Mealing, C.E. Morris, unpublished observations). Modeling can then be useful to predict the behavior of systems (i.e., nodes of Ranvier) with left-shifted Nav channels. In Ch. 5 we explore the stability and firing patterns of systems with left-shifted Nav channels. We also explore whether left-shifted Nav channels could cause the degradation of the ion gradients necessary for normal cell function.

Left-shifted kinetics of Nav channels could also play a role in neuropathic pain, by contributing in the generation of ectopic action potentials. It has been shown experimentally that subthreshold oscillations, membrane potential oscillations below the threshold for action potential firing, are linked to neuropathic pain. In Ch. 6, we lay the basis for a theoretical study of subthreshold oscillations.

Before these studies and accompanying results are presented, we present an overview of the subject.

3.1 Nav Channel Structure

This section, based on the works by Catterall[57], Yu[58] and Hille[30], presents a very brief overview of basic voltage-gated sodium channel structural features.

Voltage-gated sodium (Nav) channels are transmembrane membrane proteins which can selectively permeate sodium channels. Upon membrane depolarization Nav channels open and inactivate within a few milliseconds. The three key features of Nav channels are: ion selectivity, voltage-gated opening and fast inactivation. The complete three-dimensional

structure of Nav channels has not yet been resolved, but electrophysiological and biochemical experiments have provided insight into their structural properties.

Nav channels are composed of a complex of one large α subunit and possibly one or more smaller β subunits; the subunits are separate proteins which assemble to form the larger complex. All the essential elements (ion pore, selectivity filter, fast inactivation, voltage-sensors) are contained in the α subunit; it basically is the sodium channel. β subunits modify the kinetic properties of the α subunit (i.e., modify opening and closing), but are not essential for channel function. β subunits are not of central interest in this work and we will not discuss them further. The basic structure of a sodium channel (an α subunit) is shown in Fig. 3.1.

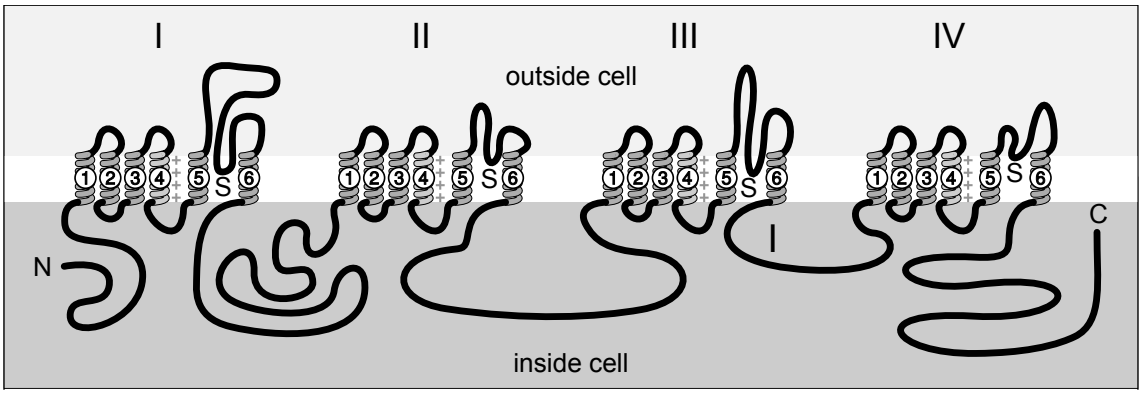

Figure 3.1 Schematic representation of a Nav channel α subunit. This schematics represents the protein partially unfolded: the protein sequence, starting from the N-terminal is arranged so that all transmembrane units (circled 1 to 4 of each domain I-IV) are on the same line. The complete folded structure of a Nav channel is not known, but the four domains arrange as in Fig. 3.2 to form the channel. The S4 helices (shown with + to represent positive charges) act as voltage-sensors. The reentrant loops forming the selectivity filter (the pore region) are identified with an S, and the inactivation gate (the part of the protein which blocks the open pore) with an I. The N- and C-terminal (the ends of the protein) are also shown. Modified from [59].

Nine α subunits have been identified (Nav1.1-Nav1.9), all sharing some basic structural properties. Their α subunit are composed of a single protein which, when folded, forms four similar domains (I-IV), each of them being composed of 6 transmembrane helices (S1-S6). The S4 helix of each domain, containing positive charges, acts as the voltage sensor: upon depolarization, their outward (i.e., towards the exterior of the cell) movement triggers a conformation change which opens the pore region.

The S5 and S6 helices of each domain are connected by a reentrant loop: the loop connects both extracellular ends of S5 and S6, but a part of the loop passes inside the membrane. These four loops (one from each domain) form a structure at the extracellular end of the pore which acts as a selectivity filter which only lets sodium ions through.

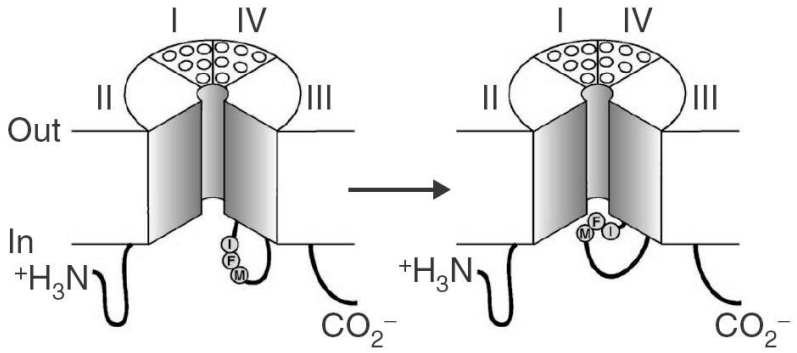

Figure 3.2 Cartoon depicting the folded Nav channel with the IFM segment of the inactivation gate moving to obstruct the pore of a Nav channel. The transmembrane helices (S1 to S6) are shown as circles in domains I and IV (and omitted for domains II and III for clarity). Reproduced under BioMed Central copyright and license agreement from [58].

Inactivation of the channel is controlled by a cytoplasmic segment linking domains III and IV which, within milliseconds of channel opening, moves in a position to occlude the pore (see Fig.3.2). Inactivation depends on the presence of three hydrophobic amino acids (isoleucine, phenylalanine and methionine; IFM) in the inactivation gate. Interestingly, if the inactivation gate is mutated so as to be unable to perform its function, peptides containing this motif may act as inactivation gates[60].

3.1.1 More on Nav channels

Knowing the structure of Nav channels is not enough to understand their complete behavior, even less so that of excitable membranes. Nav channels are voltage-gated: they change conformation in response to changes in membrane potential. They are also highly specific, only sodium ions can go through these channels.

At the resting potential (~ -60 mV), Nav channels are mainly non-conducting. They however have this feature of "window" currents (sometimes called "persistent" currents[61]): their open probability at the resting potential is non-zero, so monitoring a patch with a few channels will reveal a flickering conductance[62].

Depolarization causes the S4 helices, which act as voltage sensors (see Fig. 3.1) to move up in the bilayer (i.e., activate), causing the channel to change conformation and to open a sodium-selective pore. Note that in normal conditions the external Na concentration is high (with a reversal potential $\sim +50$ mV) so sodium ions will flow towards the inside, thus further depolarizing the membrane, further opening Nav channels. This positive feedback mechanism provides the basis for action potential generation, which we will review in the next section.

Nav channels do not remain open if potential is kept depolarized: they inactivate after a brief period. Opening of the channel favors the binding of the inactivation particle (the IFM segment, see Fig. 3.2) to the pore region, thus blocking the pore and rendering the channel silent (i.e., non-conduction) even though it is still "open". If the membrane is then repolarized, the voltage sensors will return to their original positions (i.e., de-activate). This lowers the affinity of the inactivation particle to the pore region which unbinds from the pore, enabling a subsequent pore opening.

Nav channels can be blocked by certain drugs. Tetrodotoxin (TTX) (the blowfish toxin) is probably the most widely used in laboratories as it selectively binds to the pore region of Nav channels rendering them silent. When an event is reported to be "TTX-sensitive" (e.g., the rise in axonal calcium after stretch injury[63]) it means that Nav channels are involved in the event in some way.

3.2 The Hodgkin-Huxley model

The Hodgkin-Huxley (HH) model[64] describes the permeability changes and action potential generation in an active membrane. Although it does not describe the underlying molecular mechanism, the HH model provides a useful tool for predicting the electrical response of an active membrane. We will here follow the description of the model given by Hille[30] and Gerstner and Kistler[65] albeit in a more "physicist-friendly" way.

A few notions are required to understand the HH model: reversal potential and resting potential. Reversal potential of ion species X, E_X, is the potential difference between the inside and outside of the cell necessary to stop ion flow through an open permeation pathway. It is linked to ion concentration by:

$$E_X = \frac{RT}{zF} \ln\left(\frac{[X]_o}{[X]_i}\right), \tag{3.1}$$

where R is the ideal gas constant, T temperature, z the valence of ion X, F is the Faraday constant and $[X]_o$ and $[X]_i$ the exterior and interior concentrations of ion X. Reversal potentials used in the HH model are given in table 3.1. For a derivation of the equation see Annexe A.

Resting potential is simply the steady-state potential of a system. For a neuron it is typically around ~ -50 to ~ -80 mV. Polarized is used to mean negative potential inside the cell compared to the exterior. Similarly, depolarized means the interior of the cell is more positive than its resting potential. Positive ions flowing from the exterior to the interior of a cell depolarize it.

The HH model essentially considers the membrane as an electrical circuit (see Fig. 3.3): changes in membrane potential (the potential difference on either side of the bilayer membrane) are caused by currents flowing through the membrane. Such currents are divided in three parts: the sodium current (I_{Na}), the potassium current (I_K) and the background (or leak) currents (I_{leak}). Note that the HH model does not consider propagation of action potentials along an axon, it rather considers the change in potential of a unit area of axonal membrane. It can be (and has) adapted to model propagation of action potentials in axons. Also note that in the HH model, currents are given per unit area ($\mu\mathrm{A/cm}^2$), the same applies for conductances ($\mathrm{mS/cm}^2$) and capacitance ($\mu\mathrm{F/cm}^2$) (see table 3.1).

Considering the time-derivative of the well-known capacitor equation ($CV = Q$), the main equation of the HH model is:

$$-C_m \frac{dV_m}{dt} = \sum_i I_i = I_{Na} + I_K + I_{leak}, \tag{3.2}$$

where C_m and V_m are the membrane capacitance and potential respectively (and the $-$ sign accounts for the sign convention used for currents: positive ions flowing towards the inside entail a negative current).

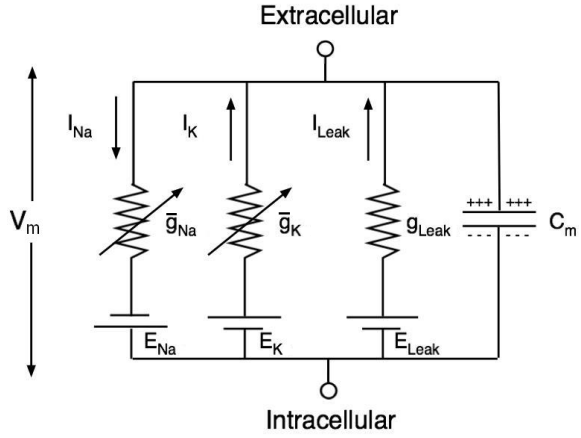

Figure 3.3 Equivalent electrical circuit for the HH model. Positive current is taken such that an influx of positive charges depolarizes the membrane. At rest, membrane potential (V_m) is about -60 mV. The sodium and potassium conductances are shown with an arrow to indicate that they are variable, whereas g_{leak} is constant. $\bar{g}_{Na} = m^3 h g_{Na}$ and $\bar{g}_K = n^4 g_K$ (variables are defined in the text).

3.2.1 Leak current

The leak current is assumed to be ohmic and to have a fixed conductance:

$$I_{leak} = g_{leak}(V_m - E_{leak}), \tag{3.3}$$

where g_{leak} is the leak conductance and E_{leak} is the leak reversal potential such that $(V_m - E_{leak})$ is the driving force for the leak current. g_{leak} does not change with time nor with potential, it is a fixed conductance and is not associated with sodium or potassium. It is due to the permeability of the membrane to ions; it is easy to describe as it behaves exactly like a common resistor would (except that it does not reverse at 0 mV).

3.2.2 Potassium current

The potassium current (I_K) is slightly more complex to describe. Upon depolarization (V_m going toward more positive values), potassium conductance increases before saturating at a steady-state value, then when the membrane is repolarized it decreases exponentially (always with the steady-state values being function of membrane potential; see Fig. 3.4). Such a mechanism can be modeled by assuming that potassium channel opening is controlled by four separate (and identical) "particles" which all need to be in the correct position for ions

to permeate through the channel. Taking the probability for a "particle" to be in the open conformation to be n, the probability of the channel being open (all "particles" in the correct position) is given by n^4. The potassium current is then written:

$$I_K = n^4 g_K (V_m - E_K), \tag{3.4}$$

where g_K is the maximal value of the potassium conductance (such that $n^4 g_K$ gives the conductance) and E_K is the potassium reversal potential. Assuming the transition between closed and open conformation for each "particle" to be first-order we have:

$$\frac{dn}{dt} = \alpha_n (1 - n) - \beta_n n, \tag{3.5}$$

where α_n and β_n are voltage-dependent transition rates obtained from experimental results and are given by:

$$\alpha_n = \frac{0.01(V_m + 55)}{1 - \exp\left(-(V_m + 55)/10\right)}, \tag{3.6}$$

$$\beta_n = 0.125 \exp\left(-V_m/80\right). \tag{3.7}$$

In Eqs. 3.6 and 3.7, V_m is expressed in units of mV and α_n and β_n in units of $(\text{ms})^{-1}$. Eq. 3.5 can also we written in a different form:

$$\frac{dn}{dt} = \frac{n_\infty - n}{\tau_n}, \tag{3.8}$$

where n_∞ is the steady-state value of n and τ_n is the time constant of the change of n. n_∞, τ_n are related to α_n and β_n through:

$$n_\infty = \frac{\alpha_n}{\alpha_n + \beta_n}, \tag{3.9}$$

$$\tau_n = \frac{1}{\alpha_n + \beta_n}. \tag{3.10}$$

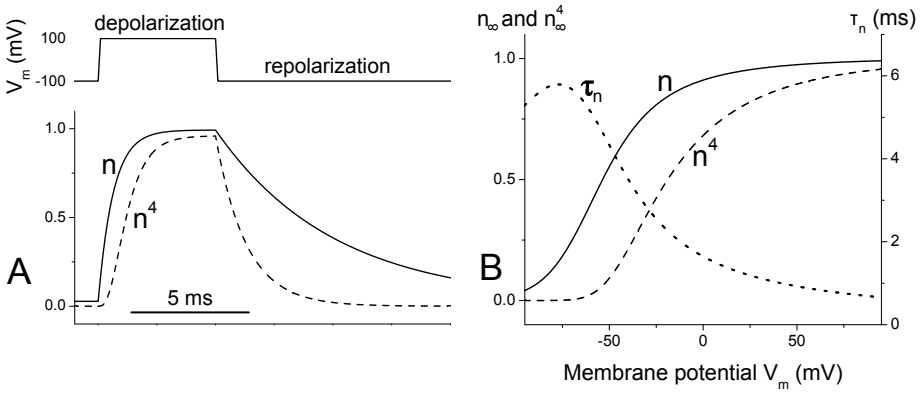

Figure 3.4 A. n and n^4 during a depolarizing and a repolarizing steps (from -100 to 100 to -100 mV). B. Steady-state open probability (n_∞ and n_∞^4) and time constant (τ_n) as functions of membrane potential (V_m). Voltage-gated potassium channels open when depolarized and close when repolarized as their opening is controlled by n^4. Upon step depolarization, they open slower than sodium channels, which is important for action potentials to occur. Generated using the values in table 3.1.

3.2.3 Sodium current

The sodium current, I_{Na}, results from the activity of voltage-gated sodium (Nav) channels (introduced in the previous section). The behavior of I_{Na} is slightly different from I_K: upon depolarization I_{Na} rapidly increases before decaying exponentially. When repolarized, no further current is elicited. Hodgkin and Huxley[64] modeled this behavior using again four "particles", but of two different types, which must all be in the "open" conformation for current to pass. The first type of "particle", the m "particle", is in the closed conformation when polarized and opens upon depolarization. The second type of "particle", the h "particle", is in the open conformation when polarized and closes upon depolarization (see Fig. 3.5). In a sodium channel, there are 3 m "particles" and 1 h "particle" such that the probability of the channel being open is given by m^3h. The process of the m "particles" moving into the open conformation in a sodium channel is called activation (m^3) and the process whereby the h "particles" moves into the closed position is called inactivation. The sodium current is then written:

$$I_{Na} = m^3 h g_{Na}(V_m - E_{Na}), \tag{3.11}$$

where g_{Na} is the maximal sodium conductance and E_{Na} is the sodium reversal potential. Eq. 3.11 assumes that an open channel conducts current in an ohmic fashion. In the HH

model activation and inactivation are taken to be completely independent processes: there is no interaction between m and h.

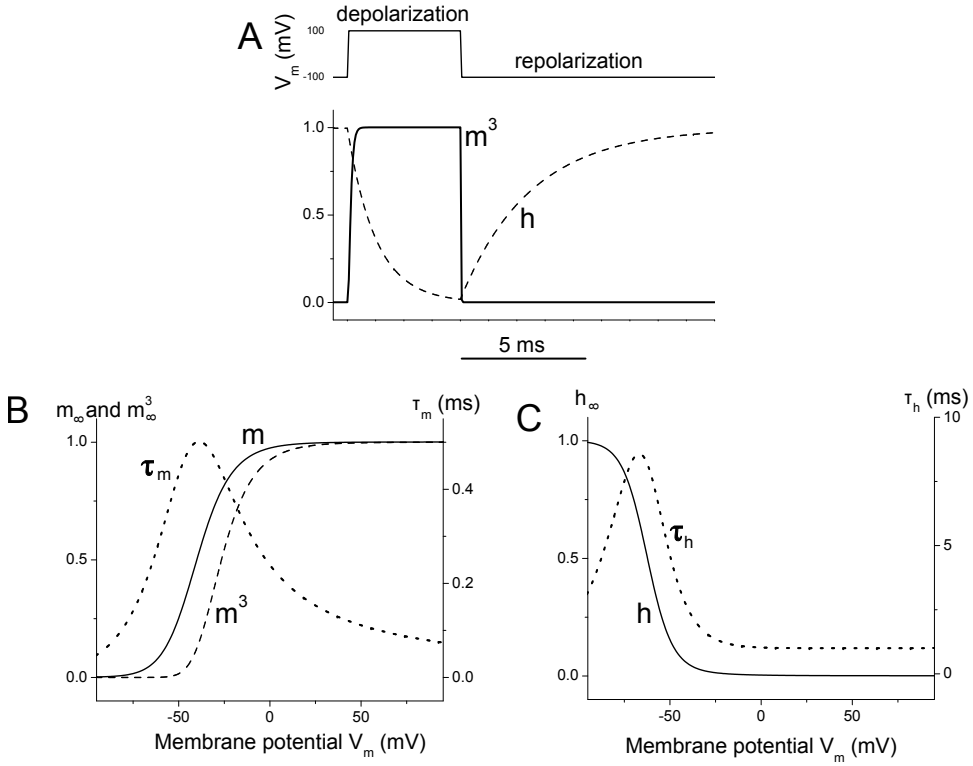

Figure 3.5 A. Response of the m and h "particles" upon depolarization and repolarization (from -100 to 100 to -100 mV). The m "particle" is faster than the h "particles". B. and C. Steady-state values of m and h and their time constants. Note the different time scales used in B and C. Generated using the values in table 3.1.

As for the n "particle", the transition of m and h are assumed to be first-order:

$$\frac{dm}{dt} = \alpha_m(1-m) - \beta_m m, \tag{3.12}$$

$$\frac{dh}{dt} = \alpha_n(1-h) - \beta_h h, \tag{3.13}$$

where α_m and β_m are the transition rates of the m units and α_h and β_h are the transition rates of the h unit. The rates are given by:

$$\alpha_m = \frac{0.1(V_m + 40)}{1 - \exp\left(-(V_m + 40)/10\right)}, \tag{3.14}$$

$$\beta_m = 4\exp\left(-(V_m + 65)/18\right), \tag{3.15}$$

$$\alpha_h = 0.07\exp\left(-(V_m + 65)/20\right), \tag{3.16}$$

$$\beta_h = \frac{1}{1 + \exp\left(-(V_m + 35)/10\right)}. \tag{3.17}$$

Again these equations use V_m in units of mV and the rates in units of $(\text{ms})^{-1}$. Similarly to Eq. 3.8, Eqs. 3.12 and 3.13 can be rewritten using the steady-state values (m_∞ and h_∞) and the time constants (τ_m and τ_h):

$$\frac{dm}{dt} = \frac{m_\infty - m}{\tau_m}, \tag{3.18}$$

$$\frac{dh}{dt} = \frac{h_\infty - h}{\tau_h}. \tag{3.19}$$

m_∞, τ_m, h_∞ and τ_h are related to α_m, β_m, α_h and β_h through:

$$m_\infty = \frac{\alpha_m}{\alpha_m + \beta_m}, \tag{3.20}$$

$$\tau_m = \frac{1}{\alpha_m + \beta_m}, \tag{3.21}$$

$$h_\infty = \frac{\alpha_h}{\alpha_h + \beta_h}, \tag{3.22}$$

$$\tau_h = \frac{1}{\alpha_h + \beta_h}. \tag{3.23}$$

3.2.4 Window currents

Emerging from the transient sodium current are window currents. Such currents are the result of the overlapping activation (m_∞^3) and inactivation (h_∞) curves. For a certain range of potentials, the channels have a non-zero steady-state open probability. Window currents do not require additional modeling as they are intrinsically the same currents as the transient currents: window currents naturally emerge from transient currents and could have been named "steady-state transient currents".

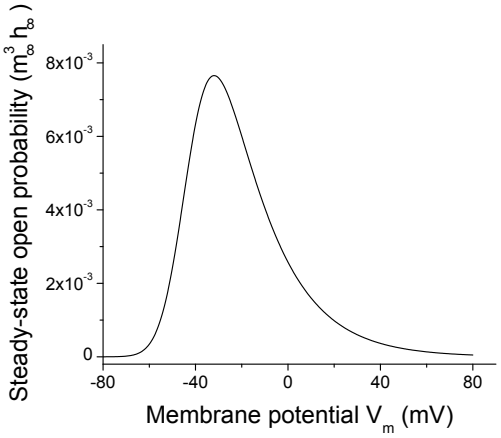

Figure 3.6 Steady-state open probability ($m_\infty^3 h_\infty$) in the HH model gives rise to window currents due to a non-zero steady-state conductance.

Table 3.1 Hodgkin-Huxley Model Parameters

Membrane capacitance	C	=	1	μF/cm^2
Transient Na conductance	g_{Na}	=	120	mS/cm^2
Transient K conductance	g_K	=	36	mS/cm^2
Leak conductance	g_{leak}	=	0.3	mS/cm^2
Na reversal potential	E_{Na}	=	50	mV
K reversal potential	E_K	=	-77	mV
Leak reversal potential	E_{leak}	=	-54.4	mV

The steady-state open probability is given by $m_\infty^3 h_\infty$ and the window conductance by $g_{Na} m_\infty^3 h_\infty$, so in essence, Fig. 3.6 presents a scaled version of window conductance. Steady-state open probability is centered at about -30 mV and extends from ~ -60 to ~ 40 mV; with a maximal open probability of 0.008 (see Fig. 3.6).

3.2.5 Complete model

The main equation (Eq. 3.2) can now be rewritten to include the parameters described above:

$$-C_m \frac{dV_m}{dt} = m^3 h g_{Na}(V_m - E_{Na}) + n^4 g_K (V_m - E_K) + g_{leak}(V_m - E_{leak}) + I_{stim}, \quad (3.24)$$

where a term, I_{stim}, was added to Eq. 3.24 to simulate stimulating current. It can be used to simulate any shape of stimulus in order to study the response of the model membrane.

The variables n, m and h encompass all the channel properties (i.e., the time dependence and the voltage dependence). They vary according to Eqs. 3.9, 3.12 and 3.13 to imitate the permeability variation of active membrane (due to voltage-gated channels) to changes in membrane potential.

3.2.6 Action Potentials

The remaining part of this discussion uses the parameters found in table 3.1. The parameters used in the HH model can be modified to better model different situations. A particular system could, for example, have more sodium channels, and hence g_{Na} would be larger. Another system could have different internal and external ion concentrations, and E_{Na} and E_K would be different.

If the system as described above, using parameters in table 3.1, is subjected to a 1 ms depolarizing pulse (I_{stim}), either of two scenarios can occur. 1) If the pulse is of weak amplitude, the potential increases during the pulse and, once the pulse stops, the system returns to its original state. 2) If the pulse is strong enough, the ensuing depolarization opens enough sodium channels (i.e., m increases) to generate a positive feedback through which the system depolarizes until sodium channels inactivate(h decreases), stopping depolarizing sodium currents. Potassium channels finally open (n increases) increasing polarizing currents. This is an action potential (see Fig. 3.7).

The whole process of action potential relies on the different time constant of the processes: sodium channel opening (m) has to be faster than both sodium channel inactivation (h) and potassium channel opening (n) (see the time constants of m, h and n in Fig. 3.4 and 3.5). If, say, inactivation was faster than channel opening, action potentials would not occur as sodium channels would inactivate before opening (or as soon as they opened, preventing depolarization).

The refractory period is the period of time after an action potential when another action potential cannot be elicited. One feature of the HH model is its ability to reproduce the refractory period of an active membrane. If a second stimulating pulse (with the same amplitude) follows the first one, a second action potential may not be elicited, depending

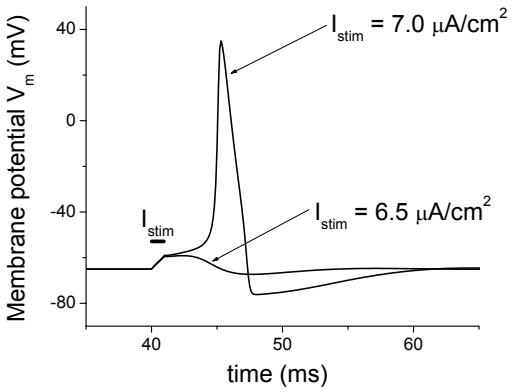

Figure 3.7 Membrane potential response to a 1 ms depolarizing pulse (I_{stim}). The response varies with the pulse amplitude: a subthreshold pulse ($I_{stim} = 6.5$ μA/cm^2) generates a tonic response which dissipates rapidly after the pulse ends. A suprathreshold pulse ($I_{stim} = 7.0$ μA/cm^2) generates a positive feedback response: an action potential. The black line shows the duration of the pulse (1 ms).

on the time interval between the pulses. Immediately after an action potential, the channels must recuperate from inactivation: the slow h "particle" must return to its steady-state value (see Fig. 3.5). Inactivated channels cannot contribute to the depolarizing current needed for the action potential. Additionally, there is an excess of open potassium channels (compared to resting state); this excess of open K channels must be allowed to close before an action potential can be elicited with the same pulse amplitude. A stronger pulse could generate an action potential during the refractory period. For the values used here, the refractory period is about 20 ms (see Fig. 3.8).

If instead of stimulating in a pulse fashion, the stimulus is continuous, then the system responds in different ways depending on the stimulating current. A weak continuous stimulation initiates a single action potential followed by a series of subthreshold oscillations before the system relaxes to a new slightly depolarized steady-state. A strong enough continuous stimulation causes repetitive action potentials (see Fig.3.9).

In nonlinear dynamics terms, such a repetitive firing pattern is considered a stable limit cycle: for any set of starting V_m, m, h and n the system will eventually (after a long enough period of time) settle in this repetitive firing behavior. To each value of I_{stim} corresponds a limit cycle with a precise amplitude of V_m oscillations. A deeper nonlinear dynamics study of the HH model is however outside the scope of this work (see e.g., [66] and references

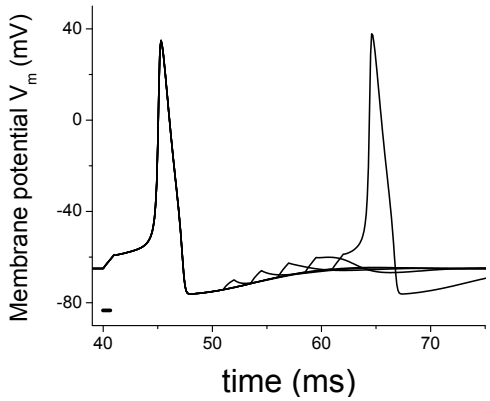

Figure 3.8 A stimulating pulse (applied at 40 ms) generates an action potential response, a second pulse is applied 10, 12.5, 15, 17.5 and 20 ms after the first one. Only the pulse applied after 20 ms elicits a second action potential: the refractory period of the system is ~ 20 ms.

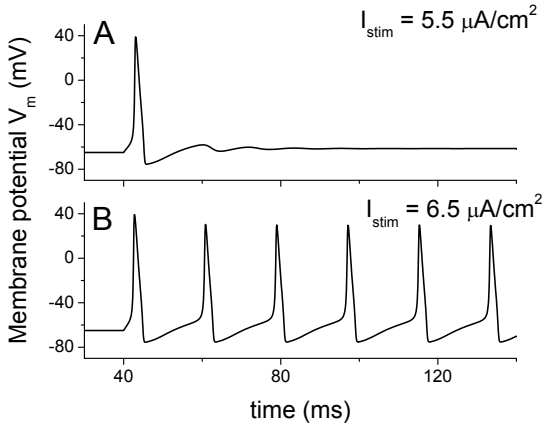

Figure 3.9 A. A weak stimulating current ($5.5\ \mu\mathrm{A/cm}^2$) generates a single action potential followed by a few subthreshold oscillations. B. A stronger stimulating current ($6.5\ \mu\mathrm{A/cm}^2$) causes the system to enter a repetitive firing mode. In both figures, stimulation begins at 40 ms.

therein for more on the topic).

3.3 Gating Charge

It this section we do not consider inactivation as it results from a different process than activation (i.e., the binding of the inactivation particle to the pore region). Activation is the movement of the voltage sensors which causes the opening of the pore region; it corresponds

to the three m "particles" of the HH model. Activation, and its counterpart "deactivation", entail a net movement of charges inside the channel. The calculation presented here is a simplistic calculation as it assumes that all the charges involved in gating move from the bottom of the membrane to the top. This may not be the case; a large number of charges may be involved in the gating process, all of which moving across different distances in the membrane. What we calculate here is a resulting net charge.

The gating charge, or the charge movement, of an opening voltage-gated channel can be estimated using equilibrium thermodynamics[64]. At equilibrium the ratio of occupancy of two states (P_{open} and P_{closed}) is given by the Boltzmann distribution:

$$\frac{P_{open}}{P_{closed}} = \exp\left(\frac{-\Delta E}{kT}\right), \tag{3.25}$$

where ΔE is the energy difference between the open and closed states. This energy difference can be separated into two parts: 1) the intrinsic energy difference between the closed and open conformations E_0 and 2) the displacement of electrical charges across a potential difference:

$$\Delta E = E_0 - zeV_m, \tag{3.26}$$

where z is the number of elementary charges (e) that move across the potential difference V_m (i.e., z is the gating charge). Combining Eq. 3.25 and 3.26 yields:

$$\frac{P_{open}}{P_{closed}} = \exp\left(-\frac{E_0 - zeV_m}{kT}\right). \tag{3.27}$$

Assuming $P_{open} + P_{closed} = 1$ the open probability is then given by:

$$P_{open} = \frac{1}{1 + \exp\left((E_0 - zeV_m)/kT\right)}. \tag{3.28}$$

Hence the gating charge determines the slope of P_{open} with respect to membrane potential (see Fig. 3.10). Moreover, by setting Eq. 3.26 equal to zero, the open probability midpoint can be found to be a combination of E_0 and z through: $V_{0.5} = E_0/ze$.

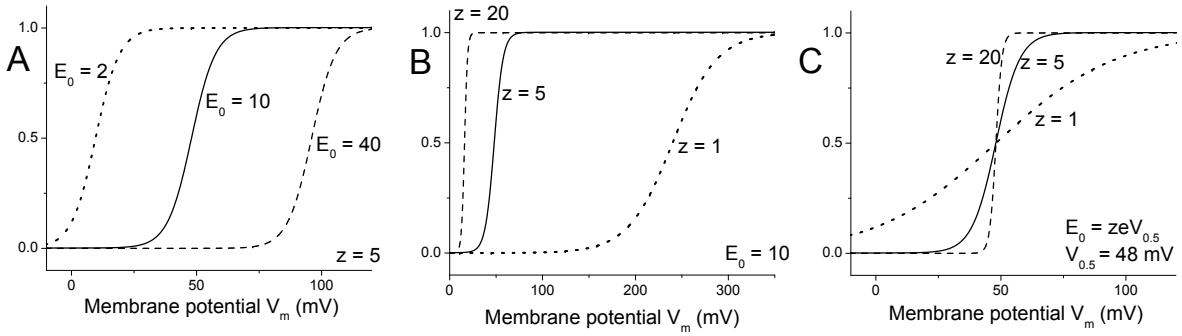

Figure 3.10 Channel open probability (P_{open}) for different values of the gating charge (z) and the intrinsic energy difference between states (E_0). A. $z = 5$ with three different values of E_0 showing how changing E_0 left- or right- shifts channel activation. B. Changing the gating charge changes both the activation midpoint and the slope of activation. C. Keeping the midpoint constant by adjusting E_0 clearly shows the effect of the gating charge on the activation slope. Values used here (including the membrane potential range) are arbitrarily selected to maximally show the effect of parameter changes.

Note that a change in gating charge cannot account for the left-shift of activation in Nav1.6 channels detected by Wang *et al.*[55] as a change in gating charge not only entails a shift in the midpoint of the activation(V) (m^3), but also changes its slope. No such change in slope of activation(V) has been detected. Only a change in E_0 can account for the left-shift observed.

This gating charge model is quite simplistic as it assumes that every charge moves across the whole potential difference V_m. This is most likely not the case in voltage-gated channels as complex structural changes undergone upon gating are bound to move different parts of the channel by different distances. It is likely that more charges than the number calculated using these equations are involved in voltage-sensing. Yet, simplistic as it is, this calculation remains useful as it gives some insight into the structural changes (i.e., charge displacement) involved in channel gating.

This model also has another interesting consequence: if E_0 changes, the activation midpoint, $V_{0.5}$, also changes (without changing the slope of the activation(V) curve). Elaborating the model, E_0 could be composed of different parts, one of them being the interaction between the channel and the lipid bilayer. Changing e.g., lipid composition, membrane tension or curvature would change the energetics of each channel state and thus modify E_0, which also means right- or left- shifting the activation(V) curve of a channel.

3.4 Schwarz Model

In this section we review the model of a firing node of Ranvier in the human peripheral nervous system by Schwarz *et al.*[67] and the main results of this model. Nerves from excess graft material (and from an amputated left arm) were used to measure current at human nodes of Ranvier in 11 fibres.

The procedure to measure current involves dissecting axons and mounting them in a measurement chamber, a process which might easily traumatize axons. In fact, 8 fibres (of 19 total) were identified as damaged because of their smaller current amplitude and axoplasmic sodium accumulation. Whether all the axons used were partially traumatized is a distinct possibility given the difficulty of the experiment.

Currents were measured using a nodal voltage-clamp technique[68]. The results show a large Na transient current, a rapid and a slow K current and an unspecified nonspecific leak current (assumed to be linear with potential). Interestingly the K current only marginally contributes to the action potential repolarization phase, the leak current primarily taking up that role. The slow K current however stops repetitive action potential trains after just a few action potentials.

The model, based on HH formulation, reproduces experimental data for human nodes of Ranvier. The basic equation relating current and potential is:

$$\frac{dV_m}{dt} = -\frac{I_{total} + I_{stim}}{C_{nodal}}, \tag{3.29}$$

where V_m is the transmembrane potential, I_{stim} is the stimulating current (if applicable) and C_{nodal} is the nodal membrane capacitance. I_{total}, the total membrane current, is given by:

$$I_{total} = I_{Na} + I_{Kf} + I_{Ks} + I_{leak}, \tag{3.30}$$

where I_{Na}, I_{Kf}, I_{Ks} and I_{leak} are the sodium, fast potassium, slow potassium and leakage currents respectively and are given by:

Table 3.2 Schwarz model parameters

Nodal membrane capacitance	C_{nodal}	=	1.4	pF
Na Permeability	P_{Na}	=	3.52×10^{-9}	$\mathrm{cm^3 s^{-1}}$
Fast K conductance	g_{Kf}	=	15	nS
Slow K conductance	g_{Ks}	=	30	nS
Leak conductance	g_{leak}	=	30	nS
External Na concentration	$[\mathrm{Na}]_o$	=	154	mM
Internal Na concentration	$[\mathrm{Na}]_i$	=	35	mM
K reversal potential	E_K	=	-84	mV
Leak reversal potential	E_{leak}	=	-84	mV
Resting potential	$E_{resting}$	=	-84	mV

$$I_{Na} = m^3 h P_{Na} \frac{V_m F^2}{RT} \left(\frac{[Na]_o - [Na]_i \exp(V_m F/RT)}{1 - \exp(V_m F/RT)} \right), \tag{3.31}$$

$$I_{Kf} = n^4 g_{Kf} (V_m - E_K), \tag{3.32}$$

$$I_{Ks} = s g_{Ks} (V_m - E_K), \tag{3.33}$$

$$I_{leak} = g_{leak} (V_m - E_{leak}), \tag{3.34}$$

where F is Faraday's constant, R the perfect gas constant, T temperature, E_K the potassium reversal potential and E_{leak} the leak reversal potential. m, h and n are the HH-type "particles", and s is a similar "particle" controlling the activation of slow potassium currents (for the model parameters, see table 3.2). Note the different formulation for I_{Na} than what is used in the HH model (Eq. 3.11). The formulation here is the Goldman-Hodgkin-Katz formulation[69, 70] and is an improvement upon the other formulation as it includes rectification: current is not a strictly linear function of potential, but deviates from linearity at potentials close to the reversal potential.

The rate of change of the m, h, n and s "particles" take the form:

$$\frac{dx}{dt} = \alpha_x (1 - x) - \beta_x x, \tag{3.35}$$

where x can be m, h, n or s. Note that this equation is incorrectly written in the article[67] where it is given with $+\beta_x x$. The transition rates α and β for each "particle" take the form:

Table 3.3 Schwarz model - transition rates

Rate constant	A $(\text{ms})^{-1}\ (\text{mV})^{-1}$	B (mV)	C (mV)
α_m	1.86	-18.4	10.3
β_m	0.0860	-22.7	9.16
α_h	0.0336	-111.0	11.0
β_h	2.30	-28.8	13.4
α_n	0.00798	-93.2	1.10
β_n	0.0142	-76.0	10.5
α_s	0.00122	-12.5	23.6
β_s	0.000739	-80.1	21.8

$$\alpha_m, \alpha_n, \alpha_s = \frac{A(V_m - B)}{1 - \exp[(B - V_m)/C]}, \tag{3.36}$$

$$\alpha_h, \beta_m, \beta_n, \beta_s = \frac{A(B - V_m)}{1 - \exp[(V_m - B)/C]}, \tag{3.37}$$

$$\beta_h = \frac{A}{1 + \exp[(B - V_m)/C]}. \tag{3.38}$$

The corresponding parameters (A, B and C) at 20 °C are given in table 3.3. Note that the A parameter corresponding to β_h has units of $(\text{ms})^{-1}$ (not $(\text{ms})^{-1}\ (\text{mV})^{-1}$). Other parameters of the model are given in table 3.2.

When subjected to a constant stimulating current (0.9 nA is used here, see Fig. 3.11), the model has an initial spike followed by a smaller peak and then peaks of decreasing amplitude. The two main differences with the HH model are 1) repolarization here is mainly carried by the leak conductance, and 2) the slow K conductance gradually (over the course of a few action potentials) increases the repolarizing current, thus reducing action potential peak amplitude. In effect, the slow K conductance prevents the system from repetitively firing over a prolonged period.

When the slow K conductance is removed (i.e., $g_{Ks} = 0$ nS), the system has a repetitive firing mode, with the first action potentials being larger, and then all the following being identical (see Fig. 3.12). The reason the first action potential is of larger amplitude is that

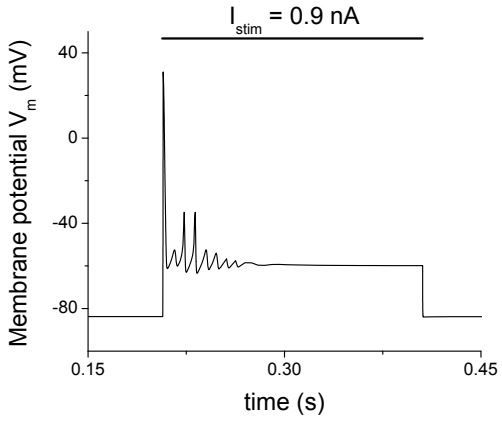

Figure 3.11 Train of action potentials in the Schwarz model with the slow K conductance. The stimulating current used is $I_{stim} = 0.9$ nA.

the system begins the action potential at a more polarized potential, hence with smaller K conductance, and more Na channels available. This feature is caused by the constant leak conductance repolarization: the system repolarizes only enough to fire again. In a system repolarizing with a variable K conductance there is an undershoot, the slowly closing K channels hyperpolarize the membrane after an action potential. This ensures that every action potential begins at the same potential, and hence have the same height.

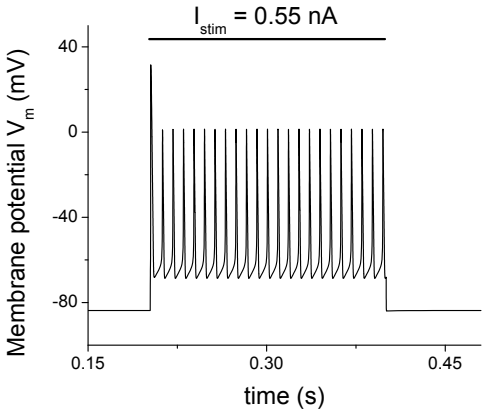

Figure 3.12 Train of action potentials in the Schwarz model without the slow K conductance. The stimulating current used is $I_{stim} = 0.55$ nA.

To summarize, the Schwarz model for a human node of Ranvier is a construction based on the HH model and is not in itself a fundamentally new model. It is however useful as it models, for the first time, a human node of Ranvier, showing how a slow conductance

can prevent repetitive firing and how the leak conductance can repolarize the node after an action potential, a job taken by potassium channels in the Hodgkin-Huxley squid axon model.

3.5 Overview of experimental techniques

3.5.1 Patch-clamp

The patch-clamp[71] is an experimental technique used to study bilayer embedded ion channels. A glass micropipette with a micrometer-sized tip opening is put in contact with the studied cell surface. The area covered by the micropipette forms the "patch", containing a few (sometimes even only one) ion channels. The lipid bilayer adheres to the pipette interior wall to form the gigaohm seal (a seal with a resistance in the $G\Omega$ range), making it possible to isolate membrane current from background noise. Membrane potential is then imposed on the patch, and the resulting current is measured. Alternatively, current can be kept constant and changes in membrane potential measured. Fig. 3.13 shows the basics of patch clamp (in cell-attached mode).

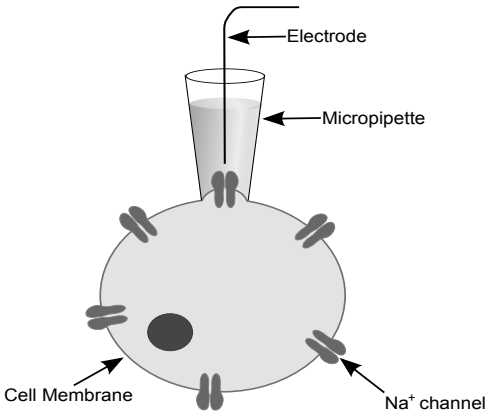

Figure 3.13 Cartoon of the patch-clamp technique in the cell-attached mode. Modified from[72].

The patch-clamp technique can be used in different modes (summarized in Fig. 3.14). The first mode, cell-attached, is when the patch remains attached to the cell. This configuration is used by Wang *et al.*[55] to study left-shift of activation curves of Nav channels after trauma (in the form of pipette aspiration); extra care was taken not to traumatize the patch during gigaohm seal formation.

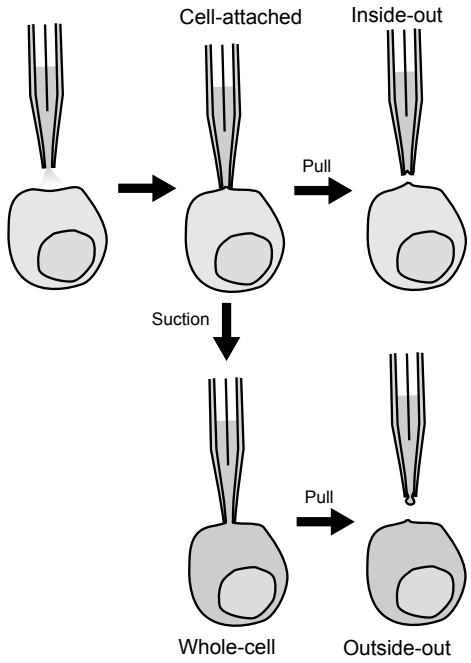

Figure 3.14 Cartoon depicting the different patch-clamp modes. Modified from[73].

Starting from the cell-attached configuration, pulling back the pipette from the cell detaches the patch and exposes the side that was on the interior to the bath solution, hence the name "inside-out".

Starting again from the cell-attached configuration and applying suction to rupture the patch (keeping the rest of the cell intact) yields the whole-cell mode: the cell remains attached to the pipette with its interior exposed to the pipette content.

Finally, the outside-out configuration is obtained from the whole-cell mode by pulling the pipette away from the cell. The membrane portion forming the gigaohm seal remains attached to the pipette but ruptures from the cell. It then reforms at the tip of the pipette, but exposing what used to be the exterior of the cell to the bath solution (thus the name "outside-out").

Using different modes to measure Nav1.6 kinetics yields different results, as will be seen in section 3.7.

3.5.2 Measurement protocols

The basic protocol used to study channels (and the current they allow) is the "voltage step". The idea is to maintain potential at a certain value V_{hold} and then step (and hold there) at another value V_{step}. Current is monitored during this procedure (see Fig. 3.15). "Current families" are obtained by repeating the above procedure (from the same V_{hold} to different V_{step}) with incrementally larger values of V_{step} (see Fig. 3.17). In terms of the HH model, this procedure yields curves of $g_{Na}m^3h(V_m - E_{Na})$ as functions of time.

Activation(V) (or $g(V)$, see Fig. 3.16) curves are obtained by dividing the maximal (peak) current obtained with each voltage step by the driving force (the difference between membrane potential and the reversal potential) and plotting these against V_{step}. The sodium current is given by Eq. 3.11, $I_{Na} = g_{Na}m^3h(V_{step} - E_{Na})$. When using the peak current for each voltage step, it is assumed that the h "particle" is so slow moving compared to the m "particle" that it stays fixed until the peak is reached. This approximation is justified because the m "particle" is about 10 times faster than the h "particle" (see Fig. 3.5). Dividing by the driving force $(V_{step} - E_{Na})$ yields $g_{Na}m^3h$, and then normalizing the curve to one removes g_{Na} and the assumed constant h thus essentially yielding m^3. Hence activation(V) (and $g(V)$) correspond to $m^3(V)$ from the HH model.

Availability(V) (i.e., the fraction of channels that are not inactivated; the h particle in the HH model) is obtained in a slightly different way. Potential is held at V_{hold} and then stepped to a pulse potential V_{pulse} for a set amount of time ($\sim$ 100 ms) and then stepped to 0 mV. Current is monitored throughout the procedure. The maximal current obtained at 0 mV is divided by the driving force ($-E_{Na}$ for sodium) and plotted against V_{pulse}. The resulting curve is normalized and hence corresponds to the HH h particle. The rationale is similar as for obtaining activation(V). The h "particle" is allowed to reach its equilibrium value at V_{pulse}. When stepping to 0 mV, the value of h is assumed constant until the peak is reached, and m is always the same as the step is always to 0 mV. By dividing by the driving force and normalizing, the value of $h(V)$ is obtained.

3.6 Membrane trauma and Na^+ leak from Nav1.6 channels

In this section, we review the work by Wang *et al.*[55] who used the patch-clamp method as well as dye-loaded cells mounted on a uniaxial stretcher to determine that activation and

inactivation of Nav1.6 channels irreversibly left-shift upon trauma (stretch).

Such left-shift would render channels "leaky" which could underlie the rapid TTX-sensitive Ca^{2+} increase observed in traumatic brain injuries[63]. Since the increase occurs rapidly after trauma (< 2 min), well before any proteolytic damage to Nav channels is detected[74], the change in Nav channel would have to be of a mechanical nature.

3.6.1 Nav1.6 is irreversibly affected by membrane trauma

αNav1.6+β1B subunit transfected *Xenopus laevis* oocytes patches were gently formed (so as to avoid trauma) and current was monitored before and during pipette aspiration (see Fig. 3.15). Stretch caused Nav1.6 currents to irreversibly change: current onset and decay became faster, current at -40 mV dramatically increased and the change did not revert (measured after 1 minute).

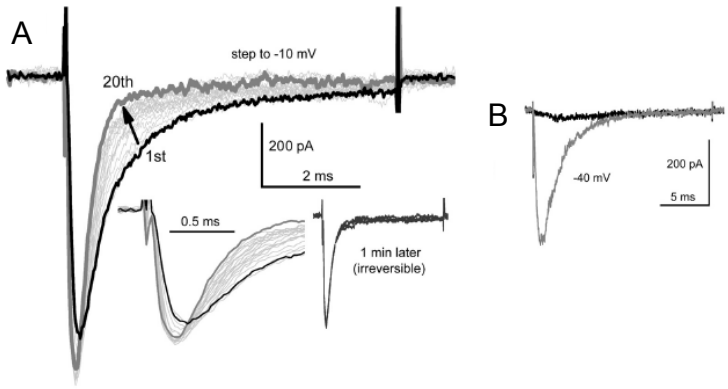

Figure 3.15 A. Current response ($I_{Na}(t)$) of αNav1.6 + β1B-subunits channels to a step depolarization to -10 mV while the patch is stretched. The voltage-step procedure is repeated at 1 Hz while trauma is applied. *Left inset:* early part of the response showing that the maximum current increased and occurred earlier. *Right inset:* Current traces 1 minute later (with same stretch) showing that the change in current response is the same: the change is irreversible and has saturated. B. Pre- (black) and post-stretch (grey) currents obtained with a voltage step to -40 mV showing a dramatic increase in response current. In terms of the HH model, these curves represent $I_{Na}(t) = g_{Na}m^3(t)h(t)(V_{step} - E_{Na})$. Wang *et al.*, Am. J. Physiol. Cell, 2009,[55] Am Physiol Soc, used with permission.

Plotting g(V) (corresponding to m^3 from the HH model) and availability(V) (corresponding to h) before and after stretch of moderate intensity reveals that both curves left-shift after stretch (see Fig. 3.16). Both curves are shifted $\sim$20 mV in the hyperpolarized

direction. This estimate is a lower bound for the maximal possible left-shift as: 1) the pre-stretch curve may be already traumatized (left-shifted) by the formation of the pipette seal and 2) only moderate stretch is used so the left-shift may not be maximal.

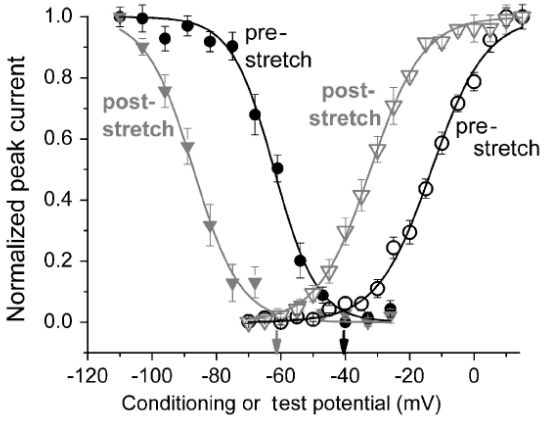

Figure 3.16 Activation(V) (g(V), or m^3 from the HH model, open symbols; see Sec. 3.5.2) and availability(V) (or h from the HH model, closed symbols) pre- (black) and post-stretch (grey). Both curves are left-shifted by the same amount ($\sim$20 mV). Wang *et al.*, Am. J. Physiol. Cell, 2009,[55] Am Physiol Soc, used with permission.

The first possibility such results evoke is the separation of the β subunit from the α subunit. The α subunit contains all the essential channel parts (voltage sensor, selectivity filter etc) and does not require β subunits to function (β subunits are known to modulate Nav channel activity (see e.g., [75] and references therein)). However this is not what happens here: patch-clamp experiments on oocytes expressing αNav1.6 channels only (without any β subunit) yield the same result, irreversible acceleration of both current rise and decay as seen in Fig. 3.17.

Current as a function of potential for a patch with particularly strong transient and steady-state current under a slow potential ramp is shown in Fig. 3.18. Before and after stretch comparison reveals that steady-state currents (as elicited by the slow negative-going ramp) also left-shift under trauma.

Current rescaling is used to test channel left-shift. Current traces taken before and after stretch, at 20 mV intervals, are rescaled (in current only) to have the same maximal current (see Fig. 3.19). The traces completely overlap proving that the channels are shifted by 20 mV in that patch. The rescaling of maximal current intensity accounts for the difference in

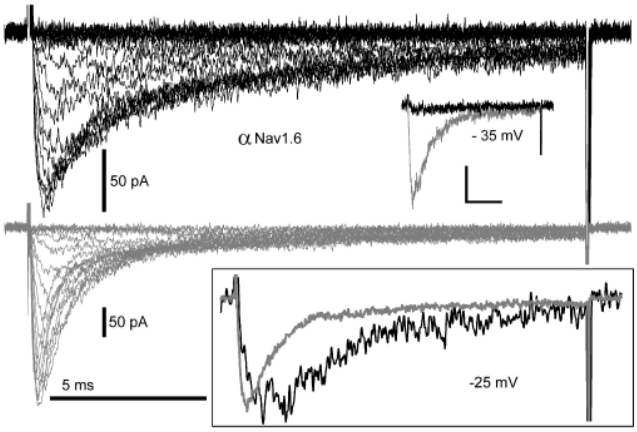

Figure 3.17 Current families (I_{Na})for αNav1.6 channel before (black) and after (grey) stretch obtained by voltage steps from $V_{hold} = -110$ mV to -70, repeating the procedure incrementing the step potential by 5 mV until +15 mV. *Insets*: Comparison (before and after) of traces at two potentials showing the current is modified by stretch. Wang *et al.*, Am. J. Physiol. Cell, 2009,[55] Am Physiol Soc, used with permission.

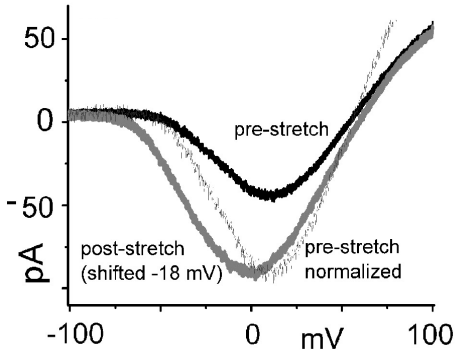

Figure 3.18 Current as a function of potential for a patch with particularly strong persistent current (demonstrated by the fact that current does not inactivate at depolarized potentials), for a 2 mV/ms negative-going voltage ramp (from +100 to −100 mV). Currents elicited by the voltage ramp left-shift post-stretch (dark grey), compared to pre-stretch (black). Wang *et al.*, Am. J. Physiol. Cell, 2009,[55] Am Physiol Soc, used with permission.

driving force at the two potentials used. The traces otherwise overlapping show that the channels have the same kinetics at those different potentials. This also proves that both activation and inactivation are affected to the same extent by trauma. Relating to the HH model, the curves in Fig. 3.19 represent $g_{Na}m^3h(V_{step} - E_{Na})$. When stepping to a different potential, the m and h "particles" should have different kinetics as their time constants

are functions of the potential (see Fig. 3.5). Rescaling the currents essentially removes the $g_{Na}(V_{step} - E_{Na})$ such that what is plotted is $m^3h(t)$. These curves, measured with two V_{step} both 20 mV apart should not overlap, but they do because the stretch causes the kinetics of m and h to left-shift identically.

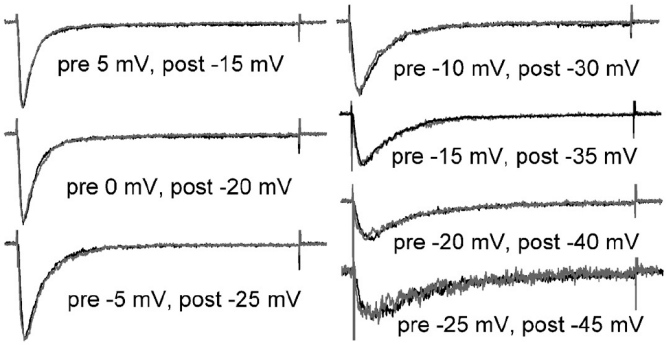

Figure 3.19 A series of current rescaling: current traces from voltage steps to the potentials indicated before (pre, black) and after (post, grey) stretch measured 20 mV apart are rescaled (in current) and completely overlap showing that channels kinetics pre-stretch are the same as post-stretch at 20 mV less (hyperpolarized): the channel kinetics are shifted by 20 mV. Wang *et al.*, Am. J. Physiol. Cell, 2009,[55] Am Physiol Soc, used with permission.

3.6.2 Na dye experiment

Window currents result from the overlap of activation(V) (g(V) or m^3 from the HH model) and availability(V) (h) curves. The left-shift of both activation(V) and availability(V) should also left-shift window currents, which would render the channels "leaky" because of an increased steady-state conductance at the resting potential. To test this, Na dye-loaded HEK cells were traumatized using a uniaxial stretcher and the change in fluorescence was monitored (see Fig. 3.20).

Fluorescence intensity increases rapidly ($\sim$2 min) upon trauma indicating that Na ions flow in (i.e., Nav channels become "leaky"). Measurement of fluorescence at 30 minutes did not reveal any further increase. TTX significantly diminished fluorescence intensity showing that at least part of the Na leak is due to Nav1.6 channels. However TTX did not fully abolish the rise in fluorescence intensity, this could be due to imperfect TTX action, rapid pore formation and resealing in the lipid bilayer, etc.

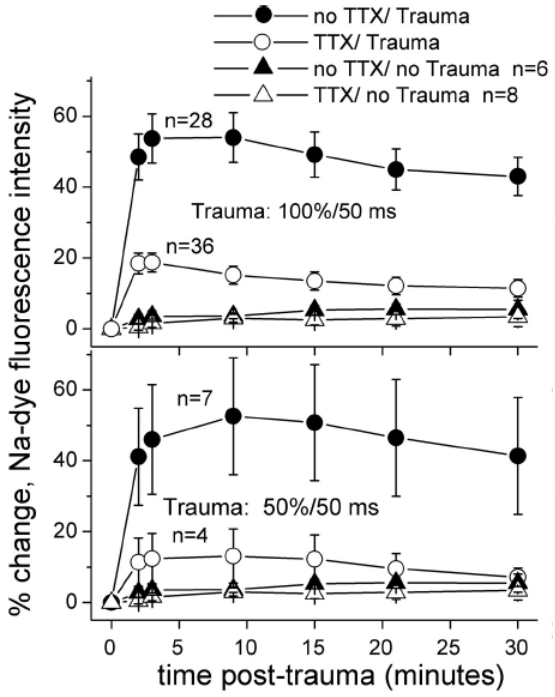

Figure 3.20 Increase in fluorescence intensity upon trauma in Nav1.6-expressing HEK cells. Fluorescence increase stabilizes after ~ 2 minutes and is reduced by TTX. Fluorescence increase indicates that trauma renders the cell membrane permeable to sodium, presumably due to the left-shift of the Nav channel window conductance region. TTX-sensitivity indicates that the change in Na is due to Nav channels. Top: The sample is strained 100% during 50 ms, Bottom: the sample is strained 50% during 50 ms. Wang *et al.*, Am. J. Physiol. Cell, 2009,[55] Am Physiol Soc, used with permission.

3.6.3 Mechanism of left-shift

The results obtained cannot be interpreted as an increase in patch area or number of channels, nor can it be interpreted as a uniform increase in open probability (see Fig. 3.21). Such scenarios would increase the maximal current obtained (peak current of an I-V relation, a plot of the steady-state current as a function of potential), but cannot account for the shift in peak position observed. Only the left-shift scenario correctly explains the results observed.

Such a scenario implies a window current region displaced towards hyperpolarized potentials (i.e., closer to the resting potential) which render Nav channels "leaky". How exactly trauma causes channels to left-shift is unknown. As shown above, disrupted αNav1.6 interactions with β subunits does not hold as an explanation.

A possible explanation is that Nav1.6 in intact membranes resides in specific lipid

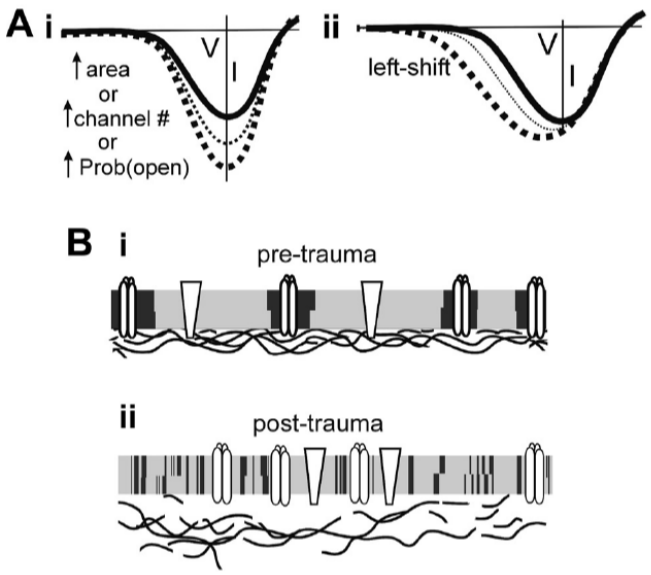

Figure 3.21 A.i and ii. Hypothetical I-V relations in different scenarios: i. increased patch area, increased number of channels and uniform open probability increase would not shift the I-V relation whereas left-shift of channel activation and inactivation does. B.i. In an intact membrane, channels sit in specialized microdomains which, upon trauma/stretch/bleb formation (ii.) are disrupted. The channels now operating in a different environment do not "feel" the same energetic barrier for their transitions thus causing left-shift of both activation and inactivation. Wang *et al.*, Am. J. Physiol. Cell, 2009,[55] Am Physiol Soc, used with permission.

microdomains. Trauma-induced bleb formation (see Sec. 3.8.1) might disrupt such microdomains causing Nav1.6 channel kinetics to left-shift. Some membrane components are known to modulate Nav channel activity (e.g., fatty acids cause left-shift whereas cholesterol causes right-shifts). For activation, changes in membrane composition would change the energy barrier for the voltage-sensor transition movement (either increasing it – right-shift, or decreasing it – left-shift), as it would be easier for a voltage sensor to move in a more fluid lipid bilayer. The mechanism and barriers involved in inactivation being poorly understood, it is hard to speculate on the precise mechanism causing the left-shift of inactivation (availability).

3.7 Measured Properties of Nav1.6

The data for activation ($g(V)$) of Nav1.6 channels from different sources (Schwarz *et al.*[67], Rush *et al.*[76], Wang *et al.*[55], Chatelier *et al.*[62], Hu *et al.*[77], Chen *et al.*[78] and Burbidge

et al.[79]) is compiled in Fig. 3.22 and Table 3.4. Some sources provide activation midpoint and slope[62, 77, 78, 79], others provide graphical information[55, 76] (and again Ref.[79]) from which we extracted and fitted the points using Eq. 3.39. Ref. [67] provides a model of sodium current, which we simulated and fitted using Eq. 3.39 to obtain a midpoint (x_0) and a slope (dx):

$$P_{open} = \frac{1}{1 + \exp\left(\frac{x_0 - x}{dx}\right)}. \tag{3.39}$$

Even though the slope of $g(V)$ remains roughly the same (5.7[77] for Hu *et al.* to 8.5[55] for Wang *et al.*), the $g(V)$ midpoints vary over a wide range (from -43.9[77] to -13.6[78]).

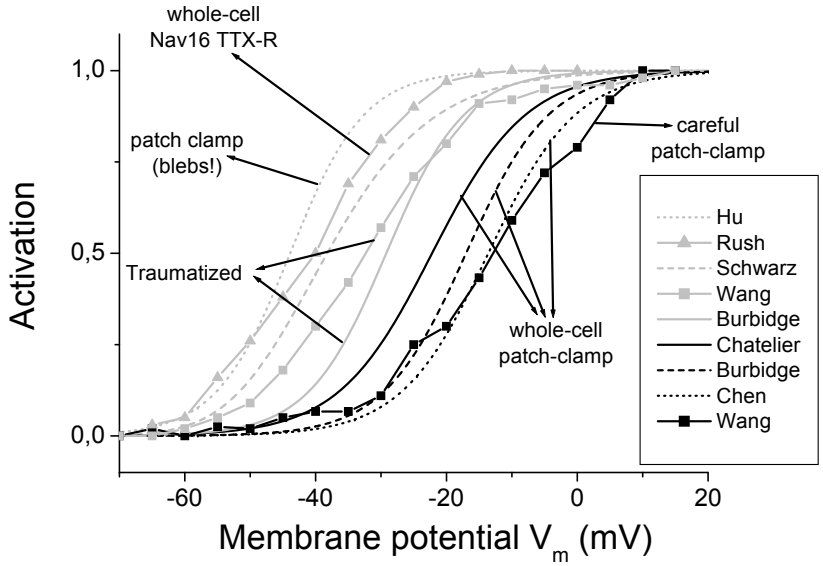

Figure 3.22 Activation, g(V), curves for Nav1.6 channels from different studies[67, 76, 55, 62, 77, 78, 79]. The data can be separated in two groups: intact (the rightmost group) and traumatized (the leftmost group). The left-shifted activation from Wang *et al.*[55], and Burbidge *et al.*[79] is shown as dashed curves. In Wang *et al.*, the left-shift occurs because of trauma; in Burbidge *et al.* the only difference was a change in solutes, which caused a left-shift of Nav kinetics.

There were notable differences in the experimental conditions of these studies. Schwarz *et al.*[67] used human axons from the peripheral nervous system to measure the activity of channels at nodes of Ranvier using the axonal voltage-clamp technique described by

Table 3.4 Nav1.6 activation data from different sources is compiled: activation ($g(V)$) midpoints and slopes, channel type, experimental method used to obtain the data and system in which the channel was expressed are presented. The activation data is presented in graphical form in Fig. 3.22.

	g(V) midpoint (mV)	g(V) slope (mV)	Channel	Method	Expressed in
Rush *et al.*[76]	−41	7.5	Y371S Nav1.6	Whole-cell clamp	Nav1.8-null DRG neurons
Schwarz *et el.*[67]	−37.6	7.6	hNav1.6	Node clamp	Native system
Chatelier *et al.*[62]	−22.2	7.2	hNav1.6	Whole-cell clamp	HEK cells
Burbidge *et al.*[79]	−17	6.4	hNav1.6	Whole-cell clamp	HEK cells
Wang *et al.*[55]	−13.3	8.5	mice Nav1.6	Cell-attached clamp	*Xenopus Laevis* oocytes
Chen *et al.*[78]	−13.6	6.7	mice Nav1.6	Whole-cell clamp	HEK cells
Hu *et al.*[77]	−43.9	5.7	rat Nav1.6	Outside-out Patch-clamp from blebs	Native system

Nonner[68]. Note that Nav1.6 is present in mammalian peripheral nervous system as demonstrated in Ref. [80, 81]. Rush *et al.*[76] expressed the TTX-resistent Y371S mutation of the mice Nav1.6 channels in mice Nav1.8-null Dorsal Root Ganglion (DRG) neurons and studied them using whole-cell patch-clamp. Wang *et al.*[55] expressed mice Nav1.6 in stably transfected *Xenopus* oocytes which they studied using cell-attached patch-clamp. Chatelier *et al.*[62] used whole-cell patch-clamp to study HEK cells stably transfected with hNav1.6 (human Nav1.6). Hu *et al.*[77] used patch-clamp from giant patches (somatic nucleated patches and isolated axon blebs) and outside-out patches to study rat prefrontal cortex sodium channels (Nav1.6 and Nav1.2). Finally, Chen *et al.*[78] transiently transfected mouse Nav1.6 into HEK cells and used whole-cell patch-clamp.

Essentially, there were 4 channels (hNav1.6, mice Nav1.6, rat Nav1.6 and TTX-R Nav1.6 (which is mice Nav1.6 Y371S mutant)) and 2 methods (patch clamp and whole-cell patch clamp) used in these studies. Note moreover that the data by Wang *et al.* is

for αNav1.6 only, no β-subunit was expressed; this could have an impact on the activation curve.

Presumably, the Y371S mutant form of mice Nav1.6 has different kinetics than the other channels since that mutation renders it TTX-resistent. This would not be surprising since TTX is a pore blocking toxin. It binds from the exterior side to the reentrant loop between helices S5 and S6 of each domain[82] (the loop forming the selectivity filter).

Ignoring that data from the list, we are left with 3 channels and 2 methods. Rat and mouse Nav1.6 are probably closely related, and so could hNav1.6 be. Assuming they have indistinguishable channel kinetics, the two different methods used would be the factor that separates the experimental data into two groups.

On one hand, we have the "intact" group, consisting of the data from Wang *et al.*, Chen *et al.*, Burbidge *et al.* and Chatelier *et al.* and on the other hand we have Schwarz *et al.* and Hu *et al.* with "left-shifted" data. The "left-shifted" group both used techniques that could damage the cells (Schwarz *et al.* dissected nerves; Hu *et al.* worked with patch-clamp technique on blebs). Those in the "intact" group used whole-cell patch clamp, a technique which should not damage the cell.

Note that Schwarz *et al.* do mention that even though "Care was taken that the nerve fibre to be isolated was never stretched and retained a wavy appearance throughout the dissection", "In [some] nerves where action potentials could be measured the amplitude was smaller and the threshold potential was higher. These changes indicated that the fibers might have been damaged during dissection and mounting, leading to axoplasmic Na accumulation and to increased leakage current"[67]. So it would not be surprising if the data they report includes some mildly traumatized nodes and hence some partly left-shifted Nav channels.

Wang *et al.* and Burbidge *et al.* present interesting cases. The data from Wang *et al.* is in the "right-shifted" group even though cell-attached patch-clamp was used, a technique which should left-shifts channel (by creating blebs). This is because they were studying trauma and hence were careful in establishing the patch-clamp not to traumatize the patch. Both the intact and left-shifted activation(V) from Wang *et al.* were included in Fig. 3.22. Burbidge *et al.* used whole-cell clamp while studying transient and persistent Nav1.6 currents. They noticed that persistent currents declined over 15-30 minutes when they used CsF in the pipette solution; using CsCl stabilized persistent currents. They

measured Nav1.6 activation both after the decline in persistent currents and with stabilized persistent currents (using CsCl). It is possible that the decline they observed in persistent current is actually a left-shift: currents becoming left-shifted, when observed at a fixed potential, would seem to decrease (see Ch. 4). This is supported by their data for Nav1.6 activation being left-shifted when using CsF (declining persistent currents) compared to using CsCl (stable persistent currents). Fig. 3.22 plots both their activation curves CsCl as a full line and CsF as a dashed line. They both fit well with the intact and left-shifted groups respectively.

Note that not all experiments used Nav1.6 channels in the same environment; this could also possibly contribute to the left- or right-shift of the channels. Additionally, the experiments might not have all been carried at the same temperature, further contributing to the channel's relative shift.

3.8 Blebs

3.8.1 Blebs in general

Blebs are protrusions of the cell membrane caused by detachment (or breaking) of the underlying actin cortex[83] (see Fig. 3.23). They are known to occur during cytokinesis (cell division)[84], are involved in cell motility[85] and apoptosis (programmed cell death)[86]; they also occur in nodes of Ranvier following trauma[56]. In the first two cases, the blebs are dynamic: they form and retract. During apoptosis, blebs do not retract. After trauma, it is not known whether blebs do retract, but presumably, if given enough time, an injured membrane can heal.

Blebs are formed by a disruption of the cell membrane-cortex interactions either by a detachment of the cell membrane from the cortex or a local rupture of the cortex. The cortex, made primarily of spectrin and actin (cytoskeletal proteins), normally maintains a number of weak interactions with the cell membrane[87, 88]; if these interactions are broken, the membrane detaches from the cortex and is pushed outward by the cell's hydrostatic pressure (normally counterbalanced by cortical tension[87, 89]). This protrusion grows by filling with cytosol for about ~ 30 s to a spherical size of $1 - 10$ μm[87].

Mechanistically, blebs grow by two processes: 1) a flow of lipids in the plane of the membrane and 2) further detachment of the cell membrane from the cortex. Lipid flow

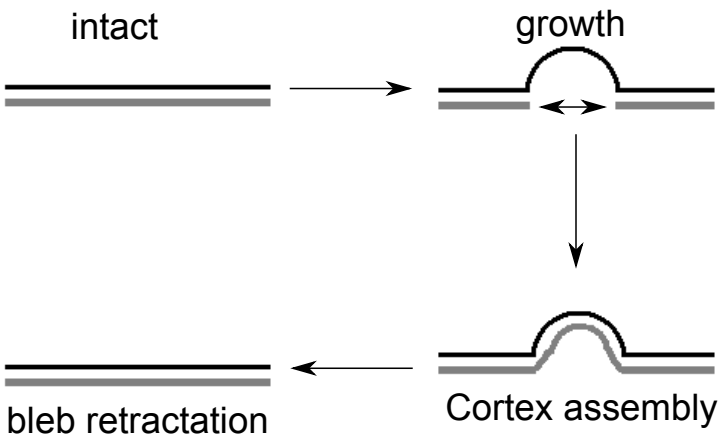

Figure 3.23 Bleb nucleation-retractation cycle: nucleation, growth, cortex assembly and retractation. The cell membrane is shown in black and the actin cortex in grey.

keeps the bleb's neck size constant and increases the bleb's total surface as well as the angle between the bleb and the cell body; detachment of cell membrane increases the neck size, but decreases the angle. The relative contribution of the two processes is unknown; presumably lipids flow until the angle is such that more membrane detaches from the cortex. The ensuing change in bleb shape would then drive more lipids to flow into the bleb. Additionally, any wrinkles present in the cell membrane at the bleb would unfold when the cell membrane is pushed outward by the cell's hydrostatic pressure, further contributing to bleb growth.

After bleb growth has stopped, the actin cortex reforms in the bleb. Two cases are possible: 1) actin is already present in the bleb but bleb growth outpaces cortex reformation, or 2) the bleb is devoid of actin and a (yet unknown) signal triggers actin cortex reconstruction. Once the cortex has reformed, motor proteins (such as myosin) power the retractation of the bleb to its original position in an intact membrane.

3.8.2 Blebs at nodes of Ranvier

Blebs are the first histopathological change observed at nodes of Ranvier after trauma[56] (see Fig. 3.24). How could a blebbed membrane contribute to Nav channels left-shift? As stated above, blebbed membranes are detached from the cell cortex which normally maintains a number of interactions with the membrane. These interactions may serve as barriers to lateral diffusion in the cell membrane[87] and hence to maintain organized microdomains around Nav channels. Disruption of the membrane-cortex interactions would then disrupt

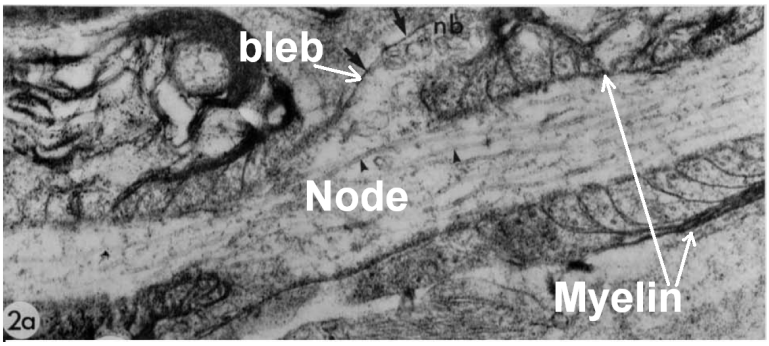

Figure 3.24 Electron micrograph of a traumatized myelinated axon showing a blebbed node of Ranvier. The bleb, node and myelin (on one side of the node) are indicated in white. Reprinted (with relabeling) by permission from John Wiley and Sons: Microscopy Research and Technique[56], copyright 1996.

these microdomains (as well as cause bleb formation) exposing the Nav channels to a different environment. The voltage sensors sitting in the membrane would then experience different forces thus lowering (or raising) the energetic barrier for their transition, causing a left-shift in channel kinetics.

3.9 Articles review

The area of trauma and modulators of neuronal membrane excitability is quite active. We conclude this introduction by providing a short review of some important papers covering excitability, trauma induced Ca increase, neuropathic pain and Nav channel kinetics modulation.

1948 Hodgkin[90] established three classes of neuronal excitability. Class I excitability refers to axon which fire spontaneously at rest, with the firing frequency varying smoothly with injected current. Class II excitability describes neurons that only fire when injected current reaches a threshold value. Finally Class III excitability is when the neurons do not fire, or fire a single spike when stimulated. In the HH model (and in the Schwarz model) the system exhibits Class II excitability. In our model, left-shift of Nav channels triggers a change in excitability class.

1985 Patlak and Ortiz[91] observed that the inactivation process of Na currents has two time constants, the slower one they labeled “slow inactivation”. Interestingly,

the slow inactivation during a voltage step was dependent on holding potential. They postulated that Nav channels can function in two different modes, each with its own inactivation time constant.

1996 Maxwell[56] studied the effect of stretch injury on an axon with transmission electron microscopy. Mild axonal trauma (mild in the sense that it does not break the axon apart right away) detaches the membrane at nodes of Ranvier from the underlying cortex, thus forming blebs. Moreover they show the cytoskeleton at nodes of Ranvier to be disrupted by trauma; a sign of an increased internal calcium concentration.

2000 Richardson, McIntyre and Grill[92] compared the transmission properties of three different models of myelin (the electrical insulator wrapped around the axons, except at nodes of Ranvier). The simplest model assumes only a simple resistance between adjacent nodes. The second model refines the first one by considering that the myelin is not a perfect insulator and hence adds parallel conductance and capacitance between the internode (the region covered by myelin) and the exterior. The last model represents the myelin with two layers of conductance and capacitance between the interior and exterior. This last model proves to be the most physiologically accurate, but also the most computationally demanding.

2001 Wolf, Stys, Lusardi, Meaney and Smith[63] studied the increase in axonal calcium concentration which follows trauma using a Ca-sensitive dye to monitor changes in concentration. By removing extracellular Ca, they showed that the increase in intracellular Ca came from the exterior environment (as opposed to intracellular Ca buffers). In the presence of TTX the rise in Ca was blocked, thus indicating that Nav channels mediate the Ca influx. They thus suggested that misbehaving Nav channels cause depolarization and depletion of the Na gradient. In turn, the Na/Ca exchanger (which uses the Na and Ca gradients to work) reverses and uptakes Ca; depolarization also causes the voltage gated Ca

channels to open, letting Ca in.

2002 Taddese and Bean[61] studied persistent currents in tuberomammillary neurons. The persistent currents they observed are closely related to HH window currents. An allosteric model was established where inactivation is not directly voltage-dependent, but activation dependent and hence inactivation draws its apparent voltage-dependence from activation. Persistent currents arise from the non-zero steady-state occupancy of the open-state (making it similar to HH window currents which arise from the overlap of activation and inactivation). They suggested that these persistent currents could generate spontaneous activity in any neuron; an idea which we apply in the context of left-shifted Nav channels.

Hogg, Lewis and Adams[93] investigated the effect of ciguatoxin on neurons using patch clamp. Ciguatoxin induces spontaneous activity and subthreshold potential oscillations. Interestingly, they report that ciguatoxin left-shifts activation (they do not mention inactivation) of Nav channels. Essentially they report a left-shifted Nav channel causing spontaneous firing and subthreshold oscillations in a neuron. Knowing that neuropathic pain is linked to subthreshold oscillations, it wouldn't be surprising if abnormal kinetics of Nav channels were involved there too.

2003 Tokuno, Kocsis and Waxman[94] showed that blockade of Nav channels with TTX causes dorsal and ventral nerve roots to hyperpolarize. They argue that this suggests the presence of persistent Na currents but do not specify whether this persistent current results from a Nav channels unable to inactivate, or from the window conductance of Nav channels.

2004 Iwata *et al.*[95] studied axonal trauma. The first evidence of trauma is the rapid TTX-sensitive increase in internal Ca concentration mediated by mechanically injured Nav channels. This rise in calcium mediates further damage to the axon, including the proteolysis (degradation) of Nav channels, further disrupting

already misbehaving Nav channels and further increasing levels of internal Ca. This sequence of events (summarized in Fig. 3.25) presents a positive feedback mechanism whereby moderate trauma can eventually degenerate into, possibly, diffuse axonal injury.

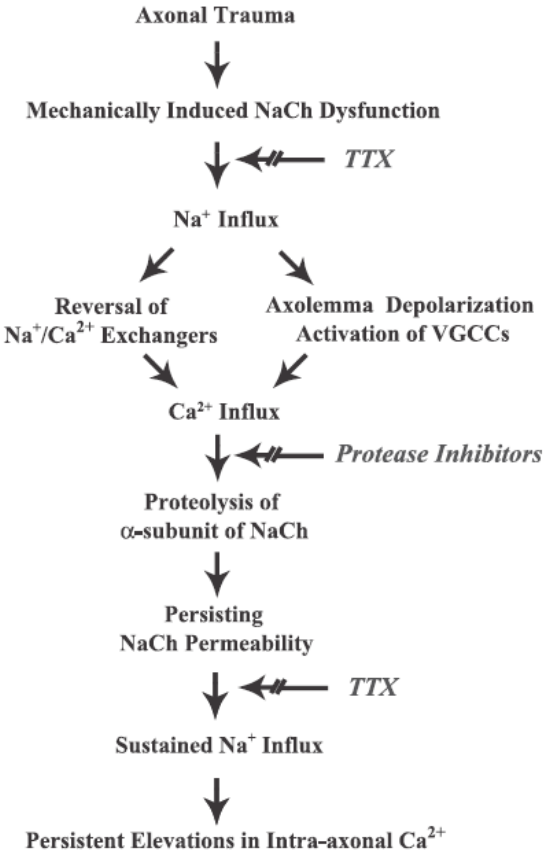

Figure 3.25 Pathway of internal Ca increase. The axonal trauma mechanically induces a malfunction of Nav channels (NaCh), causing a TTX-sensitive Na influx. This influx 1) depolarizes the axolemme causing activation of voltage-gated Ca channels (VGCCs) and 2) reversal of Na/Ca exchangers resulting in a rise in internal Ca. As a result, Nav channels are degraded (by Ca-activated proteases) causing further malfunction of the channel. These pathways can be blocked, either by TTX, or by protease inhibitors, as indicated. Reproduced with permission from [95].

2006 Shirahata *et al.*[96] report that Ankyrin-G, a protein which mediates attachment of transmembrane proteins to the spectrin cytoskeleton, radically reduces the persistent current produced by Nav1.6 channels (transfected in TsA201 cells, a variation of HEK cells). They measure persistent currents as steady-state

currents after a voltage step, thus it could be "window current". Considering their data (Fig. 3 in particular) which show that transient currents are left-shifted by ankyrin-G, persistent currents instead of being globally reduced, could have been left-shifted too by ankyrin-G. A left-shift of window conductance would give the impression of a reduction of persistent current at e.g., 0 mV (see Ch. 4).

2008 Villalba-Galea, Sandtner, Starace and Bezanilla[97] proposed that the S4 segment (the voltage-sensor) of voltage-gated proteins changes conformation from a 3_{10} helix (active) to an alpha-helix (a less tightly packed helix, relaxed) when held at depolarized potentials. They suggest that this change of conformation of the voltage-sensor is associated to the "slow-inactivated" state, a non-permeating state from which the return to the closed (active) state is slow. Four conformations of the voltage sensor are possible: closed-active, open-active, closed-relaxed and open-relaxed. We suggest (see Ch. 4) that this change of conformation might prevent the inactivation particle from binding to the channel thus making the relaxed mode a "non-inactivating" mode; a source of persistent currents.

Prescott, De Koninck and Sejnowski[98] found that by varying a single parameter the excitability of a Morris-Lecar model[99] could be modified. They used extensive nonlinear dynamics analysis to study the changes in firing behaviour (from single spike, to phasic firing to tonic firing). This study is relevant to our work as even though they used a different model, they studied the effect of shifts of channel kinetics (mainly in Kv kinetics) on firing patterns. A Morris-Lecar model would have been unsuitable for our study as inactivation, which is not considered in Morris-Lecar models, was required.

2009 Ochab-Marcinek, Schmid, Goychuk and Hänggi[100] studied whether noise (originating from a finite number of ion channels) could facilitate the propagation of action potentials in a myelinated axon. They used simple resistors as connectors between adjacent nodes of Ranvier and endowed the nodes with HH kinetics. The internode resistance was set just below the propagation threshold. Low noise does not allow propagation, and high noise only allows action potentials to propagate over short distances (each node experiencing large potential fluctua-

tions). The optimal number of channel in a node (obtained through the optimal noise level) is close to the actual physiological values.

Thomas, Hawkins, Richards, Xu, Gazina and Petrou[101] investigated the reason why fever can lead to seizure. Specifically, they studied the modification of the kinetics of Nav1.2, the sodium channel present at the axon initial segment (AIS), by temperature in HEK cells using patch-clamp technique. Their results indicate that not only activation of Nav1.2 becomes faster with elevated temperature, but it also left-shifts, causing the AIS to become more excitable. This change in neuronal excitability could be the cause of seizures.

McGinn, Kelley, Akinyi, Oli, Liu, Hayes, Wang and Povlishock[74] showed that following traumatic brain injuries calpain, a calcium-activated protease, cleaves spectrin, one of the major constituents of the cytoskeleton. This result highlights the fact that following trauma, internal level of Ca rise enough to activate calpain.

Devor *et al.*[102, 103, 104, 105, 106] studied neuropathic pain and showed that it is underlied by ectopic discharges. They provide evidence that Aβ afferent neurons (normally signalling touch and vibration information) undergo excitability changes. They also show that nerve injury enhances subthreshold membrane potential oscillations in neuropathic pain model[104]. These oscillations are possibly caused by "delayed Na current", currents with a slow inactivation[102]. Changing the total Na conductance in a computer model with slow-inactivating Na currents changes the window of injected current necessary to obtain different firing patterns (oscillations, burst firing and tonic firing).

2010 Lorincz and Nusser[107] used immunogold and immunofluorescence labelling techniques to study the localization of Nav1.6 channels. They show that the most Nav1.6-rich regions of the axon are the nodes of Ranvier and the initial segment (the portion of the cell between the body and the axon).

Börjesson, Parkkari, Hammarström and Elinder[108] showed that charged fatty acids shift the voltage dependence of K channels. They used three differently

charged fatty acides with the same backbone to show that the negative charge left-shifts channel activation whereas a positive charge right-shifts it. The neutrally charged fatty acid has no effect on K channels. They also use a HH-type model to simulate the excitability of a system with shifted K channel activation, showing that a -5 or $+5$ mV shift of K channel activation is the equivalent of a 3-fold increase or decrease in K channel conductance. They suggest that this electrostatic tuning of excitability could constitute a powerful pharmacological approach in the treatment of ion channel (and excitability) related conditions.

Chatelier, Zhao, Bois and Chahine[62] used patch-clamp techniques to study persistent currents in Nav1.6 transfected HEK cells. Through single channel recordings, they identified rapid opening of Nav channels, possibly due to window conductance. They also show a trace (Fig. 5, third trace) exhibiting open channels that do not inactivate (possibly "mode switched" into the relaxed mode). This mode switch seems to be a rare event; only one of six traces had this behaviour.

Hasenstaub, Otte, Callaway and Sejnowski[109] studied the energetic cost of action potentials using experiments and simulations. They showed that a neuron having the capacity to fire at a higher frequency automatically consumes more ATP per spike (or per spike train), even if the high frequency capacity is not solicited. Channel expression and function in a neuron is set to maximize firing frequency capacity and minimize energy consumption. The left-shift of Nav channels presumably disrupts this equilibrium.

Having introduced the topic, we now present the two papers resulting from this work. The first one proposes experimental voltage-step protocols to study traumatized Nav channels. The second studies the changes in excitability and ion homeostasis in a traumatized node of Ranvier. In Ch. 6 we also present our preliminary work on subthreshold oscillations generated by left-shifted Nav channel operation.

Chapter 4

Identifying the "leaky" states of native Nav channels in traumatized neurons: simulation and theory for $I_{Na}(V,t)$ during trauma of cell-attached patches

P-A Boucher, B Joós and CE Morris

Identifying the "leaky" states of native Nav channels in traumatized neurons: simulation and theory for $I_{Na}(V,t)$ during trauma of cell-attached patches

Pierre-Alexandre Boucher[a], Béla Joós[a], Catherine E. Morris[b]

[a]*Institut de physique Ottawa-Carleton*
Campus de l'Université d'Ottawa
Ottawa, Ontario, Canada, K1N 6N5
[b]*Neurosciences, Ottawa Health Research Institute*
Ottawa, Ontario, Canada, K1Y 4E9

Abstract

Stretch/shear injury of axons renders their voltage-gated sodium channels (Nav) pathologically leaky. The mechanically-induced blebbing at Nav-rich axolemma, we hypothesize, causes this lethal change (Wang et al 2009 Am J Physiol 297:823). In Nav1.6-rich oocyte membrane patches (cell-attached) blebbed by pipette aspiration, progressive and irreversible hyperpolarizing shifts ("left-shift") of both activation and availability occur. Determining whether native Navs respond similarly will require challenging brain-slice patching, so clamp protocols suitable for extracting mechanistic information from small irreversibly changing macroscopic currents are needed. Anticipating this, we test assorted ramp and step protocols on a simulated Nav1.6-like $g_{Na}(V)$. Simulations include mixes of intact and left-shifted (20 mV) transient and non-inactivating channels. We show: 1) where left-shifted $g_{Na}(V)$ underlies traumatized leaky Navs, the oft-used practice of characterizing the "leakiness" of a Nav channel population by the ratio steady-state/peak $I_{Na}(0\text{ mV})$ could be misleading. 2) relatively fast positive-then-negative-going sawtooth clamp will distinguish changes in non-inactivating from those in transient-based "persistent" $g_{Na}(V)$ as membrane trauma worsens. 3) during progressive bleb formation, selected multi-step protocols run continually could reveal whether left-shift of transient $g_{Na}(V)$ operation occurs as an all-or-none or a graded process. The former would signify disruption of discrete (putative) Nav-modulator interactions (e.g., Nav/ankyrinG binding) while the latter could suggest that a progressively less orderly bilayer surround explains the progressive left-shift. 4) Where transient and non-inactivating Nav channels (same activation parameters; relative abundance 0.0075) co-exist, ramps indicate that after traumatic left-shift of both populations, transient channel subthreshold activity would be the likelier initiator of excitogenicity.

1. Introduction

During traumatic brain injury, shear/stretch of axonal membranes in affected tissue directly alters the behavior of voltage-gated sodium channels (Nav). Leaky Nav channels lead eventually to hyperactivated axonal Ca^{2+}-proteases that degrade the spectrin skeleton, thereby creating the untreatable condition (evident by brain imaging) of "diffuse axonal injury"[34]. Using Na-dye loaded HEK cells with recombinant Nav channels[31], we determined that Nav1.6 - the isoform of adult myelinated axons - is directly rendered "leaky" by stretch trauma of intact cells. Further, we showed via cell-attached oocyte patch-clamp of macroscopic Nav1.6 current (see Fig. 1A), that this "leaky" condition coincides with a hyperpolarizing (leftward) shift of the activation and steady-state fast inactivation (or availability) kinetics of the channels. This irreversible shift, we argue, could be pivotal in the excitotoxicity of dif-

fuse axonal injury and in ectopic excitogenicity such as occurs with neuropathic pain in damaged axons. Importantly, an automatic consequence of coupled left-shifting of activation and inactivation is the leftward displacement of window current arising from the overlap of these two processes. In axons, left-shifting Nav channel operation moves window conductance closer to (or, in extreme cases, beyond) the resting potential.

From indirect evidence (not from voltage clamp), it has been hypothesized that trauma increases a non-transient form of sodium current, variously termed persistent or non-inactivating [26]. Terms applied to the many manifestations of non-transient I_{Na} do not always imply the same mechanisms. Even "window I_{Na}", the steady-state product of transient I_{Na} (our "I_{tr}") as described in the Hodgkin and Huxley [10] model (hereafter, HH) (see Fig. 3), can be conflated with other steady-state versions of I_{Na} [22, 35]. The literature alludes to delayed, late, persistent and steady-state I_{Na} [1, 14], to non-inactivating mode or "modal" I_{Na} [21] (similar to our I_{ni}), to mixed "non-inactivating" current [36], to various slowly-inactivating versions of I_{Na} [32] or to "slow mode" I_{Na}[12], to subthreshold persistent I_{Na}[27], to "late events" and to "re-openings" (as evident in single channel recordings)[7]. It is often uncertain what kinetically distinct open state(s) account for these currents, especially since several Nav isoforms[37], each with particular sets of fundamental and "modulated" kinetics, can occur in native membranes. "Persistent current" has a broad semantic range. It signifies various open states with disparate unitary and macrcoscopic Nav current manifestations (e.g., [12, 21, 28, 29]) that fall outside the range for classic (i.e., HH like) fast-inactivating I_{Na}.

The Taddese and Bean [27] allosteric Markov model for neuronal Nav channel activation/inactivation yields a "subthreshold persistent current" that closely tracks availability(V) and that strongly resembles the coupled version of HH window current used here and in our studies of post-trauma excitability [4]. Specifically, in our model (designed to be consistent with recombinant macroscopic currents[31]), changes in m and h voltage dependence are always coupled, as occurs (albeit by a different formalism) in the allosteric

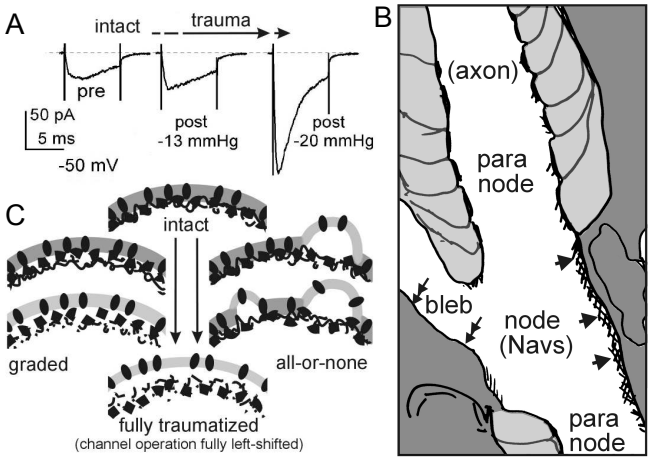

Figure 1: **Membrane trauma and Nav channels. A**. "Left-shift" as seen from I_{Na} in a cell-attached patch (recombinant αNav1.6/β1; experimental conditions as in [31]), during steps to −50 mV before pipette aspiration, as labeled (i.e., as the membrane is made progressively more traumatized). **B**. Cartooned tracing of a transmission electronmicrograph of a stretch-traumatized myelinated axon from optic nerve. The node of Ranvier has a mix of normal-looking (arrowheads) and blebbed (double-headed arrows) nodal axolemma; the paranodal regions are indicated (modified from Fig. 2a of Maxwell [19]. **C**. Cartoon depicting two possible scenarios by which a membrane could go from intact to fully traumatized during mechanically-induced bleb formation. These are not mutually exclusive possibilities. At the graded extreme, the entire population of channels contributing to macroscopic I_{Na} (black ovoids) simultaneously experiences kinetically significant and progressively more extensive changes in the membrane. At the all-or-none extreme, each channel is either normal or has experienced a kinetically significant local change (e.g., local bilayer de-adhesion/thinning, as depicted; irreversible loss of a specific chemical modulator is another possibility). The endpoints correspond to intact and traumatized node of Ranvier as described by Maxwell [19] who shows that a single traumatized node can be partially intact-looking, partially blebbed; this is captured in our model by the parameter pair AC and LS_{AC}. In intact plasma membrane, bilayer adheres to the actomyosin-spectrin skeleton[6] which stabilizes localized arrangements of bilayer lipids[16]; fully traumatized (blebbed) membrane has lost the adhesions and with them whatever microdomain organization they fostered. Channel-bearing bilayer is depicted thick in intact and thin in blebbed membrane (with altered grey tones to suggest an altered average lipid constitution) but the bilayer-mechanical and/or membrane-chemical changes that cause left-shift during bleb-inducing trauma are not known.

model. In some reports, recombinant Nav1.6 yields such large (relatively speaking) steady-state currents near 0 mV[25] that it would be hard not to invoke I_{ni}. Elsewhere, large I_{ni} is seen only sporadically in whole-cell recordings [5, 7, 33]. For recombinant Nav1.6 in HEK cells, non-inactivating or modal events have been observed at the single channel level in cell-attached patches, but appear to represent a rarely visited gating mode and to generate $\ll 1\%$ of total current[7]. Nevertheless, in computational models, an I_{ni} conductance mechanism has been the usual embodiment of "persistent sodium current"(see e.g., McIntyre and Grill [20]).

If the non-inactivating modes occur in axons[26] (and/or somata) as has been suggested, and if they left-shift (along with I_{tr}) during membrane trauma, it becomes even more difficult to ascertain the kinetic properties (and by extension, the molecular nature) of "TTX-sensitive sodium leak" in injured neurons[11, 34]. We therefore consider situations in which trauma left-shifts I_{ni} along with I_{tr}.

Mammalian CNS white matter fixed directly after traumatic stretch shows, in electronmicrographs, blebbed axolemma at the nodes of Ranvier[19]. These mechanically-induced blebs are the earliest consequence of the mechanical insult (see Fig. 1B). Nodes of Ranvier are the short lengths of myelin-free axolemma that constitute the brain's most Nav1.6-rich membranes[17]. If left-shifted $g_{Na}(V)$ in nodal blebs underlies trauma-induced "Nav leak", then it is the channels in blebs that are the key targets for neuroprotective Nav blockers. Though Nav blockers are being tested clinically for their ability to salvage the traumatic penumbra[3] the specifics of their molecular targets are not understood. Blebbing of Nav-rich membrane also occurs in ischemic brain injury, with axon initial segments being especially vulnerable [23] and since NMDA channel blockers do not protect the axon initial segment, inappropriately open Nav channels are considered the likely culprit.

During cell-attached patch clamp, pipette aspiration of sufficient intensity and duration causes mechanical (traumatic) blebbing. Recombinant neuronal Nav channels expressed in *Xenopus* oocytes (Nav1.6[31] and Nav1.2 (P.F. Juranka, W. Lin, C.E. Morris, unpublished observations)) are susceptible to this blebbing trauma. Comparable experiments are required on native brain channels, using neurons in situ, or as near to in situ as possible. Because acute isolation or culture of primary neurons modifies the plasma membrane's mechanical properties[30] and probably many biochemical properties too, acute brain slice is the preparation of choice. But the experiments will be challenging. Preliminary cell-attached patch-clamp recordings on cortical neuron somata in rat brain slices (M. Martina, G. Mealing, C.E. Morris, unpublished observations) confirm that recording the kinetics of native Nav (Nav1.2) channels in pyramidal neurons in slices is feasible. Nav density in the soma is lower than in axon initial segments. The latter represents an even more difficult, but not impossible[13] prospect for cell-attached recording. Curiously, a recently-reported technique for characterizing native axonal Nav channel kinetics involves patching axonal blebs shed from brain slice bleb patch; clearly that will not serve for comparing Nav kinetics before, during and after blebbing trauma. With cell-attached recordings, a high-K solution zeroes the cell once a gigaohm seal forms, but it swells all cells; this makes one patch per slice the limit. Moreover, since trauma is irreversible (on the time scale of experiments) only one pass is possible. Improving signal-to-noise via a second pass, or probing the time course of trauma in a given patch with a series of different protocols, is out of the question. Given the clinical importance of understanding how native Nav channels respond to mechanically-induced blebbing, and the high bar for success, simulations and theoretical studies such as presented here are warranted. They should help with devising protocols that can generate maximally information-rich data sets from one-pass experiments on brain slice patches.

2. Model and simulations

2.1. Model

We approximate voltage-clamped macroscopic Nav1.6 currents as observed in cell-attached patches of *Xenopus* oocytes (see Fig. 2) using a HH-type model. For the modeled conductance, the goal is to "pre-test" clamp protocols that might prove useful in exploring irreversible trauma-induced modifications in recombinant and, more importantly, native Nav1.6

and Nav1.2 channels. Cell-attached patch recordings on neurons will not always yield "pure" Nav channel current, but the point of this modeling effort is not to predict patch currents in detail, it is to capture the broad features of observed (from oocyte patches) and expected (from cortical neuron patches on the soma or axon initial segment) I_{Na} before, during, and after a membrane trauma caused by pipette aspiration.

Transient sodium current, I_{tr}, is modeled after Schwarz et al. [24]'s HH type[10] description of peripheral human node of Ranvier currents as:

$$I_{tr} = m^3 h g_{tr}(V_m - E_{Na}), \tag{1}$$

with V_m the membrane potential, $g_{tr} = 20$ nS the maximal conductance through Nav channels and E_{Na} the sodium reversal potential. m and h are the activation and inactivation variables - such that m^3h gives the open probability of a channel - and are given by:

$$\frac{dm}{dt} = \alpha_m(1-m) - \beta_m m, \tag{2}$$

$$\frac{dh}{dt} = \alpha_h(1-h) - \beta_h h, \tag{3}$$

with rate constants, taken from Schwarz et al. [24], given by:

$$\alpha_m = 1.86\frac{(V_m + 18.4)}{1 - \exp\left((-18.4 - V_m)/10.3\right)}, \tag{4}$$

$$\beta_m = 0.086\frac{(-22.7 - V_m)}{1 - \exp\left((V_m + 22.7)/9.16\right)}, \tag{5}$$

$$\alpha_h = 0.0336\frac{(-111 - V_m)}{1 - \exp\left((V_m + 111)/11\right)}, \tag{6}$$

$$\beta_h = \frac{2.30}{1 + \exp\left((-28.8 - V_m)/13.4\right)}, \tag{7}$$

with voltages in mV, and rates in $(ms)^{-1}$.

The HH formulation assumes that inactivation (availability) and activation are independently voltage-dependent processes, but in our model we always shift them by the same amount, effectively coupling them. Since binding of the fast inactivation particle is inherently voltage independent but limited by (and hence "kinetically coupled to") the voltage dependent activation process, this works well to mimic experimental data (see Fig. 2Eiii and Wang et al. [31]).

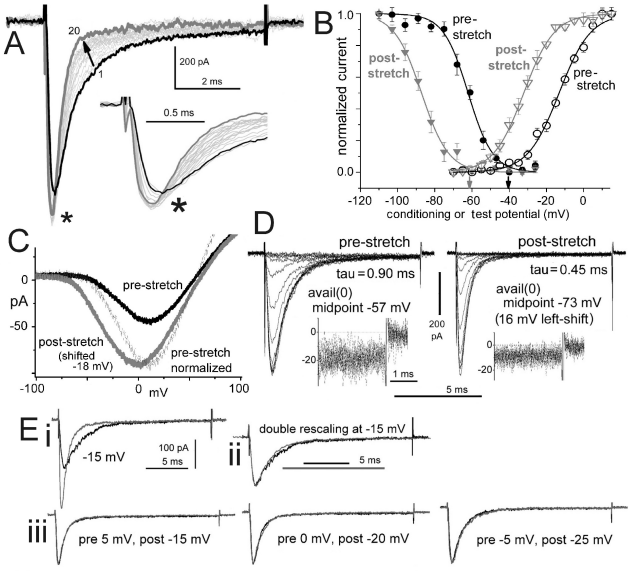

Figure 2: **Key findings about Nav1.6 trauma** (modified from [31]) **A**. I_{Na} near $g(V)_{max}$ during pipette aspiration (20 steps to −10 mV, 1 Hz; inset expands early I_{Na}). Noise, inevitable with single-sweep recordings used to monitor a continually changing time course, leaves it unclear if the pattern of change (asterisks) reliably reflects underlying kinetic changes. **B**. Traumatic stretch causes an irreversible hyperpolarizing shift of the Nav1.6 activation and fast inactivation Boltzmanns. **C**. Ramp currents (+100 mV down to −100 mV at 2 mV/ms) before and after stretch. **D**. Availability families pre and post trauma; tau-inactivation and steady-state current (expanded insets) at 0 mV both decrease. **E**. V_m-dependent Nav activation limits fast inactivation, conferring on macroscopic fast inactivation its voltage-dependent time course. **i** With trauma, macroscopic activation and fast inactivation accelerate irreversibly to essentially the same extent. **ii** Consequently, with appropriate time rescaling, normalized currents pre/post trauma overlap (see double-rescaled I_{Na} during steps to −15 mV pre/post trauma), and, **iii** depending on the extent of trauma, some particular value of hyperpolarization (20 mV in the example shown) predicts the post-trauma time courses of I_{Na}. This justifies the simple co-shifting of the HH formulation to various extents (in voltage) to model various extents of trauma.

It is not known whether the trauma-induced left-shift observed experimentally [31] is an all-or-none or graded process (see Fig. 1). For an all-or-none process, an individual channel is either intact or fully traumatized (left-shifted) whereas for a graded process, the mechanical insult left-shifts the entire affected population as a series of (arbitrarily small) steps. In either case, both the relative amount of the excitable system's channel-bearing membrane subjected to trauma and the intensity of that trauma need to be specified. This is dealt with by modeling Nav channel trauma with two parameters: the fraction of affected channels (AC) and the left-shift (in millivolts) of these affected channels (LS_{AC}). The total I_{tr} is then the sum of contributions from intact and shifted channels:

$$I_{tr} = (m^3h(1-AC) + m_{LS}^3 h_{LS} AC)(V_m - E_{Na})g_{tr}, \quad (8)$$

with m_{LS} and h_{LS} the activation and inactivation variables for left-shifted channels calculated by replacing V_m in Eqs. 4 to 7 by $(V_m + LS_{AC})$. Shifted channels retain the same (unitary) conductance and reversal potential, only their kinetic midpoints are modified.

Non-inactivating sodium current, I_{ni}, is taken to arise from a subpopulation of Nav channels (fixed relative to the total population at a ratio of 0.0075) that do not inactivate but that otherwise are kinetically identical to the Nav channels responsible for the transient current, I_{tr}. Chatelier et al. [7] (their Fig 5, third trace) give an example of a recombinant Nav1.6 channel in a several-channel patch temporarily behaving like this. Thus the kinetics of m_{ni}, the non-inactivating current activation variable, are given by Eqs. 4 and 5 and:

$$I_{ni} = m_{ni}^3(V_m - E_{Na})g_{ni}, \quad (9)$$

where g_{ni} is the maximal non-inactivating conductance.

2.2. Ramp Simulations

For negative- and positive-going ramps, ramp clamp is simulated by equilibrating at +150 mV (depolarized) then ramping at −2 mV/ms (unless specified differently) to −150 mV (hyperpolarized) - or the opposite, as appropriate.

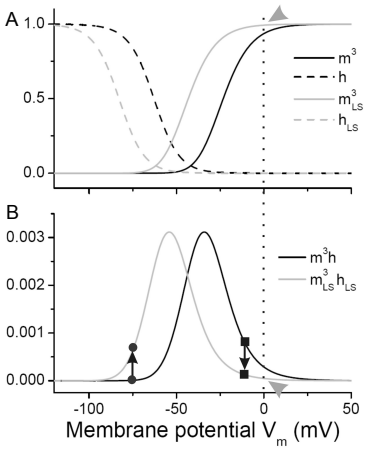

Figure 3: **The transient current component of I_{Na}. A**. Equilibrium plots for the activation (m) and inactivation (h) variables of intact and 20 mV left-shifted Nav channels. **B**. A steady-state open probability or window conductance (m^3h) results from overlap of activation and inactivation in Nav channels. For the intact case, m^3h yields "window current" between about −60 to 20 mV. Left-shifting both m and h left-shifts the window conductance $m_{LS}^3 h_{LS}$. Note that with left-shift, window conductance increases at values near typical neuronal resting potential (−75 mV is highlighted here; black circles) while decreasing near 0 mV (e.g., black squares at −10 mV).

2.3. Step Simulations

To simulate $I(t)$ traces during step protocols, the system is equilibrated at some potential, V_{hold}, then stepped to V_{step}. Experimentally, trauma time courses are monitored by stepping to some test potential at ∼ 1 Hz while the membrane patch is being traumatized. In simulations, the V_{hold} to V_{step} protocol is repeated but either the number of affected channels (AC) or the left-shift of the affected channels (LS_{AC}) is augmented to simulate progressively deeper trauma. For all simulations, E_{Na} = 60 mV.

3. Results

3.1. Use of ramp clamp

Fig. 4 shows that for negative-going ramps, current is nearly the same for 2 mV/ms and 0.1 mV/ms ramps, indicating that the faster ramp (requiring only 100 ms for a 200 mV excursion) is slow enough. For the positive-going ramps, however, 2 mV/ms partially stimulates I_{tr} indicating that this is "too fast". Although ramping at 0.1 mV/ms gives "pure" I_{ni} either way, it requires 2 s per 200 mV ramp excursion.

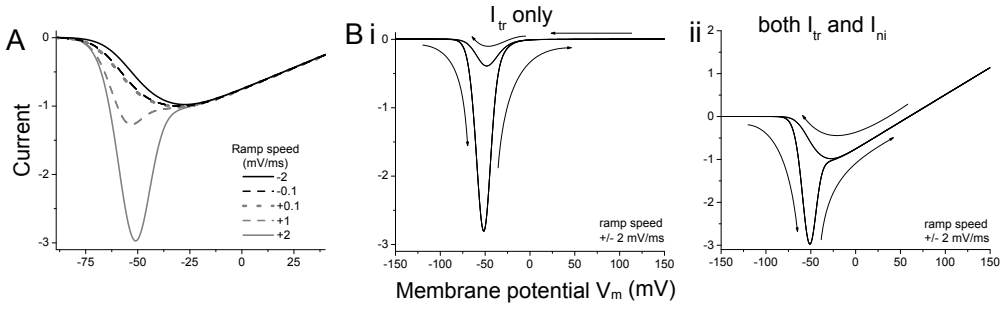

Figure 4: **Ramp and sawtooth clamp A**. Current responses to negative-going (black) and positive-going (grey) voltage ramps of various speeds (g_{ni}/g_{tr} = 0.0075), normalized to the peak current of the negative 0.1 mV/ms ramp. Above ~ −10 mV all plots overlap. Fast positive ramps activate I_{tr} as well as I_{ni}. **Bi,ii**. Current hysteresis (arrows indicate how voltage is applied) expected during sawtooth ramp clamp if, as labeled, only I_{tr} flows, or if both I_{tr} and I_{ni} contribute.

Except for the sawtooth clamp of Fig. 4B, negative-going 2 mV/ms ramps are used for further simulations here. Ramps in this speed range would be practicable with native channels in neuron patches, where low channel density would probably necessitate averaging many tens of ramp excursions before and again after trauma. Moreover, for higher channel densities (e.g., axon initial segments), repeated fast sawtooth ramps could allow for capture of a developing trauma during a sustained bout of pipette aspiration. Fig. 5C illustrates this point with single ramp traces of Nav1.6 current in an oocyte patch before and after increasingly intense bouts of aspiration. Fig. 4Bi, ii show simulated current elicited by a sawtooth clamp (time sequence indicated by arrows) of −150 to +150 to −150 at 2 mV/ms repeated twice; the two trajectories overlap completely, indicating that the ramp captures a dynamic steady-state. If membrane patches tolerated the voltage extremes poorly, brief plateaux (at say −120 and +80 mV) could be interjected. Fig. 4Bi shows the hysteresis expected if a patch had only I_{tr} and 4Bii shows what the same sawtooth yields with I_{ni} present. A sawtooth at this speed should simultaneously detect changes in window-like and non-inactivating variants of I_{Na} during the course of trauma. Of course the current amplitudes must exceed the background noise. If nothing else, an ensemble average of the sawtooth currents should reveal the size of (I_{ni} + I_{tr}) as they reversed near E_{Na}. Note that I_{tr} elicited by ramps becomes maximal at more hyperpolarized voltages than the peak of m^3h (the window conductance) (see Fig. 3).

When left-shifted Nav channel operation is involved, it is incorrect simply to consider Nav channels "leakier" only if, at or near 0 mV (see vertical line, arrowheads in Fig. 3B), the ratio [steady-state current]/[peak current] is higher in the experimental vs the control condition. If g_{ni} and/or g_{tr} increased, the ratio would change in this way, but if left shift was responsible for the "leak", it would not. In that case, the only change evident at 0 mV would involve the decreased "0 mv tails" of steady-state I_{tr} . This reasoning would also apply when comparing mutant vs WT Nav channels, drug-modulated vs control Nav channel operation, or here, trauma-modulated vs intact Nav operation.

4. Determining if non-inactivating Nav channels shift with membrane trauma

Fig. 5C illustrates cell-attached patch currents for recombinant Nav1.6 during a negative-going ramp. Non-inactivating current is evident. If all the channels contributing to this ramp current were capable of inactivation, then, based on Fig. 3, steady-state I_{tr} should be near-zero at depolarized potentials. Since, instead the ramp I_{Na} is ever-increasing as 0 mV is approached, non-inactivating channels must be contributing. Modeling g_{ni} as 0.75% of g_{tr} (Fig. 5A) gives a qualitative match with Fig. 5C.

It is notable (Fig. 5Ai) that maximal I_{ni} occurs at a more depolarized potential than the maximal transient (window) ramp current. The latter is a function of activation, inactivation and driving force such that $m^3h(V_m - E_{Na})$ is maximized. For I_{ni} the maximum is a function of only activation and driving force such

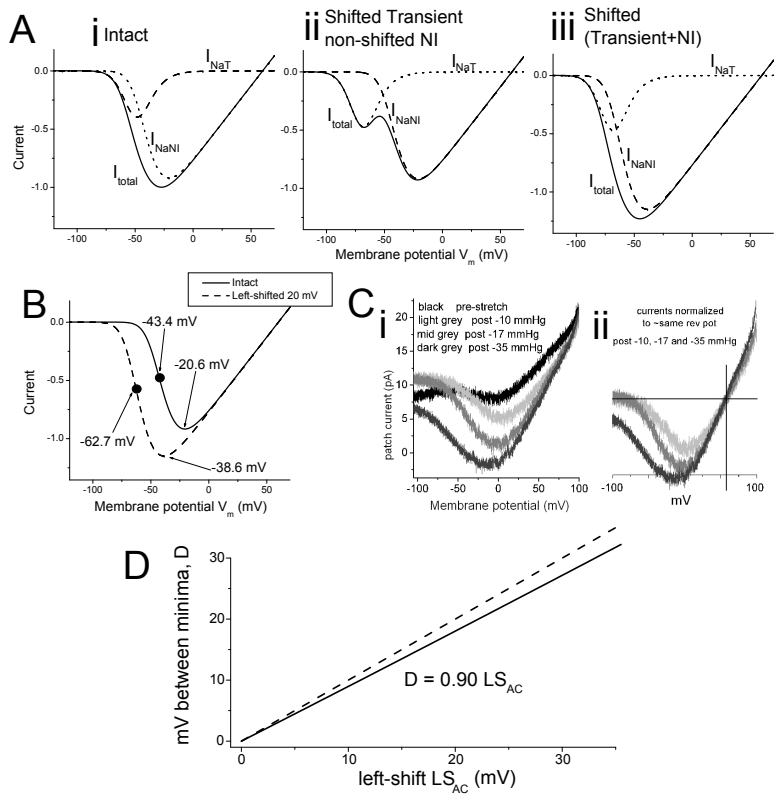

Figure 5: **Ramp currents and trauma. A**. Simulated I-V relations for a ramp starting at +150 mV to −150 mV at 2 mV/ms. The three curves are for I_{tr}, I_{ni} and their sum I_{total}. For depolarized potentials I_{ni} is non-zero whereas it is zero for I_{tr}. "Peak" I_{ni} amplitudes are at more depolarized potentials than those for I_{tr}. **B**. Simulated I-V relation for intact and left-shifted (20 mV) non-inactivating currents only. Membrane potential is ramped from +150 mV to −150 mV at 2 mV/ms. Although I_{ni} activation is left-shifted by 20 mV, the distance between the current minima (−20.6 mV intact and −38.6 mV left-shifted) is 18 mV. Similarly, the current midpoint (shown with dots) (−43.4 mV and −62.7 mV) is shifted by 19.3 mV. **Ci**. A raw data set (obtained as in Fig. 2C) for ramp current measured after increasingly large ∼ 20 s bouts of suction at the values listed; as frequently occurs with ramps, baseline drift was an issue. **ii**. The 3 best-behaved traces are "normalized" on the current axis till each has the same reversal potential; this Nav1.6-based I_{ni} appears to have left-shifted with trauma. **D**. Numerical solution of Eq. 10 fitted with a straight line whose slope (0.9) indicates that the voltage gap between the non-inactivating ramp current minima is less than LS_{AC}. The dashed line represents a slope of 1.

that $m_{ni}^3(V_m - E_{Na})$ is maximized. Essentially, (ramp) I_{ni} depends on a single Boltzmann function whereas (ramp) I_{tr} depends on the product of two Boltzmanns (activation and availability).

For the chosen conductance ratio $g_{ni}/g_{tr} = 0.0075$, the simulation was run in 3 different scenarios: both intact, only g_{tr} left-shifted, both g_{tr} and g_{ni} left-shifted to the same extent. Comparing simulations to data like that in Fig. 5C (see also Fig. 2C) will make it possible to assess whether both transient and non-inactivating Nav1.6 currents left-shift with membrane stretch. Certainly, recombinant g_{tr} left-shifts[31] and if it were the only component to do so, ramp traces would show a hump (see Fig. 5Aii, total current) in the case of widely separated (∼ 20 mV) I_{tr} and I_{ni}. Since the recombinant traces showed no evidence of humps, a simple interpretation is that both I_{ni} and I_{tr} left-shifted with membrane trauma.

It will generally be easier, in experiments, to measure a maximal ramp I_{ni} than to determine the g_{ni} midpoint (e.g., see double-hump ramp currents in Fig. 2A(a and b) of Wu et al. [36]). In simulation of g_{ni} left-shift, the maximal I_{ni} moves "down" and leftward due to increased open probability at more hyperpolarized potentials. However, the difference between intact and left-shifted maximal I_{ni} is less than the trauma-induced left-shift of the underlying kinetics. For a 20 mV left-shift, the distance between the maxima is 18 mV (−20.6 mV for intact $I_{ni}(V)$, −38.6 mV for left-shifted $I_{ni}(V)$) as seen in Fig. 5B. This requires further explanation.

Maximal I_{ni} is found by requiring that the derivative of I_{ni} (Eq. 9)versus membrane potential be zero, which yields the relation:

$$3m_{ni-min}^2(V_{min} - E_{Na})\frac{dm_{ni}}{dV_m} + m_{ni-min}^3 = 0. \qquad (10)$$

Here, m_{ni-min} is the steady-state value of m_{ni} for "minimum" I_{ni} (=maximal negative amplitude, by convention), and m_{ni-min} is a function of both V_m and of the left-shift (LS_{AC}). Eq. 10 can be solved numerically for V_{min} which is a function of LS_{AC}. Fig. 5D plots the displacement of maximal I_{ni} for a left-shifted g_{ni} vs its left-shift. Approximating the

solution as a straight line, the slope factor is 0.9, and hence the displacement of the maximal I_{ni} grows more slowly than the left-shift of the channel kinetics. A slope factor of 1 would require that $m_{ni}(V)$ be infinitely steep. Similar considerations apply for current midpoints (instead of minima), which are (see Fig. 5B) −43.4 and −62.7 mV for a midpoint shift of 19.4 mV (i.e., $< LS_{AC} = 20$ mV).

For recombinant Nav1.6, Wang et al. [31] observed an 18 mV post-stretch left-shift of (predominantly) non-inactivating ramp current (see Fig. 2C) in a recombinant system where trauma-induced left-shift I_{tr} left-shift averaged $\sim$ 20 mV. That is anecdotal, but if $g_{ni}(V)$ and $g_{tr}(V)$ do left-shift together, trauma probably modulates their voltage-sensor motions the same way.

4.1. The molecular process: all-or-none versus graded

For an individual Nav channel, trauma-induced shift could bespeak an all-or-none event or a graded process (Fig. 1). An all-or-none change would result from a discrete molecular "lesion" event (e.g., mechanical dissociation from G-ankyrin, exposure of a binding site for, say, a modulatory G-protein, dissociation/association of a regulatory lipid molecule). A graded shift at the individual channel level would likely result from a progressively changing membrane environment such as a graded increase in bilayer fluidity and/or thickness. From a clinical perspective, it will be important to uncover the molecular mechanism of trauma-induced left-shift.

After trauma in oocyte patches[31] (Fig. 2B), Nav1.6 activation (and availability) curves remain parallel to the pre-trauma curves, but it was not ascertained if maximal trauma had been achieved. Parallel shifting indicates that all channels left-shifted equally but does not permit unequivocal determination that the underlying process is graded and not all-or-none. Both can potentially yield a parallel shift: in graded response scenarios, activation curves must remain parallel as there is only one population; in all-or-none scenarios, trauma severe enough to affect every channel leaves only one (left-shifted) population.

In principle one could sort this out using patches with only one or two Nav channels, but in practice, this is not feasible. Given the tiny membrane area needed for single channel patches, gigaohm sealing itself would likely pre-traumatize the membrane. In any case, Nav channel density is $>$ 150 channels μm^{-2} where neurons are most susceptible to membrane injury, the axon initial segment[17, 23] - far too high for single channel recording.

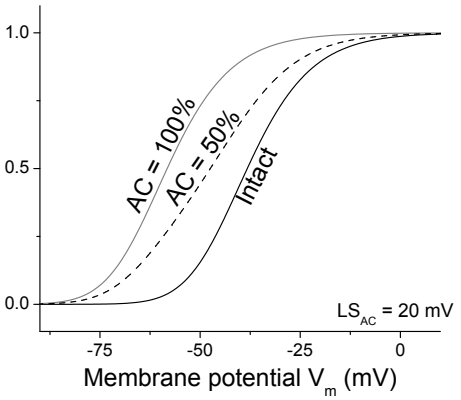

Figure 6: **Activation curves and trauma scenarios.** Activation boltzmann (m^3) for an intact population ($AC = 0\%$), a half intact half left-shifted population ($AC = 50\%$,$LS_{AC} = 20$ mV) and a fully left-shifted population ($AC = 100\%$,$LS_{AC} = 20$ mV). When there are two populations of channels ($AC = 50\%$) the slope of the combined activation is shallower than that of a single (intact or left-shifted) population.

Thus, experimental approaches involving macroscopic current are needed to distinguish between graded and all-or-none left-shift processes. With macroscopic current, it is crucial to ascertain (for a given bout of pipette aspiration) whether all or only a fraction of the channels contributing current have left-shifted. Ideally, application of even more intense aspiration pressure would "saturate" the shift, but, given the ever-present risk of patch rupture, some finesse is required.

Fig. 6 shows activation curves of three systems: one intact ($AC = 0\%$), one fully traumatized ($AC = 100\%$, $LS_{AC} = 20$ mV) and one partially traumatized ($AC = 50\%$, $LS_{AC} = 20$ mV). The partially traumatized system sums the $AC = 0\%$ and $AC = 100\%$ cases and accordingly has a shallower slope than the other 2 cases. Had left-shift of affected channels been very large (say $LS_{AC} = 100$ mV), a clear plateau at 0.5 would have been evident.

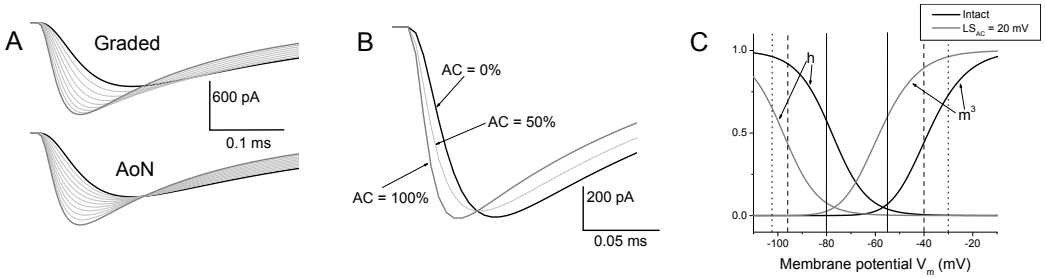

Figure 7: **Use of step protocols.** **A**. Current response to a potential step from −120 mV to −30 mV with the graded (top) and all-or-none (bottom) mechanisms showing progressive trauma from intact (black lines) to fully left-shifted (dark grey). This set of potentials does not allow the left-shift mechanism to be easily identified. **B**. Current responses in the all-or-none mechanism using LS_{AC} = 20 mV, V_{hold} = −110 mV, V_{step} = −10 mV for three different values of AC. The $AC = 0\%$ and $AC = 100\%$ cases intersect, and all the other traces (only $AC = 50\%$ is shown here for clarity) go through that point. **C**. Activation (m^3) and inactivation (h) for an intact (black line) and fully left-shifted (grey) channel. The potentials used in the voltage step simulation are also shown here as vertical lines: dotted: −102 to −30 mV; dashed: −96 to −40 mV; solid: −80 to −55 mV. These potentials were chosen for illustration purposes because they yield intact and fully left-shifted traces with approximately equal maximum currents.

Alternatively, if channels in (say) 5 sub-regions of clamped membrane were shifted by 20, 40, 60, 80 and 100 mV respectively, the activation curve would have a very shallow slope. If the provenance of such a curve was misconstrued, incorrect assumptions about molecular mechanisms would result. Interestingly, for a mechanosensitive channel (MscL), Chiang et al. [8] report this kind of circumstance: structural data show that MscL expands ∼ 20 nm^2 on opening, but recording conditions during membrane stretch generate a shallow activation curve that, were one to assume a two-state channel, would yield an estimate of only ∼ 6 nm^2. For Nav1.6 channels, we pointed out that non-parallel activation(V) curves would have left open the possibility of an all-or-none process. The MscL example highlights an additional point, namely, that an assumption of uniform membrane mechanics is made in this analysis, but with the caveat that insofar as channel left-shift results from changes in membrane mechanics, such changes are modeled implicitly in AC and LS_{AC}.

4.2. Use of multistep protocols

In graded Nav responses, a single population of channels left-shifts progressively until a maximal value "X" mV is attained; the time course will vary with pipette aspiration intensity. In all-or-none responses, the relative weight of two distinct populations (intact channels or ones left-shifted by X mV) changes, with the X-shifted portion increasing progressively with trauma. The two scenarios differ starkly enough that, during aspiration-induced patch trauma, they could be exploited to distinguish all-or-none from graded responses, without generating a time series of well-resolved activation curves. Step protocols are needed, that, as trauma progresses, yield qualitatively different patterns of traces for each scenario.

To simulate a graded process, a voltage step protocol is run repeatedly while incrementally sliding the black lines in Fig. 7C (and Fig. 3A) towards the grey lines whereas for an all-or-none process, every channel behaves as either intact or "X"-shifted (black and grey lines in Fig. 7C). To illustrate the importance of appropriate step and holding potentials, note the outcome (Fig. 7A). Noiseless traces would be required to distinguish the 2 scenarios (based on the crossover point in the all-or-none case); as Fig. 2A illustrates, single sweep patch traces captured during the course of pipette aspiration trauma are inherently noisy. Ruling out the all-or-none case from a pattern of traces such as this would be unwise. However, the basic approach is easily enhanced with multistep protocols (e.g., an 8-step, 4 voltage protocol with two V_{hold} and two V_{step} levels) that greatly increase the likelihood that distinctive-looking graded or all-or-none patterns of traces are resolved.

A useful protocol (see Fig. 8) will include 1) a V_{hold} at which availability ($h(V)$) is less for the left-shifted than the intact case (e.g., −105 mV in Fig. 7C), 2) a V_{step} where activation ($m^3(V)$) is greater

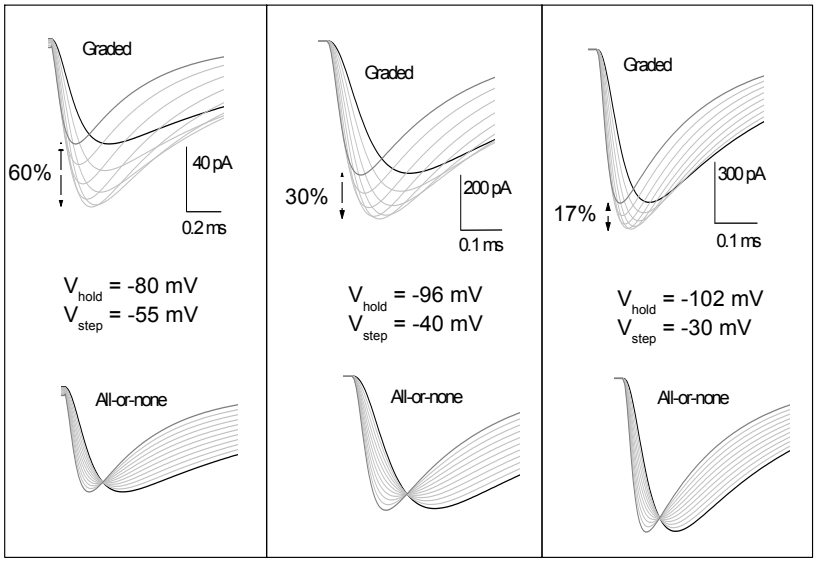

Figure 8: **Optimal step protocols for distinguishing graded from all-or-none responses.** Simulated current traces during depolarizing steps: left: from −80 to −55 mV, middle: from−96 to −40 mV and right: from −102 mV to −30 mV simulated with the graded (top row) and all-or-none (bottom row) mechanisms. Intact responses: black lines; partially traumatized: light grey lines; fully traumatized: dark grey lines.

for the left-shifted case (e.g., −30 mV), and 3) a set of V_{hold} and V_{step} where intact and fully left-shifted system have approximately equal currents. This last condition is not *sine qua non*, but in the face of experimental noise would make the difference between the mechanisms more easily detectable.

In an all-or-none process, the above scenario does not yield a particularly different result from using any other holding and step potentials; the graded response can, however, be distinguished. As the channels become incrementally left-shifted, the increase of $m^3(V)$ at V_{step} ensures an increase in peak current until decreasing $h(V)$ causes peak current to fall.

This distinctive increase-then-decrease of peak current as trauma progresses could be identified experimentally: it never occurs for an all-or-none mechanism, where total current - always the sum of contributions from the two populations (i.e., AC = 0% and AC = 100%) - never exceeds the envelope of the two. In an all-or-none process, peak current either increases or decreases with increasing AC, depending on which curve (initial/intact or final/traumatized) has the biggest peak current. Moreover, the pattern of currents as trauma deepens features has a fixed crossover point that is absent for graded changes in a single population. The unique crossover point (all-or-none case) is explained by total current being constrained between AC = 0% and AC = 100%; all intermediate traces must intersect at the same time point as do the extremes.

In the graded mechanism the situation is different: AC is fixed at 100% but LS_{AC} increases gradually. For small left-shifts, the value of $m(V)$ at V_{step} increases and its time constant becomes smaller thus resulting in a larger peak current. However as the left-shift increases, $h(V)$ at V_{hold} also decreases to a point where peak current no longer increases with left-shift but starts decreasing. This behavior allows the scenarios to be unequivocally distinguished (as seen in Fig. 8): with all-or-none, all the intermediate traces between the initial (intact) and final (fully left-shifted) condition have a smaller peak amplitude than either the initial and the final curves. In the graded case, all the intermediate traces have a larger peak current than the initial and final curves.

5. Discussion

Mechanisms underlying the "TTX-sensitive Na^+ leak" of mechanically damaged neurons[2, 34] remain unknown. Nevertheless, from recombinant patch clamp and immunohistochemistry of the CNS[19] it is plausible that the initial mechanically-induced I_{Na} change (prior to calcium excitotoxicity[11]) bespeaks left-shifted operation of Nav channels in mechanically-blebbed[31] axolemma. Recombinant Nav current is monitored before, during and after trauma-level pipette aspiration of cell-attached patches. Native channels in brain slice preparations need to be subjected to comparable procedures. To facilitate progress in the very challenging slice preparation, we have computationally tested ramp and step protocols to see which might best reveal transient and persistent components of I_{Na} change with progressively deeper membrane trauma. The rationale for and benefits of specific protocols are given in the Results section, so we will not reiterate those here. Instead we briefly discuss how the model we used constrains our findings, thereby implying where protocols for native channels might usefully be adjusted to take those constraints into account.

We modeled $I_{Na}(V,t)$ using a standard HH formulation except that, to mimic trauma, the Boltzmann curves for activation and availability were always left-shifted by exactly the same amount. This mimics the effect of aspiration-trauma on recombinant human Nav1.6 current and straightforwardly acknowledges the kinetic coupling of (inherently voltage-insensitive) inactivation to (inherently voltage-sensitive) activation. Parameter values reported for human node of Ranvier Nav channels[24] (now known to be Nav1.6 channels[5]) were used in the model. Strikingly, window conductance (m^3h) was still appreciable near 0 mV, providing a qualitative explanation for an unexpected experimental observation[31], namely that steady-state recombinant Nav1.6 current near 0 mV decreases with trauma. Our assumption prior to doing those experiments[31] had been that any steady-state I_{Na} near 0 mV would reflect a "persistent sodium current" that would increase with trauma, thereby explaining post-trauma TTX-sensitive Na^+ leaks. This proved to be entirely wrong. Nevertheless, as seen here, observed decrease is readily explained, qualitatively speaking, by trauma-induced left-shift of I_{tr}. Moreover, in a companion publication[4], we show that left-shifted I_{tr} would dissipate an axon's Na^+ gradient, thus triggering Ca-excitotoxicity.

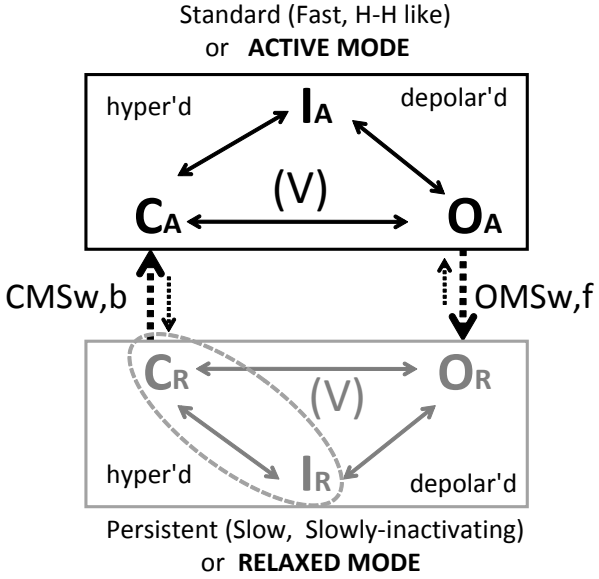

Figure 9: **A simplified scheme suggesting how g_{tr} and g_{ni} might interact.** Nav channel states are reduced to a lumped closed state (C), an open state (O) and an inactivated state (I) with voltage sensor motions (V) enabling the channel to get from C to O. There are two modes, Active (A) and relaxed (R), hence the subscripts on C,O,I. Once in $\mathbf{O}_A$ the channel can undergo the **f**orward **m**ode-**sw**itch transition (OMSw,f) into a variously long-lived ("persistent") state, O_R. Then, if the membrane hyperpolarizes, the channel will enter $\mathbf{C}_R$ and thence, via the **b**ack **m**ode-**sw**itch (CMSw,b) to C_A, the state favored at a strongly hyperpolarized V_{hold}. As implied by the multiple labels for each two gating modes, ACTIVE mode would supply traditional I_tr, including window current, whereas RELAXED mode would supply slowly-inactivating or "non-inactivating" persistent current. Drugs like riluzole and ranolazine[35] act by stabilizing I_R and C_R (dashed ellipse). For both ischemic and traumatic axonal blebs[23], a highly desirable trait for neuroprotective Nav blockers would be an even higher affinity for I_R and C_R in blebbed than in intact membrane.

Although an allosteric Markov modification of HH elegantly produces a subthreshold persistent I_{Na}[27], it generates no non-inactivating type I_{Na} and so would not have provided a comprehensively better model here. Nav channels (including Nav1.6) do produce the type of "persistent" currents that we modeled via g_{ni}, even though they are decid-

edly elusive, both theoretically and experimentally speaking[5, 7, 25, 33]. Recombinant Nav1.6 in HEK cells yield, in our experience, several-fold larger whole-cell ramp currents with negative-going slow ramps (unpublished observations) than with standard (moderately fast) positive-going ramps[5]. In the present work, we suggest using moderately fast negative-going ramps as part of sawtooth waveforms as a way to distinguish I_{tr} from I_{ni} in ramp currents. However, our model for I_{ni} does not assume that the two components can interchange kinetically. When they do (in situ) the hysteresis observed is likely to be even more dramatic than what is depicted here, and the slow ramps we eschewed might well need to be reincorporated. The efficacy of ultra slow negative-going ramps in "growing" the amplitude of I_{ni} would suggest that a kinetic scheme like that in Fig. 9 was operating. This scheme posits that activated Nav channels undergo a slow voltage-independent "Mode Switch" transitions. Native cardiac (Nav1.5) channels evidently do so[21], as do HCN2 pacemaker channels[18]. In fact, Villalba-Galea et al. [29] suggest that in all voltage-gated proteins, a slow conformation change of the voltage sensor (possibly from a rigid 3_{10}-helix to a relaxed α-helix) or mode-switch (see Lin et al. [15]) becomes likely when a sensor is in its "active" state. Presumably Nav channel inactivation particles bind poorly for relaxed (compared to active state) channels so a "slow-mode persistent current" results. Seen at the single channel level, "non-inactivating" ("modal") channels or late- reopening channels[31] might result from excursions into the relaxed mode. While these ideas are interesting and important, it would have been premature to explicitly include such provisions in our model for persistent current. We instead used a kinetically simple, fully non-inactivating conductance (g_{ni}).

Assuming native neuronal Nav channels left-shift in blebbed membrane, it will be important to ascertain how. A simple possibility consistent with findings to date is that the more fluid bilayer of a blebbed (versus intact) plasma membrane lowers the barrier for the rate-limiting voltage sensor movement leading to opening. This could result in a graded process wherein all the channels in a patch collectively left-shift with progressive trauma. In an all-or-none mechanism the blebbing process would have to be locally completed in a single step, such that any individual channel is either intact or left-shifted and trauma progresses in a patch by increasing number of channels in blebs. In this vein a possibility with some appeal is that physical anchoring of Nav channels (via ankyrin, perhaps) keeps channels in a strongly right-shifted kinetic state until physical disruption of the Nav-anchor interaction occurs. Other all-or-none possibilities unrelated to bleb formation per se would include physical exposure of previously cryptic binding site for some abundant ligand or loss of bound bilayer-resident modulator ligand. What we show here is that during sustained aspiration-induced trauma, current responses to depolarizing voltage-steps (with carefully chosen V_{hold} and V_{step}) would differ qualitatively in graded vs all-or-none scenarios, allowing the class of mechanism to be identified.

Native I_{tr} and I_{ni} might well respond to trauma in the same way as recombinant Nav1.6 channels, i.e., irreversibly left-shifted I_{tr} operation plus left-shifted and augmented g_{ni} (as per Fig. 2). If so, for both recombinant and native settings, a unifying explanation suggests itself, based on the scheme in Fig. 9, and on the fundamental mechanosensitivity of voltage-gated channels: the bleb-bilayer in which Nav channels are embedded post-trauma promotes the OMSw,f transition and/or inhibits CMSw,b while simultaneously favoring (lowering the barrier for) the rate-limiting voltage sensor motions leading from C to O. In other words, trauma-induced change in the bilayer mechanics of this channel, would simultaneously change rates for multiple transitions in the channel, as occurs with Kv channels[9]. An important goal would then be to ask how known and putative neuroprotective reagents - be they Nav inhibitors[2, 35] or non-specific reagents like PEG[3] - further affect gating of bleb-resident Nav channels.

References

[1] Agrawal, N., Hamam, B., Magistretti, J., Alonso, A., Ragsdale, D., 2001. Persistent sodium channel activity mediates subthreshold membrane potential oscillations and low-threshold spikes in rat entorhinal cortex layer V neurons. Neurosci. 102 (1), 53–64.

[2] Ates, O., Cayli, S., Gurses, I., Turkoz, Y., Tarim, O., Cakir, C., Kocak, A., 2007. Comparative neuroprotective effect of sodium channel blockers after experimental spinal cord injury. J. Clin. Neurosci. 14 (7), 658–665.

[3] Baptiste, D., Austin, J., Zhao, W., Nahirny, A., Sugita, S., Fehlings, M., 2009. Systemic Polyethylene Glycol Promotes Neurological Recovery and Tissue Sparing in Rats After Cervical Spinal Cord Injury. J. Neuropathol. Exp. Neurol. 68 (6), 661.

[4] Boucher, P.-A., Joós, B., Morris, C., 2010. Traumatic brain injury, axonal sodium loading and excitogenicity: modeling the impact of left-shifted Nav channel operation at blebbed nodes of Ranvier. in thesis.

[5] Burbidge, S., Dale, T., Powell, A., Whitaker, W., Xie, X., Romanos, M., Clare, J., 2002. Molecular cloning, distribution and functional analysis of the NaV1. 6. Voltage-gated sodium channel from human brain. Mol. Brain Res. 103 (1-2), 80–90.

[6] Charras, G., Coughlin, M., Mitchison, T., Mahadevan, L., 2008. Life and times of a cellular bleb. Biophys. J. 94 (5), 1836–1853.

[7] Chatelier, A., Zhao, J., Bois, P., Chahine, M., 2010. Biophysical characterisation of the persistent sodium current of the Na v 1.6 neuronal sodium channel: a single-channel analysis. Pflügers Archiv Eur J Physiol 460, 1–10.

[8] Chiang, C., Anishkin, A., Sukharev, S., 2004. Gating of the large mechanosensitive channel in situ: estimation of the spatial scale of the transition from channel population responses. Biophys. j. 86 (5), 2846–2861.

[9] Finol-Urdaneta, R., McArthur, J., Juranka, P., French, R., Morris, C., 2010. Modulation of KvAP Unitary Conductance and Gating by 1-Alkanols and Other Surface Active Agents. Biophys. J. 98 (5), 762–772.

[10] Hodgkin, A., Huxley, A., 1952. A quantitative description of membrane current and its application to conduction and excitation in nerve. J. Physiol 117, 500–544.

[11] Iwata, A., Stys, P., Wolf, J., Chen, X., Taylor, A., Meaney, D., Smith, D., 2004. Traumatic axonal injury induces proteolytic cleavage of the voltage-gated sodium channels modulated by tetrodotoxin and protease inhibitors. J. Neurosci. 24 (19), 4605.

[12] Ji, S., Sun, W., George, A., Horn, R., Barchi, R., 1994. Voltage-dependent regulation of modal gating in the rat SkM1 sodium channel expressed in Xenopus oocytes. J. Gen. Physiol. 104 (4), 625.

[13] Kole, M., Ilschner, S., Kampa, B., Williams, S., Ruben, P., Stuart, G., 2008. Action potential generation requires a high sodium channel density in the axon initial segment. Nat. Neurosci. 11 (2), 178–186.

[14] Kovalsky, Y., Amir, R., Devor, M., 2008. Subthreshold oscillations facilitate neuropathic spike discharge by overcoming membrane accommodation. Exp. Neurol. 210 (1), 194–206.

[15] Lin, W., Laitko, U., Juranka, P., Morris, C., 2007. Dual stretch responses of mHCN2 pacemaker channels: accelerated activation, accelerated deactivation. Biophys. J. 92 (5), 1559–1572.

[16] Lingwood, D., Simons, K., 2010. Lipid rafts as a membrane-organizing principle. Science 327 (5961), 46.

[17] Lorincz, A., Nusser, Z., 2010. Molecular identity of dendritic voltage-gated sodium channels. Science's STKE 328 (5980), 906.

[18] Männikkö, R., Pandey, S., Larsson, H., Elinder, F., 2005. Hysteresis in the Voltage Dependence of HCN Channels. J. Gen. Physiol. 125 (3), 305–326.

[19] Maxwell, W., 1996. Histopathological changes at central nodes of Ranvier after stretch-injury. Microscopy research and technique 34 (6), 522–535.

[20] McIntyre, C., Grill, W., 2002. Extracellular stimulation of central neurons: influence of stimulus waveform and frequency on neuronal output. J. Neurophysiol. 88 (4), 1592.

[21] Patlak, J., Ortiz, M., 1985. Slow currents through single sodium channels of the adult rat heart. J. Gen. Physiol. 86 (1), 89.

[22] Rakowski, R., Gadsby, D., De Weer, P., 2002. Single ion occupancy and steady-state gating of Na channels in squid giant axon. J. Gen. Physiol. 119 (3), 235.

[23] Schafer, D., Jha, S., Liu, F., Akella, T., McCullough, L., Rasband, M., 2009. Disruption of the axon initial segment cytoskeleton is a new mechanism for neuronal injury. J. Neurosci. 29 (42), 13242–13254.

[24] Schwarz, J., Reid, G., Bostock, H., 1995. Action potentials and membrane currents in the human node of Ranvier. Pflügers Archiv European Journal of Physiology 430 (2), 283–292.

[25] Shirahata, E., Iwasaki, H., Takagi, M., Lin, C., Bennett, V., Okamura, Y., Hayasaka, K., 2006. Ankyrin-G regulates inactivation gating of the neuronal sodium channel, Nav1. 6. J. Neurophysiol. 96 (3), 1347.

[26] Stys, P., Sontheimer, H., Ransom, B., Waxman, S., 1993. Noninactivating, tetrodotoxin-sensitive Na+ conductance in rat optic nerve axons. Proc. Natl. Acad. Sci. USA 90 (15), 6976.

[27] Taddese, A., Bean, B., 2002. Subthreshold sodium current from rapidly inactivating sodium channels drives spontaneous firing of tuberomammillary neurons. Neuron 33 (4), 587–600.

[28] Vanoye, C., Lossin, C., Rhodes, T., George, A., 2006. Single-channel properties of human NaV1. 1 and mechanism of channel dysfunction in SCN1A-associated epilepsy. J. Gen. Physiol. 127 (1), 1.

[29] Villalba-Galea, C., Sandtner, W., Starace, D., Bezanilla, F., 2008. S4-based voltage sensors have three major conformations. Proc. Natl. Acad. Sci. USA 105 (46), 17600.

[30] Wan, X., Juranka, P., Morris, C., 1999. Activation of mechanosensitive currents in traumatized membrane. Am. J. Physiol. 276 (2), C318.

[31] Wang, J., Lin, W., Morris, T., Banderali, U., Juranka, P., Morris, C., 2009. Membrane trauma and Na+ leak from Nav1. 6 channels. Am. J. of Physiol. 297 (4), C823.

[32] Webb, J., Wu, F., Cannon, S., 2009. Slow inactivation of the NaV1. 4 sodium channel in mammalian cells is impeded by co-expression of the β1 subunit. Pflügers Arch. Eur. J. Physiol. 457 (6), 1253–1263.

[33] Welch, N., Lin, W., Juranka, P., Morris, C., Stys, P., 2008. Traditional AMPA receptor antagonists partially block

Nav1. 6-mediated persistent current. Neuropharmacology 55 (7), 1165–1171.

[34] Wolf, J., Stys, P., Lusardi, T., Meaney, D., Smith, D., 2001. Traumatic axonal injury induces calcium influx modulated by tetrodotoxin-sensitive sodium channels. J. Neurosci. 21 (6), 1923.

[35] Wu, S., Chen, B., Hsu, T., Peng, H., Wu, Y., Lo, Y., 2009. Analytical studies of rapidly inactivating and noninactivating sodium currents in differentiated NG108-15 neuronal cells. J. Theor. Biol. 259 (4), 828–836.

[36] Wu, S.-N., Lo, Y.-C., Shen, A.-Y., Chen, B.-S., 2011. Contribution of non-inactivating Na+ current induced by oxidizing agents to the firing behavior of neuronal action potentials: experimental and theoretical studies from NG108-15 neuronal cells. Chinese Journal of Physiology 54 (1), DOI: 10.4077/CJP.2011.AMM002.

[37] Yang, R., Wang, W., Chen, J., Xie, R., Hu, S., 2009. Gabapentin selectively reduces persistent sodium current in injured type-A dorsal root ganglion neurons. Pain 143 (1-2), 48–55.

Chapter 5

Traumatic brain injury, axonal sodium loading and excitogenicity: modeling the impact of left-shifted Nav channel operation at blebbed nodes of Ranvier

P-A Boucher, B Joós and CE Morris

Traumatic brain injury, axonal sodium loading and excitogenicity: modeling the impact of left-shifted Nav channel operation at blebbed nodes of Ranvier

Pierre-Alexandre Boucher[a], Béla Joós[a], Catherine E. Morris[b]

[a]*Institut de physique Ottawa-Carleton*
Campus de l'Université d'Ottawa
Ottawa, Ontario, Canada, K1N 6N5
[b]*Neurosciences, Ottawa Health Research Institute*
Ottawa, Ontario, Canada, K1Y 4E9

Abstract

During trauma, stretch/shear experienced by axons irreversibly damages voltage-gated Na^+ (Nav) channels, causing axonal Na^+-loading, secondary Ca^{2+}-excitotoxicity and white matter degeneration. Even seemingly mild trauma can cause lethal "tetrodotoxin-sensitive Na^+ leak". Nav1.6 is the myelinated axon isoform; in traumatically-stretched mammalian cells, it immediately (< 2 min) becomes leaky. Based on recombinant Nav1.6 behavior we hypothesize that, in situ, hyperpolarizing (left)-shift of Nav1.6 channels in shear-blebbed axolemma explains the leak. Left-shifting a kinetically coupled pair of activation/availability processes effectively degrades a well-confined window conductance into a Na^+ leak. Here we model free-running nodes of Ranvier to assess how effectively left-shifted Nav channel kinetics could engender Na^+ (and hence Ca^{2+}) loading of axons. The model includes Kv and Nav conductances, a Na/K pump, and variable compartment volumes. We also follow saltatory propagation after traumatizing a single node. Particular shift ranges generate particular patterns of ectopic activity and $[Na^+]/[K^+]$ fluctuations. Depending on the fraction affected and extent of left-shift, trauma can trigger tonic or burst firing or even render the node inexcitable. Spontaneous activity dissipates the Na^+ gradient and hyperactivates the Na/K pump. Shifts severe enough to cause excitability failure do not protect the affected node (E_{Na} still dissipates) but do block action potential propagation along the axon; perhaps severe left-shift explains how head-blows immediately produce unconsciousness. An injured mid-axon node firing spontaneously due to left-shift sends action potentials towards both axon terminal and soma. Left-shifted Nav channels in damaged axons might therefore be one of the excitogenic factors in neuropathic pain discharges.

1. Introduction

A devastating aspect of traumatic brain injury is that even initially-mild axon damage tends to worsen inexorably in the hours, days, and weeks after head injuries[49]. Transient membrane poration is sometimes detected[14], but typically the initial mechanical insult does not rupture the axonal plasma membrane (axolemma)[49]. Instead, the stretch/shear forces experienced by the axolemma and the axonal cytoskeleton trigger a degenerative excitotoxic cascade[57]. As with ischemic brain injury[43], inappropriate injury-induced flux through voltage-gated sodium channels is pivotal[57]; tetrodotoxin (TTX) is highly neuroprotective in model systems (e.g., Wang et al. [56], Yuen et al. [58]). The TTX-sensitive rundown of the transmembrane Na gradient slows Ca extrusion through Na/Ca exchangers[11, 50] and Ca eventually reaches the lethally high levels at which Ca-proteases cleave spectrin[33, 43]. What first links mechanical insult to Nav channel malfunction, however, is still unclear. We postulate

that mechanically-induced bleb formation — i.e., the physical disruption of adhesive contacts between the axolemmal bilayer and membrane skeleton[6, 56] — is the culprit. Three lines of evidence support for this idea: 1) in optic nerve fixed within minutes of traumatic stretch, the first sign of trauma is blebbing of the Nav1.6 channel-rich nodes of Ranvier[28, 32], 2) abrupt stretch of recombinant Nav1.6-expressing HEK cells causes a TTX-sensitive rise in intracellular Na (Na-dye experiment) [56], and 3) for recombinant Nav1.6, mechanically-induced blebbing (via pipette aspiration of cell-attached *Xenopus* oocyte patches) causes an irreversible hyperpolarizing (left-) shift of activation and steady-state inactivation (and hence of Nav1.6 window current)[56].

All myelinated axons (central and peripheral) have Nav1.6 channels that pass transient I_{Na} (see Burbidge et al. [8]), but the nature of persistent or non-inactivating current associated with these channels[51, 54] is not well understood. It is sometimes described in models as a channel that activates and deactivates but cannot inactivate (see e.g., McIntyre and Grill [34]). But, on close examination in peripheral axons[5] it is similar to the "subthreshold persistent" I_{Na} of pacing neurons; Taddese and Bean [52] characterized this persistent current kinetically using an allosteric Markov scheme to fit to TTX-sensitive current from dynamic action potential clamp. That subthreshold persistent I_{Na} resembles a Hodgkin-Huxley (HH) window current (insofar as it is based on fast-inactivating channels), but differ in that explicit kinetic coupling forces availability (dependent on the fast inactivation particle) to borrow its voltage dependence from activation.

In cell-attached patches, we found that trauma-induced left-shift of activation and availability is kinetically coupled[56]. As described elsewhere[6], the left-shift behaves precisely like a HH sodium conductance for which each X-mV activation shift is accompanied by an X-mV availability shift. Moreover, in patch trauma experiments (macroscopic recombinant Nav1.6 current), results (i.e., decreased steady-state current near 0 mV) are routinely consistent with left-shift of a (coupled) window conductance and seldom suggestive of increased non-inactivating current[6, 56] (i.e., increased steady-state current near 0 mV). Single channel recordings of recombinant Nav1.6 current[9] also show non-inactivating (modal) gating behavior to be exceedingly rare. Had there been evidence that non-inactivating Nav1.6 gating channels increased irreversibly with trauma, the question of how axon (and possibly dendrite[28, 35]) trauma caused TTX-sensitive sodium leak would have a foregone conclusion. If, instead, as we postulate, left-shifted transient (window) current through Nav1.6 channels in traumatically blebbed axolemma is principally to blame, the leak becomes a subtler entity requiring closer inspection. Under those circumstances a precise understanding of how transient channel activity contributes to diffuse axonal injury is critical for refining neuroprotective Nav reagents (e.g., Isose et al. [20]) to allow them to more selectively target channels resident in damaged axolemma.

Here, our initial aim was to test computationally the idea that left-shifted Nav1.6 transient current could generate sufficient axonal Na leak to destroy ion gradients and hence the myelinated axon itself over the course of minutes, hours or days. On this the answer is a clear yes. Further, in testing whether model axons retain excitability various fractions of the axolemma were traumatized, we immediately encountered bursting behaviors like those linked to neuropathic pain and other manifestations of ectopic excitation. Painful human dental pulp is associated with the formation of atypically organized Nav1.6-rich axon sites[30]. Further, in a simple model of saltatory propagation along a myelinated axon, we found that left shift could interfere with and even fully block propagation. This suggests how a severe headblow affecting the thalamocortical tracts that carry the action potential traffic necessary for sustaining consciousness[31] might render a person almost instantaneously unconscious: impaired propagation by mechanically-induced left-shift.

Our findings could also have resonance for developmentally- and physiologically- regulated gating shifts in subpopulations of Nav1.6 (or other) isoforms. In this vein, voltage shifted Kv channels alter excitability patterns in model neurons[4, 40]. Voltage sensor stability, including for Nav channels [2], is inherently sensitive to both physical and chemical bilayer mechanical perturbations[15, 24, 29, 36, 39, 45]. Thus, perturbing the bilayer nano-environment

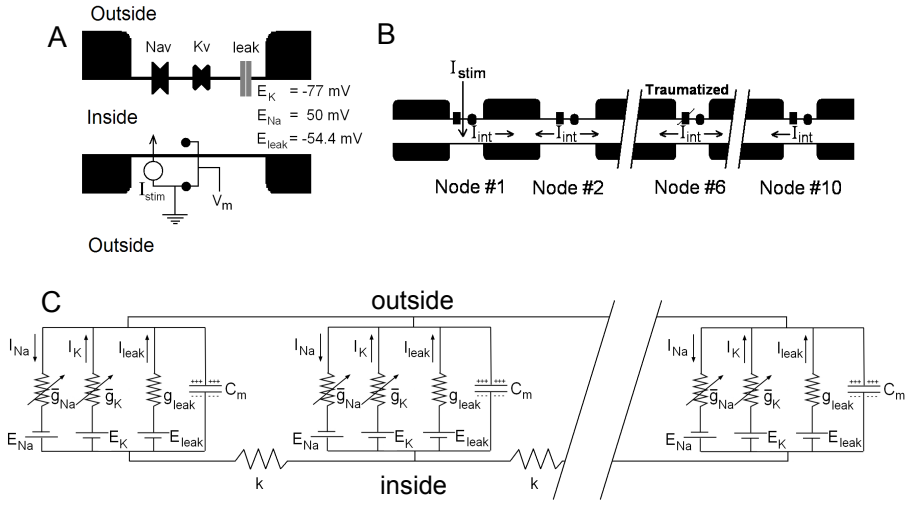

Figure 1: Cartoon representation of the model showing: **A**. a single node with the conductances modeled and reversal potentials used; **B**. a ten-node axon with one node (node 6) damaged; **C**. the equivalent circuit used, with $g_{Na}^{-} = g_{Na}m^3h$, and $g_{K}^{-} = g_K n^4$.

of a given Nav (or other voltage gated channel), whether intentional or through misadventure, can be expected to lower or raise barriers to voltage sensor repacking. Just as left-shifted operation of Nav1.6 channels in traumatized membranes may be due to the altered bilayer mechanics of the bleb[56], cell-controlled changes in the lipid surround of Nav channel subpopulations could modulate a neuron's excitability patterns. Perhaps there is even a connection between Nav channel block by dietary omega fatty acids (e.g., Bruno et al. [7], Li et al. [27]) and their neuroprotective effect[1] in a model of traumatic brain injury.

2. Model

The voltage- and time-dependent currents of the model are a transient sodium current, (I_{Na} due to Nav channels) and a non-inactivating fast potassium current (I_K due to Kv channels). There is also an ohmic leak current I_{leak}, generally attributed to chloride and potassium ions crossing the membrane but here, unspecified. In the version of the model that incorporates concentration changes, currents carried by the Na/K ATPase (pump) and leak currents specifically for Na and K ions are included.

Constant parameters used in the model are listed in table 1. Model equations were solved using a fourth-order Runge-Kutta scheme with variable time-step.

2.1. Modeling an injured axon

When modeling the voltage excursions of an injured axon, we depict each individual node of Ranvier with HH kinetics[17]. Adjacent nodes are connected via simple linear resistors, non-adjacent nodes do not interact directly. The basic equation giving the change in membrane potential at a single node as a function of time is:

$$\frac{dV_m}{dt} = \frac{-1}{C}(I_{Na} + I_K + I_{leak} + I_{int} + I_{stim}), \quad (1)$$

where V_m is the membrane potential, t is time, C is the membrane capacity of the node, I_{int} is the interaction current between adjacent nodes and I_{stim} is the stimulating current, usually only present at the initial node. Every current is assumed to be independent from one another except through membrane potential changes.

I_{Na} is modeled following Hodgkin and Huxley [17] as:

$$I_{Na} = m^3 h g_{Na}(V_m - E_{Na}), \quad (2)$$

with g_{Na} the maximal conductance through Nav channels and E_{Na} the sodium reversal potential. m and h are the voltage-dependent activation and inactivation variables - such that m^3h gives the open probability of a channel - and are given by:

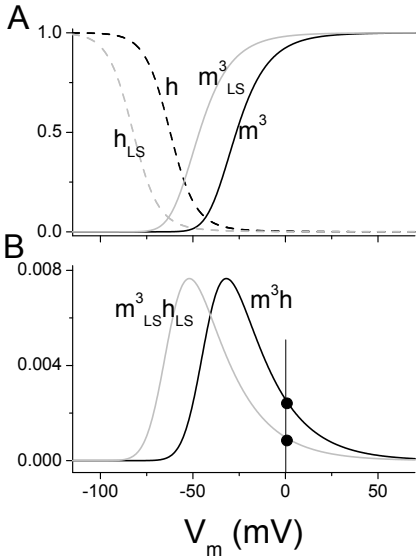

Figure 2: **A**: Equilibrium values of the activation (m^3) and inactivation (h) variables for the intact and left-shifted (20 mV) Nav channel as a function of potential. **B**: The steady-state open probability (m^3h) of the intact and left-shifted Nav channels yields a "window conductance". Note that, with left-shift, window conductance decreases at 0 mV (vertical line and circles).

$$\frac{dm}{dt} = \alpha_m(1-m) - \beta_m m, \quad (3)$$

$$\frac{dh}{dt} = \alpha_h(1-h) - \beta_h h, \quad (4)$$

with rate constants given by:

$$\alpha_m = 0.1\frac{(V_m+40)}{1-\exp(-(V_m+40)/10)}, \quad (5)$$

$$\beta_m = 4\exp(-(V_m+65)/18), \quad (6)$$

$$\alpha_h = 0.07\exp(-(V_m+65)/20), \quad (7)$$

$$\beta_h = \frac{1}{1+\exp(-(V_m+35)/10)}. \quad (8)$$

The units of potential and time in Eq. 5 to 8 and throughout this work are mV and ms respectively.

Equations 3 and 4 can be expressed in the form:

$$\frac{dx}{dt} = \frac{x_\infty - x}{\tau_x}, \quad (9)$$

where x represents the m or h variable, and with $x_\infty = \frac{\alpha_x}{\alpha_x+\beta_x}$ and $\tau_x = \frac{1}{\alpha_x+\beta_x}$. "Left-shifting" a channel consists in displacing both these functions (x_∞ and τ_x) towards more hyperpolarized potentials which is easily done by replacing the potential V_m in Eqs. 5 to 8 by ($V_m + LS_{AC}$) with LS_{AC} being the magnitude of the left-shift. This approach is justified experimentally by the findings of Wang et al. [56] and is also used in a companion paper[6] where the kinetic coupling of steady-state inactivation to activation in Nav1.6 channels is discussed further.

The irreversible left-shift of Nav.16 channel operation observed experimentally for recombinant channels in aspirated cell-attached oocyte patches[56] could result from an all-or-none process or it could reflect a graded response. It is unknown if each channel is a) either fully intact or fully shifted (i.e., maximally traumatized), or b) if all channels left-shift in a graded manner, to an extent that depends on the intensity of the trauma imposed. Accordingly, modeling the left-shift of Nav channels requires two parameters: the fraction of affected channels (AC) and the left-shift of these affected channel (LS_{AC}). Eq. 2 then becomes:

$$I_{Na} = (m^3h(1-AC) + m_{LS}^3 h_{LS} AC)(V_m - E_{Na})g_{Na}, \quad (10)$$

Shifted channels retain the same unitary conductance and driving force, only their kinetics are modified (i.e., only m and h are displaced towards more hyperpolarized potentials), see Fig. 2A. Window conductance is also left-shifted (Fig. 2B) and decreases at 0 mV. It is interesting to realize that a mutation or a drug that decreases "persistent" current as gauged by the ratio steady-state to transient current at 0 mV could achieve this by left-shifting channel activation. Via activation at the now more-hyperpolarized foot of the curve, a left-shifted Nav channel becomes "leaky" even though steady-state current at 0 mV may have measurably decreased compared to control.

Though we analyse our data in terms of mammalian systems, the model used here is based on the HH model [17] for action potentials in a squid axon. Our emphasis is on qualitative behaviors of myelinated axons rather than on quantitative specifics. As recent examples, Ochab-Marcinek et al. [38], Smit et al. [48] and Kovalsky et al. [23] also used

HH based models in simulating mammalian node of Ranvier excitability, action potential propagation in myelinated axons and aspects of ectopic discharges.

A non-inactivating potassium current contributes to membrane repolarization during action potentials and is modeled as:

$$I_K = n^4 g_K (V_m - E_K), \tag{11}$$

where g_K is the maximal potassium conductance and E_K is the potassium reversal potential, n^4 is the voltage-dependent open probability and evolves according to:

$$\frac{dn}{dt} = \alpha_n(1-n) - \beta_n n, \tag{12}$$

with:

$$\alpha_n = 0.01\frac{(V_m+55)}{1-\exp(-(V_m+55)/10)}, \tag{13}$$

$$\beta_n = 0.125\exp(-(V_m+65)/80). \tag{14}$$

I_{leak}, the leak current, is given by:

$$I_{leak} = g_{leak}(V - E_{leak}). \tag{15}$$

There are many models for myelinated axons (see e.g., Richardson et al. [41]); the simplest assume the myelin to be a perfect insulator (see e.g., Ochab-Marcinek et al. [38]) and hence each node is connected to its neighbor by a simple resistor representing the internodal axoplasmic conductance, κ. The interaction current for node i is then given by:

$$I_{int} = \kappa(V_m(i-1) + V_m(i+1) - 2V_m(i)), \tag{16}$$

at every node except the first and the last one where it is given (in a ten-node axon) respectively by:

$$I_{int} = \kappa(V_m(2) - V_m(1)), \tag{17}$$

$$I_{int} = \kappa(V_m(9) - V_m(10)), \tag{18}$$

where $V_m(i)$ is the membrane potential at node i.

2.2. Modeling an injured node of Ranvier

In this section a single injured node of Ranvier is modeled independent of any neighbors. Injected current is used in place of interactions with firing neighbors.

The basic equation for this model is:

$$\frac{dV_m}{dt} = \frac{-1}{C}(I_{Na} + I_K + I_{Napump} + I_{Kpump} + I_{Naleak} + I_{Kleak} + I_{leak}), \tag{19}$$

where I_{Napump} and I_{Kpump} are Na and K current generated by the Na/K pump and I_{Naleak} and I_{Kleak} are specific Na and K leaks needed to stabilize the system in the presence of the Na/K pump (see e.g., Kager et al. [21]) The other currents are as previously defined.

The Na/K pump is an ATP-driven transporter that uptakes 2 K^+ and extrudes 3 Na^+ per cycle. This process is weakly dependent on membrane potential and strongly dependent on the sodium and potassium binding rates and on their respective concentrations. Because the pump reverses at a very hyperpolarized potential (about −200 mV[26]), and is weakly dependent on membrane potential over the range studied, we use the pump current formulation given by Läuger [25].

$$I_{Kpump} = -2I_{maxpmp}(1+\frac{K_{mK}}{[K^+]_o})^{-2} \times (1+\frac{K_{mNa}}{[Na^+]_i})^{-3}, \tag{20}$$

$$I_{Napump} = -\frac{3}{2}I_K, \tag{21}$$

where I_{maxpmp} is the maximal current generated by the pump and K_{mK} = 3.5 mM and K_{mNa} = 10 mM.

The specific leak for ion species X (Na or K) takes the form:

$$I_{Xleak} = g_{Xleak}(V_m - E_X). \tag{22}$$

Concentrations in the interior and exterior compartment change as ions X flow in and out as given by:

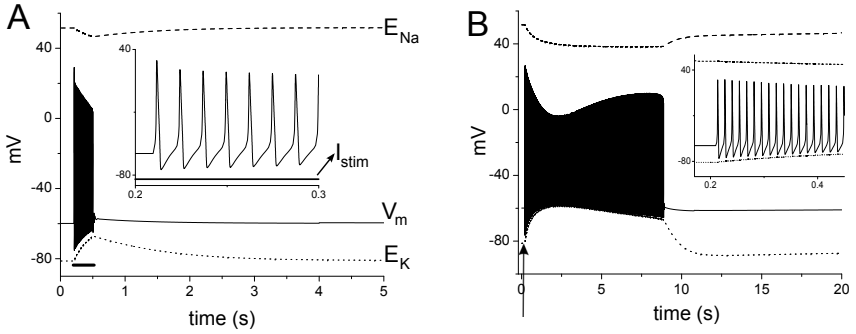

Figure 3: **A**. When a sustained current of 12 μA/cm^2 is injected (black bar), the system enters a repetitively firing mode and the ion gradients slowly dissipate. After the current injection (I_{stim}), firing stops and within a few minutes the system returns to its initial steady-state, showing that the system is stable. E_K (dotted line), E_{Na} (dashed line) and V_m (full line) are shown; this convention also applies in B and throughout this paper (Figs. 9 and 11). **B**. Immediately after receiving a mild left-shifting injury (at 200 ms, see arrow)), the system ($AC = 1$, $LS_{AC} = 1.5$ mV) fires spontaneously for a prolonged period of time (about 10 s) and then settles into a new slightly hyperpolarized (2 mV) steady-state. Note the change in time scale between A and B.

$$\frac{d[X]_i}{dt} = -\frac{I_{XT}S}{FVol_i}, \tag{23}$$

$$\frac{d[X]_o}{dt} = \frac{I_{XT}S}{FVol_o}, \tag{24}$$

where F is the Faraday constant, Vol_i and Vol_o are the volume of the interior and exterior compartment respectively, S is the surface of the node and I_{XT} denotes the total currents for ion species X (e.g., $I_{NaT} = I_{Na} + I_{Napump} + I_{Naleak}$). The reversal potential of ion species X (Na or K) is calculated as:

$$E_X = \frac{RT}{F} \ln \frac{[X]_o}{[X]_i}. \tag{25}$$

For the system to maintain a steady-state, the leak conductances and maximal pump activity need to be balanced. Since the Na/K ATPase uptakes 2 K ions for every 3 Na extruded, the leak conductances are adjusted so that the total Na and K currents have a ratio of 3/2 at the initial concentrations with the resting potential at−59.9 mV. The maximal activity of the Na/K pump is then set so that the total current is zero thus putting the system in a steady-state at those conditions.

The stability of the intact (uninjured) system is tested by verifying that it goes back to its initial state after a current injection that elicits a prolonged train of action potentials (see Fig. 3A).

Unless stated otherwise, the parameters used for the axonal and the single node models are those in table 1.

Table 1: Model parameters

Myelinated Axon Model				
Membrane capacitance	C	=	1	μF/cm^2
Stimulating current	I_{stim}	=	12	μA/cm^2
Transient Na conductance	g_{Na}	=	120	mS/cm^2
Transient K conductance	g_K	=	36	mS/cm^2
Leak conductance	g_{leak}	=	0.25	mS/cm^2
Na reversal potential	E_{Na}	=	50	mV
K reversal potential	E_K	=	−77	mV
Resting potential	V_{rest}	=	−65.5	mV
Leak reversal potential	E_{leak}	=	−54.4	mV
Internodal conductance	κ	=	0.14	mS/cm^2
Single Node Model				
Temperature	T	=	293.15	K
Volume of the inside compartment	Vol_i	=	3×10^{-15}	m^3
Volume of the outside compartment	Vol_o	=	3×10^{-15}	m^3
Surface	S	=	6×10^{-8}	cm^2
Initial inside Na concentration	$[Na]_i$	=	20	mM
Initial outside Na concentration	$[Na]_o$	=	154	mM
Initial inside K concentration	$[K]_i$	=	6	mM
Initial outside K concentration	$[K]_o$	=	150	mM
Na reversal potential	E_{Na}	=	51.5	mV
K reversal potential	E_K	=	−81.3	mV
Intact Resting potential	V_{rest}	=	−59.9	mV
K leak conductance	g_{Kleak}	=	0.1	mS/cm^2
Leak conductance	g_{leak}	=	0.5	mS/cm^2
Leak reversal potential	E_{leak}	=	−59.9	mV
Trauma variables				
Fraction of affected channels	AC	=	0 – 1	
Left-shift of the affected channels	LS_{AC}	=	0 – 20	mV

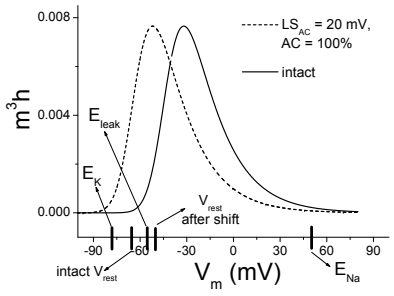

Figure 4: Steady-state open probability (window conductance) for intact and shifted (LS_{AC} = 20 mV) channels, also showing K, Na and leak reversal potentials as well as resting potentials. With all the Nav channels shifted by this amount, the resting potential changes to −50 mV; at such potential, the left-shifted channels' availability is too low to allow for action potentials upon depolarization towards the normal threshold.

3. Results

3.1. Single node - fixed concentrations

Keeping fixed concentrations simulates short timescales. Shutting down interactions with neighboring nodes limits the number of model parameters while we examine the consequences of Nav channel left-shift.

The firing frequency of the system is studied in two different scenarios: with and without stimulating current. Two parameters are systematically varied: the number of affected channels (AC) and the left-shift of affected channels (LS_{AC}). To do that, the intact system is allowed to reach steady-state (100 ms) then the left-shift (trauma) is applied (e.g., see arrowhead in Fig. 3B). After another period to allow steady-state to be reached (100 to 500 ms depending on the simulation), spike counting begins for the simulation period (typically 5 s), and, where applicable, a stimulating current (as per table 1) is turned on. Firing frequency is the number of spikes divided by the time. Numerically, a spike is counted every time membrane potential crosses a certain value in the positive direction. We typically used −15 mV, but results were not affected by the value of this parameter.

With no stimulating current, a large enough left-shift of a large enough fraction of Nav channels induces spontaneous firing. What is needed is for window current from the shifted channels to become large enough at the resting potential to depolarize the membrane past the threshold for firing. The node fires at a frequency that depends on the depolarizing window current (as it would depend on the stimulating current). However it is possible for the left-shift to be so large and to affect such a large fraction of the Nav channels that no spontaneous firing occurs. This happens if the extent of left-shift takes the window current region of the shifted channels beyond the normal resting potential. For example, 5% affected channels do not induce spontaneous firing for shifts under 12 mV. For left-shifts between 12 and 30 mV, the channel's maximal window conductance is close enough to the resting potential that window current act as stimulating current and induce spontaneous activity. For larger shifts there is no spontaneous activity because the depolarizing currents are too feeble to trigger action potentials. Small fractions of affected channels (AC) give narrow spectrum of spontaneous activity inducing left-shift (LS_{AC}).

For large fractions of affected channels, the situation is different. When the left-shift is applied, there is an initial spontaneous action potential train after which the system stops firing and settles into a new depolarized steady-state where further depolarization (e.g., from injected current) cannot generate any action potential because too many sodium channels are already inactivated (see Fig. 4); the axon becomes inexcitable.

Using stimulating currents, if the fraction of affected channels is large, then the firing frequency increases with the left-shift of affected channels until the system no longer responds to stimulating currents. However if the fraction of affected channels is small, then a very large shift will have practically no effect as the shifted channels' voltage range of operation will be far outside the range of operation of intact channels and hence shifted channels will simply have no effect on the system.

When the results for spontaneous and stimulated firing for large values of AC are taken together, four different regimes (A, B, C, D; see Fig. 6) of activity can be identified. In regime A, the system behaves very closely to the control system: it shows no spontaneous activity and activates when stimulated. Regime B exhibits both spontaneous and stimulated activity. Regime C has spontaneous activity that is,

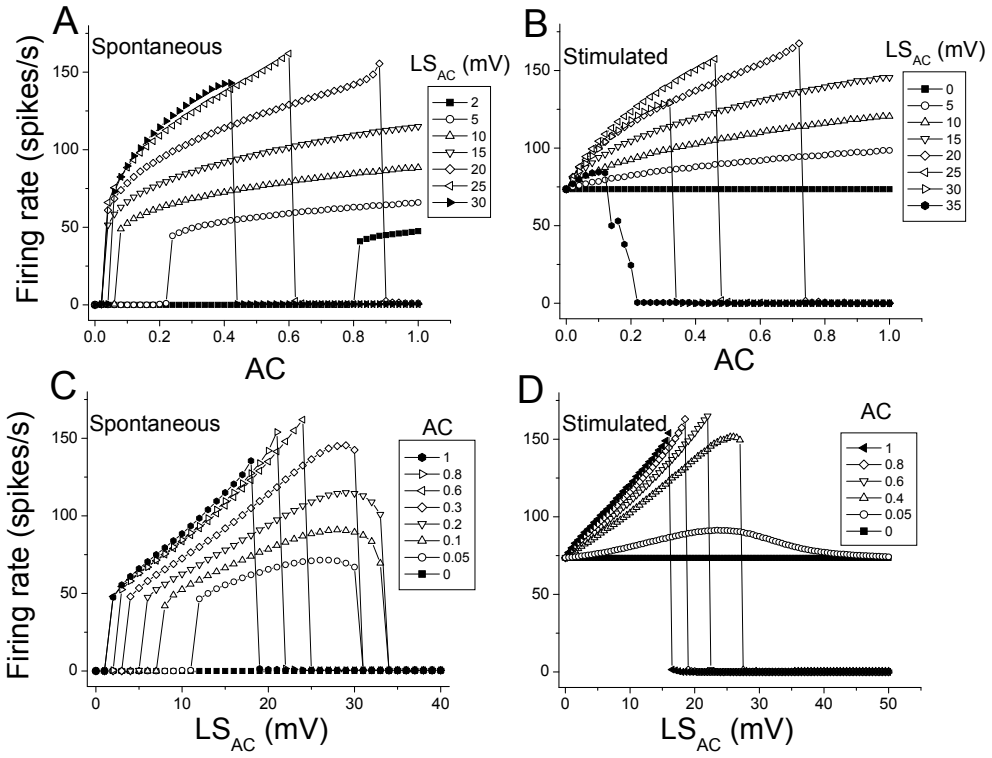

Figure 5: **A, B**: Firing rate as a function of the fraction of affected channels (AC) for different values of the left-shift of affected channels (LS_{AC}), with (**B**) and without (**A**) stimulating current (I_{stim} = 12μA/cm^2). **C, D**: Firing rate as a function of the extent of the left-shift of affected channels (LS_{AC}) for different fractions of affected channels (AC), (**D**) with and without (**C**) stimulating current (I_{stim} = 12μA/cm^2).

however, stopped by current injection and regime D which shows no sustained firing activity under any condition, becomes completely inexcitable shortly after trauma.

The most peculiar behavior is regime C where spontaneous firing is stopped by current injection. The system, which becomes inexcitable when the resting potential is too depolarized, is on the brink of that state in regime C. Thus, instead of triggering more spikes, injected current pushes the steady-state potential to an even more depolarized level rendering the system electrically silent.

3.2. Propagation along a myelinated axon

For saltatory propagation, the computational procedure used differs. Nodes are first allowed to equilibrate individually (with left-shift applied at the injured node) for 100 ms. With stimulating current applied at the initial node (if applicable) internode interaction is then turned on and the system equilibrates for another 150 ms. Action potentials frequency is then measured, typically for 5 s.

An injured node in regime B or C (see Fig. 6) fires spontaneously. These ectopically generated mid-axon action potentials propagate along the whole axon in both directions (Fig. 7), thereby sending inappropriate signals towards both axon terminals and the cell body.

A single node with a regime D injury blocks action potentials traveling down the axon, as shown in Fig. 7 bottom. Interestingly an injured node in regime C though spontaneously firing (i.e., generating ectopic excitation), stops propagation of action potentials when stimulated by incoming action potential traffic.

Though a mid-axon spontaneously firing node sends action potential in both anterograde and retrograde directions (see Fig. 6A), not all spikes are transmitted. As firing frequency in the injured node increases with LS_{AC} (keeping AC = 100%) it eventually becomes too rapid for the uninjured adjacent nodes: consecutive injured-node action potentials that occur during the refractory period of the adjacent node, are not both transmitted. Thus firing frequency at the intact adjacent node decreases. Fig. 8Ai plots firing frequency (spikes s^{-1}) for an injured node and an adjacent intact node as left-shift of affected channels (LS_{AC}) is increased. Note that all the intact nodes fire at the same frequency since spikes in intact nodes are faithfully transmitted. With increas-

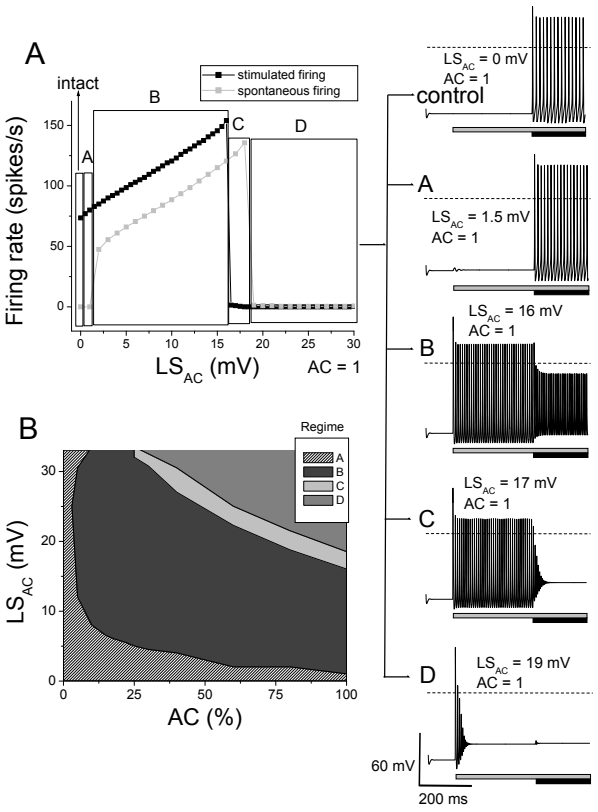

Figure 6: **A (top left)**. Four different regimes of activity (*A* to *D*, column on the right) can be identified for a single non-interacting node with fixed ion concentrations at $AC = 1$. Left-shift is applied at 100 ms and the stimulating current starts at 400 ms. The dashed line are at 0 mV. **B (bottom left)**: firing regimes as a function of both AC and LS_{AC}.

ing LS_{AC}, the system changes from propagating all ectopic spikes (1 : 1 propagation) to propagating 2 for every 3 generated at the injured node (3 : 2 propagation) to propagating 1 for every 2 (2 : 1 propagation) (see Fig. 8Aii).

What happens when there is incoming (anterograde) stimulation from node 1? Fig. 8B plots firing frequency for nodes 1, 5, 6 and 10. Node 6 is injured and as described above all "downstream" nodes (exemplified by 10) have exactly the same firing frequency. Node 5, however, lies between the stimulated node (1) and the injured node (6) and is affected both by the incoming (anterograde) action potentials from node 1 and the retrograde injured node ectopic spikes occuring at a different frequency. As a result, node 5 shows complicated erratic behavior. At nodes closer to the stimulated node (node 1), the interfering effect of the injured node is less pronounced.

It should be possible to test this scenario experimentally by monitoring firing frequency at (minimally) three distant points along a myelinated axon, comparing the effect of irreversible trauma to that of reversible agents known to left-shift Nav1.6 kinetics. At the middle point, a left-shifting agent would be applied e.g., highly localized heating[53] then, perhaps, ciguatoxin[18] and, finally, trauma. A change in firing frequency, or possibly a silencing of the most distal point would indicate a change in excitability mid-axon, if firing frequency behaves as modeled here. This would not-only confirm that trauma, like heat and ciguatoxin, causes Nav channels to left-shift, but also have implications for such conditions as neuropathic pain where ectopic generation of action potentials is the source of the condition[12].

3.3. Ion homeostasis

In this section, we study the results of the model of a single node of Ranvier, but allow the Na and K concentrations to change in time. This permits a more complete description of the situation. The firing regimes particulars identified in the previous sections do not necessarily apply when ion reversal potentials are free to change. In simulations, the system is first equilibrated for 200 ms then the left-shift (trauma) is applied.

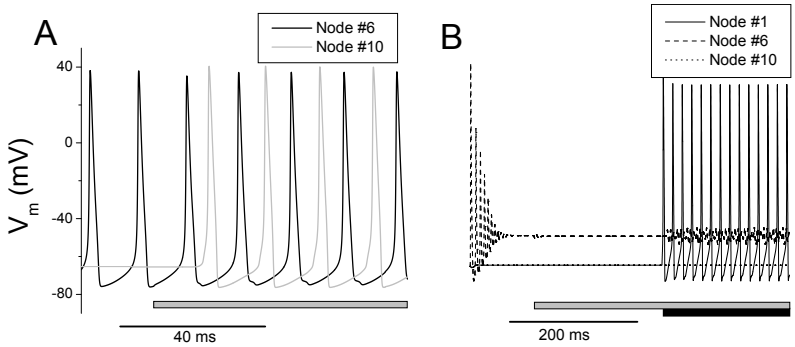

Figure 7: **A**. $V_m(t)$ at the spontaneously firing injured node (6) and at the end node (10). Node 1 also activates like node 10 (not shown). Interactions between nodes is switched on at 100 ms (grey bar). The delay between node 6 and node 10 action potentials represents the propagation time through the intervening nodes. **B**. $V_m(t)$ at the initial(1), injured(6) and end(10) nodes. The axon is stimulated at node 1 and the action potentials propagate to node 6, which is injured (from $t = 0$ ms); node 6 is in regime D, which blocks action potentials. The nodes after node 6 (exemplified by node 10) remain inactive. Internode interaction is turned on at $t = 100$ ms (grey bar), stimulating current at the initial node starts at $t = 300$ ms (black bar). The vertical axis applies for A and B.

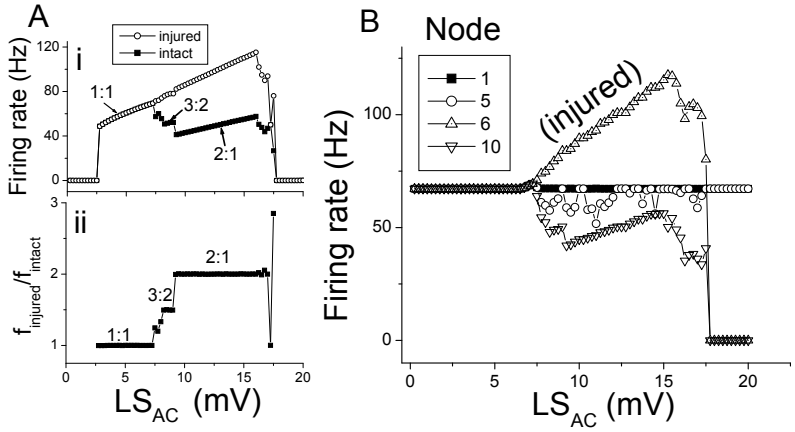

Figure 8: **A.i**. Firing frequency at injured node and intact nodes as LS_{AC} increases ($AC = 1$). All intact nodes fire at the same frequency because any AP produced in the nodes neighboring the injured node propagates faithfully to the end of the axon. **ii**. Same data set plotted as ratio of injured to intact firing frequency to emphasize how the propagation ratio diminishes with increasing left-shift (of affected channels), but only does so in integer ratios. **B**. Firing frequency for nodes 1 (stimulated), 5, 6 (injured) and 10. Nodes after the injured node behaves qualitatively as intact nodes on the left, but nodes before the injured node do not. Node 5 receives the propagated AP generated at node 1 but is also affected by node 6 firing at a faster rate.

Five different classes of behavior ("regimes") can now be identified as the fraction of affected channels (AC) and their left-shift (LS_{AC}) are varied. The previous argument regarding combination of these factors still applies: e.g., a large AC has no effect if LS_{AC} is very small and conversely.

The first regime identified characterized shows spontaneous firing then (over time) a return to an excitable steady-state (see Fig. 9Ai). Larger trauma induces a regime with periodic burst firing (Fig. 9Aii). This is similar to responses in a comparable system Kager et al. [21] upon reduction of pump activity: less hyperpolarizing current (electrogenic pump activity) yields a similar outcome to more depolarizing current (window current, in our case). Between bursts, the membrane is excitable (i.e., current injection elicits spikes). The third regime consists of sustained spontaneous activity (Fig. 9Aiii). The fourth (Fig. 9Aiv) occurs for a very limited set of AC and LS_{AC} and consists of periodic bursting at a reduced amplitude accompanied by a large dissipation of the sodium gradient (i.e., from about E_{Na} = 50 mV to 0 mV). Finally, major trauma renders the system unexcitable with, again, collapse of E_{Na}. Interestingly this regime is characterized by a hyperpolarized E_K, and by a V_m value that is unchanged from the control steady-state. E_K hyperpolarizes as pumps work extra fast to compensate the Na leak but simultaneously uptake K, thereby hyperpolarizing E_K. V_m stays unchanged because it is dominated by the unspecified leak whose reversal potential E_{leak} (by definition) is unaffected by the trauma-associated depletion of specific ion gradients. Clearly this is an oversimplification: in real cells, leaks are specific pathways (e.g., K channels, non-selective cation channels) that might be affected by trauma.

3.4. ATP depletion

The Na/K pump is fueled by ATP. If intense pump activity at a node of Ranvier depletes the ATP reserve, pumps slow or stop, not because of the re-established gradients, but because of insufficient ATP. The Na and K gradients would then rapidly dissipate, along with the Ca gradient (coupled to Na via the Na/Ca exchanger); Ca excitotoxicity and cell death would ensue.

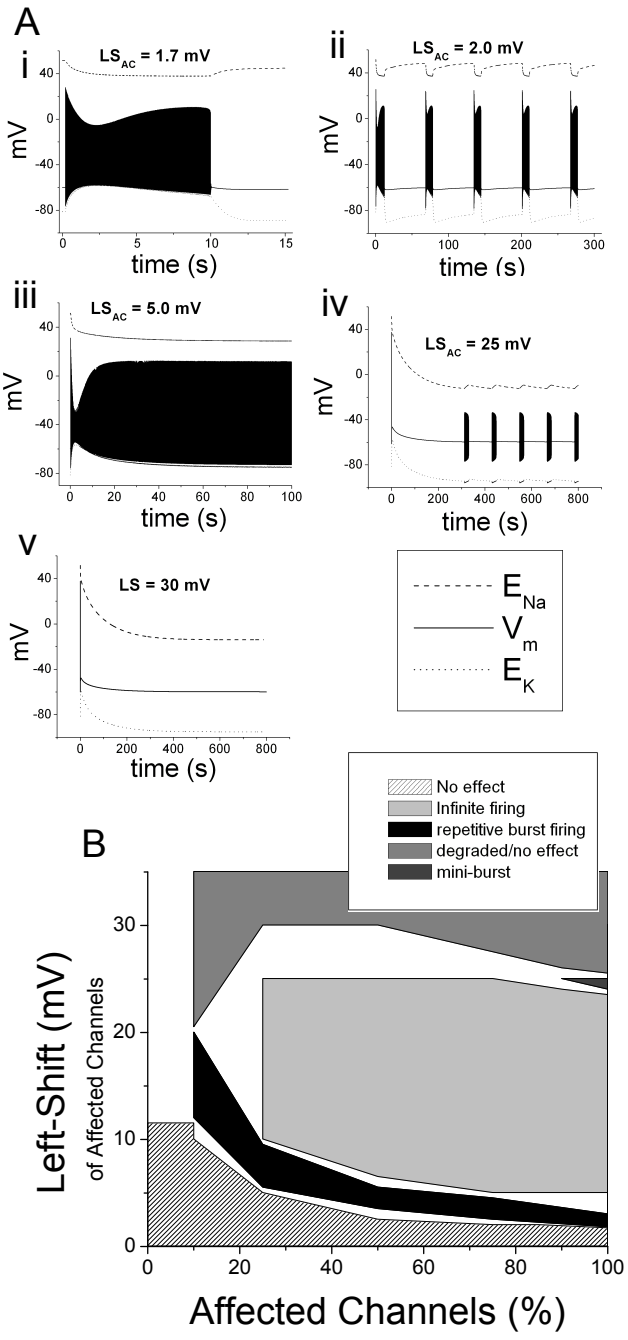

Figure 9: Classes of spontaneous activity for the system including concentrations changes. The system is initially in its intact state at its steady-state. At t = 0 ms channel kinetics are shifted (without changing the actual values of m and h at that instant) and $V_m(t)$ is followed. A selection of plots for the AC = 1 case are shown (A) along with a summary plot of system behavior (B) for values of AC and LS_{AC}. The summary plot is incomplete (as transitions between behaviors are difficult to identify), but gives a qualitative idea of the possible behaviors. The model was run for 1000 s to verify that a steady-state is reached for LS_{AC} = 1.7 mV. Note the different time scales in A.

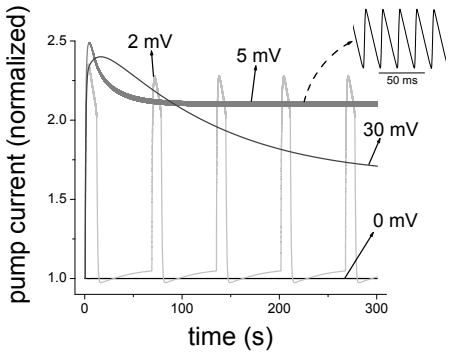

Figure 10: Pump current as a function of time for different LS_{AC} (as labeled, $AC = 100\%$)). Any level of trauma increase pump current and hence ATP usage. ATP depletion would cause the NaK pump to stop working leading to depolarization.

As left-shifted Nav channels dissipate the Na gradient, the Na/K pumps hyperactivate. Fig. 10 plots normalized pump activity with time for different LS_{AC} which serves as an index of ATP usage (per unit time). A 2 mV left-shift ($AC = 1$) causes the node to fire in bursts (as seen in Fig. 9ii); pump activity increases to 2.3 times the control level during the bursts. For a 5 mV left-shift the node enters a repetitive firing mode; pump activity increases above 2 times the control level. The thick line for $LS_{AC} = 5$ mV in Fig. 10 is a result of the rapid changes in pump activity because of nodal firing. $LS_{AC} = 30$ mV causes the Na gradient to depolarize and the K gradient to hyperpolarize; pump activity increases above 2 times control level and then slowly (over a range > 300 s) decreases to a steady state value of 1.64 times the control level.

Even the ~ 10 s of spontaneous firing elicited by the smallest left-shift in Fig. 9Ai would appreciably increase pump activity. It is easy to see that where ATP reserves were already compromised (e.g., due to trauma-related ischemia), left-shift of Nav channels would further deplete the reserves, thus slowing the pumps and further depolarizing the nodes.

3.5. Changing the volume of the extracellular compartment

In the simulations, we have assumed equal and fixed interior and exterior volumes. In reality, for axons of different calibers, the values of these parameters would vary substantially in both absolute and relative terms, and importantly, both compartment could change volume following trauma. For example, trauma-induced swelling of neighboring glia, accompanied by altered solute uptake capabilities and K channel activity in the glia could alter the effective volume of the exterior compartment[13, 22, 47] (because of e.g., bleb formation, beading, osmotic swelling etc). With changing volumes in the with-pump system, it is especially important to follow the system long enough for pump activity to slowly bring the system to its new steady-state. Illustrating the dramatic impact of compartment volume on the details of excitogenicity, Fig. 11 shows, for a spontaneously firing (traumatized) node, the effect of tripling the exterior volume: after about $\sim 10 - 20$ s, a new increased shorter duration, higher frequency bursting pattern is established.

4. Discussion

Pathological malfunction of axonal Nav channels is a common theme in traumatic and ischemic injury of brain, spinal cord and peripheral nerve. Likewise, axonal Nav channel hyperactivity generates neuropathic pain in connection with trauma and inflammation (and the attendant demyelination/remodeling) of peripheral nerves. For heterologously expressed Nav1.6, which is the myelinated axon isoform, membrane trauma progressively and irreversibly shifts the voltage range of channel activity closer to or even beyond an axon's normal resting potential[56]. More specifically, trauma causes a kinetically-coupled hyperpolarizing shift of Nav1.6 activation and availability. If, for a node's Nav1.6 population, left-shifted gating was "smeared-out" over a range of voltages, there would be concomitant "left-smearing" of window currents. In effect, trauma would generate a "subthreshold persistent current" - the traumatized Nav1.6 channels would serve as axonal pacemakers, just as Nav channels do normally in the soma of certain rhythmically firing hypothalamic neurons[52]. By this means, traumatized "transient current" could constitute, we hypothesized, the potentially lethal TTX-sensitive Na leak reported for traumatized axons[56]. In a seminal paper, in which he recorded from isolated crayfish axons, Hodgkin [16] noted that given axon preps could generate qualitatively different firing patterns as they

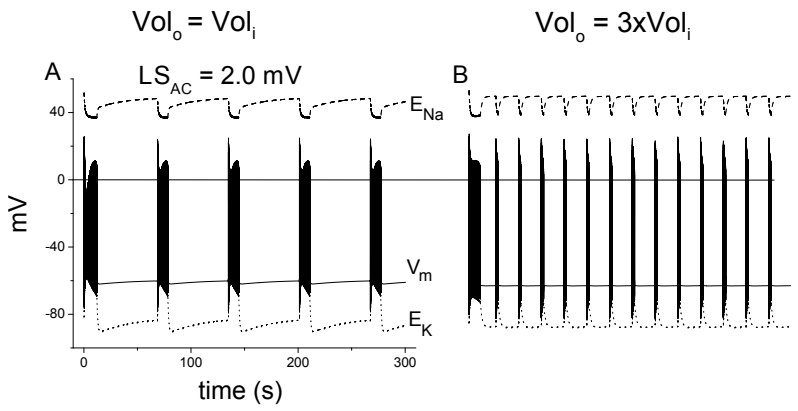

Figure 11: **A**. An injured node ($AC = 100\%$,$LS_{AC} = 2$mV) with equal interior and exterior volumes fires in repetitive bursts. **B**. A node injured in the same way as in **A** but with the exterior volume triple the interior volume has a shorter burst duration, but higher bursting frequency.

deteriorated. For internally-perfused giant muscle fibers, we likewise noted firing patterns changing with time[37]. Slow membrane blebbing - the dissociation of axo-(or sarco-)lemma from underlying cortex - and attendant irreversible left-shifts, likely explains some of the rhythmicity changes. As recently shown by Sejnowski and colleagues (e.g., [40]), the Hodgkin and Morris-Lecar analyses have been instrumental in helping show how neurons generate different patterns (regimes) of physiological rhythmicity. An implicit assumption, and one that we embrace, is that physiological and pathological rhythmicities are close kin. From cell biological, developmental, pharmacological and clinical perspectives, however, it will be critical to learn if "physiological" Nav1.6 channels become more "pathological" whenever their bilayer mechanical environments become more bleb-like.

Another possible explanation of trauma-induced TTX sensitive Nav channel leak (assessed in a companion paper [6]) is that mechanical trauma somehow increases the fraction of Nav1.6 channels active in a slow-(or non-inactivating) mode. This option is not mutually exclusive of left-shifted transient current, but we always observed that phenomenon and seldom observed non-inactivating I_{Na}[56]. We therefore explored, computationally, whether physiological damage consistent with diffuse axonal injury could be inflicted by left-shifted transient current operation alone. We tested various depths of left-shift (LS_{AC}) and fractions of affected channels (AC). Patterns of excitability and Na/K homeostasis were characterized in an isolated node. For saltatory propagation in a ten-node axon, ectopic excitation and nerve block were examined.

The clinical significance of our results hinges on whether, in myelinated mammalian axons, Nav1.6 channel operation indeed undergoes an irreversible left-shift with trauma. We know that Nav1.6 (with or without auxiliary beta subunits) behaves this way in *Xenopus* oocyte patches[56]. Further, we note that voltage clamp of blebbed-vesicles collected from rat myelinated axons in brain slices yields Nav1.6 midpoint activation values of −43.9 mV[19]. In that instance, blebbing was not seen as trauma, but as a way to access the channels for voltage clamp. This value is approximately the same than what was reported for recombinant Nav1.6 channels (rendered TTX - insensitive by a point mutation) expressed in dorsal root ganglion neurons[42]. It is however ~ 25 mV more hyperpolarized than what was reported for recombinant (human and mice) Nav1.6 channels expressed in HEK cells[8–10]. Human Nav1.6 current in myelinated axons was characterized under voltage clamp by Schwarz et al. [46] who emphasized that care was taken to avoid accidental stretch of the axons while isolating and mounting them. Unfortunately, if any accidentally stretched axons were voltage clamped, the data were not reported. Still the value reported by Schwarz et al. [46] fall closer to the values reported by Hu et al. [19], measured in blebbed-vesicles.

From our computational approach, a key result relevant to our initial question of whether left-shifted transient current could explain slowly developing diffuse axonal injury is this: mild node of Ranvier trauma elicits spontaneous activity that, for a mid-axon node, would send ectopic signals in both directions. At an affected node, mild trauma could deplete the sodium gradient enough to explain how a small patch of blebbed nodal axolemma[32] could be responsible for an axon's descent towards excitotoxic degeneration. The specifics of any traumatized axon's firing pattern are influenced, however, not solely by the channel kinetics - the combined influence of pump activity, axoplasmic volume and extracellular volume on Na and K driving forces have a large impact. In our computations, conditions consistent with excitotoxic degeneration were typically evident in tens of seconds to minutes, but small parameter changes could change this to a time scale of hours or days. Larger trauma can render a node (and hence the axon) silent and inexcitable. Even under these circumstances, however, inappropriate window current is flowing at the traumatized node and thus ion gradients become depleted. Previously[56] we suggested that left-shifted Nav channel activity might explain how a "KO punch" to the head immediately renders a victim unconscious; the present work provides some specifics for this notion. Consider the midbrain axon tracts that carry consciousness-sustaining action potential traffic[55]. Several distinct rhythmicity regimes emerged in our modeling. In each, Nav1.6 left-shift has a qualitatively different effect on an the axons' ability to propagate signals. Depending on its "LS_{AC}/AC coordinates" (Fig. 6B, Fig. 9B), a left-shifting trauma could render an axon spontaneously active (i.e., ectopically active) or could block any propagation beyond the affected node ((regimes *B* and *D* respectively of Fig. 6; regime also *C* covers both cases). A KO punch would likely be associated with wide-ranging LS_{AC}/AC for different axons such that, instantaneously, there would be increased firing rates in some axons, induction of spontaneous firing in others, and propagation block in others. The electrophysiological and anatomical substrate of consciousness is still too poorly understood[3, 44] to suggest which aspects would take precedence in a temporary disruption of consciousness. Surely, however, a blow that yielded sudden widespread occurrence of axons with at least one regime-*D* node (i.e., a node with propagation-blocking LS_{AC}/AC) would result in sudden loss of consciousness.

References

[1] Bailes, J., Mills, J., 2010. Docosahexaenoic acid (DHA) Reduces Traumatic Axonal Injury in a Rodent Head Injury Model. Journal of Neurotrauma Epub ahead of print.

[2] Banderali, U., Juranka, P., Clark, R., Giles, W., Morris, C., 2010. Impaired stretch modulation in potentially lethal cardiac sodium channel mutants. Channels 4 (1), 12–21.

[3] Blyth, B., Bazarian, J., 2010. Traumatic Alterations in Consciousness: Traumatic Brain Injury. Emerg. Med. Clin. North Am. 28 (3), 571–594.

[4] Börjesson, S., Parkkari, T., Hammarström, S., Elinder, F., 2010. Electrostatic Tuning of Cellular Excitability. Biophysical journal 98 (3), 396–403.

[5] Bostock, H., Rothwell, J., 1997. Latent addition in motor and sensory fibres of human peripheral nerve. J. Physiol. 498, 277–294.

[6] Boucher, P.-A., Joós, B., Morris, C., 2010. Identifying the "leaky" states of native Nav channels in traumatized neurons: simulation and theory for $I_{Na}(V,t)$ during trauma of cell-attached patches. in thesis.

[7] Bruno, M., Koeppe, R., Andersen, O., 2007. Docosahexaenoic acid alters bilayer elastic properties. Proc. Natl. Acad. Sci. USA 104 (23), 9638–9643.

[8] Burbidge, S., Dale, T., Powell, A., Whitaker, W., Xie, X., Romanos, M., Clare, J., 2002. Molecular cloning, distribution and functional analysis of the NaV1. 6. Voltage-gated sodium channel from human brain. Mol. Brain Res. 103 (1-2), 80–90.

[9] Chatelier, A., Zhao, J., Bois, P., Chahine, M., 2010. Biophysical characterisation of the persistent sodium current of the Na v 1.6 neuronal sodium channel: a single-channel analysis. Pflügers Archiv Eur J Physiol 460 (1), 1–10.

[10] Chen, Y., Yu, F., Sharp, E., Beacham, D., Scheuer, T., Catterall, W., 2008. Functional properties and differential neuromodulation of Nav1. 6 channels. Mol. Cell. Neurosci. 38 (4), 607–615.

[11] Craner, M., Hains, B., Lo, A., Black, J., Waxman, S., 2004. Co-localization of sodium channel Nav1. 6 and the sodium-calcium exchanger at sites of axonal injury in the spinal cord in EAE. Brain 127 (2), 294.

[12] Devor, M., 2009. Ectopic discharge in Aβ afferents as a source of neuropathic pain. Exp. Brain Res. 196 (1), 115–128.

[13] Di, X., Goforth, P., Bullock, R., Ellis, E., Satin, L., 2000. Mechanical injury alters volume activated ion channels in cortical astrocytes. Acta Neurochir. Suppl. 76, 379–383.

[14] Farkas, O., Povlishock, J., 2007. Cellular and subcellular change evoked by diffuse traumatic brain injury: a com-

plex web of change extending far beyond focal damage. Prog. Brain Res. 161, 43–59.

[15] Finol-Urdaneta, R., McArthur, J., Juranka, P., French, R., Morris, C., 2010. Modulation of KvAP Unitary Conductance and Gating by 1-Alkanols and Other Surface Active Agents. Biophys. J. 98 (5), 762–772.

[16] Hodgkin, A., 1948. The local electric changes associated with repetitive action in a non-medullated axon. J. Physiol. 107 (2), 165.

[17] Hodgkin, A., Huxley, A., 1952. A quantitative description of membrane current and its application to conduction and excitation in nerve. J. Physiol 117, 500–544.

[18] Hogg, R., Lewis, R., Adams, D., 2002. Ciguatoxin-induced oscillations in membrane potential and action potential firing in rat parasympathetic neurons. Eur. J. Neurosci. 16 (2), 242–248.

[19] Hu, W., Tian, C., Li, T., Yang, M., Hou, H., Shu, Y., 2009. Distinct contributions of Nav1. 6 and Nav1. 2 in action potential initiation and backpropagation. Nature Neurosci. 12 (8), 996–1002.

[20] Isose, S., Misawa, S., Sakurai, K., Kanai, K., Shibuya, K., Sekiguchi, Y., Nasu, S., Noto, Y., Fujimaki, Y., Yokote, K., et al., 2010. Mexiletine suppresses nodal persistent sodium currents in sensory axons of patients with neuropathic pain. Clin. Neurophysiol. 121 (5), 719–724.

[21] Kager, H., Wadman, W., Somjen, G., 2000. Simulated seizures and spreading depression in a neuron model incorporating interstitial space and ion concentrations. J. Neurophysiol. 84, 495.

[22] Kimelberg, H., 2004. Volume activated anion channel and astrocytic cellular edema in traumatic brain injury and stroke. Adv. Exp. Med. Biol. 559, 157–167.

[23] Kovalsky, Y., Amir, R., Devor, M., 2009. Simulation in Sensory Neurons Reveals a Key Role for Delayed Na+ Current in Subthreshold Oscillations and Ectopic Discharge: Implications for Neuropathic Pain. Journal of neurophysiology 102 (3), 1430.

[24] Krepkiy, D., Mihailescu, M., Freites, J., Schow, E., Worcester, D., Gawrisch, K., Tobias, D., White, S., Swartz, K., 2009. Structure and hydration of membranes embedded with voltage-sensing domains. Nature 462 (7272), 473–479.

[25] Läuger, P., 1991. Electrogenic ion pumps. Distinguished lecture series of the Society of General Physiologists. 5.

[26] Lemieux, D., Roberge, F., Joly, D., 1992. Modeling the Dynamic Features of the Electrogenic Na,K pump of Cardiac Cells. J. theor. Biol. 154, 335–338.

[27] Li, G., Sun, H., Zhang, X., Cheng, L., Chiu, S., Tse, H., Lau, C., 2009. Omega-3 polyunsaturated fatty acids inhibit transient outward and ultra-rapid delayed rectifier K+ currents and Na+ current in human atrial myocytes. Cardiovasc. Res. 81 (2), 286.

[28] Lorincz, A., Nusser, Z., 2010. Molecular identity of dendritic voltage-gated sodium channels. Science's STKE 328 (5980), 906.

[29] Lundbĉk, J., Collingwood, S., Ingólfsson, H., Kapoor, R., Andersen, O., 2010. Lipid bilayer regulation of membrane protein function: gramicidin channels as molecular force probes. J. R. Soc. Interface 7 (44), 373–395.

[30] Luo, S., Perry, G., Levinson, S., Henry, M., 2010. Pulpitis Increases the Proportion of Atypical Nodes of Ranvier in Human Dental Pulp Axons without a Change in Nav1. 6 Sodium Channel Expression. Neurosci. 169 (4), 1881–1887.

[31] Massimini, M., Boly, M., Casali, A., Rosanova, M., Tononi, G., 2009. A perturbational approach for evaluating the brain's capacity for consciousness. Prog. Brain Res. 177, 201–214.

[32] Maxwell, W., 1996. Histopathological changes at central nodes of Ranvier after stretch-injury. Microscopy research and technique 34 (6), 522–535.

[33] McGinn, M., Kelley, B., Akinyi, L., Oli, M., Liu, M., Hayes, R., Wang, K., Povlishock, J., 2009. Biochemical, structural, and biomarker evidence for calpain-mediated cytoskeletal change after diffuse brain injury uncomplicated by contusion. J. Neuropathol. Exp. Neurol. 68 (3), 241.

[34] McIntyre, C., Grill, W., 2002. Extracellular stimulation of central neurons: influence of stimulus waveform and frequency on neuronal output. J. Neurophysiol. 88 (4), 1592.

[35] Monnerie, H., Tang-Schomer, M., Iwata, A., Smith, D., Kim, H., Le Roux, P., 2010. Dendritic alterations after dynamic axonal stretch injury in vitro. Exp. Neurol. 224 (2), 415–423.

[36] Morris, C., Juranka, P., 2007. Lipid stress at play: mechanosensitivity of voltage-gated channels. Curr. Top. Membr. 59, 297–338.

[37] Morris, C., Lecar, H., 1981. Voltage oscillations in the barnacle giant muscle fiber. Biophys. J. 35 (1), 193–213.

[38] Ochab-Marcinek, A., Schmid, G., Goychuk, I., Hänggi, P., 2009. Noise-assisted spike propagation in myelinated neurons. Phys. Rev. E 79 (1), 11904.

[39] Phillips, R., Ursell, T., Wiggins, P., Sens, P., 2009. Emerging roles for lipids in shaping membrane-protein function. Nature 459 (7245), 379–385.

[40] Prescott, S., De Koninck, Y., Sejnowski, T., 2008. Biophysical basis for three distinct dynamical mechanisms of action potential initiation. PLoS Comput. Biol. 4 (10).

[41] Richardson, A., McIntyre, C., Grill, W., 2000. Modelling the effects of electric fields on nerve fibres: influence of the myelin sheath. Med. Biol. Eng. Comput. 38 (4), 438–446.

[42] Rush, A., Dib-Hajj, S., Waxman, S., 2005. Electrophysiological properties of two axonal sodium channels, Nav1. 2 and Nav1. 6, expressed in mouse spinal sensory neurones. J. Physiol. 564 (3), 803.

[43] Schafer, D., Jha, S., Liu, F., Akella, T., McCullough, L., Rasband, M., 2009. Disruption of the axon initial segment cytoskeleton is a new mechanism for neuronal injury. J. Neurosci. 29 (42), 13242–13254.

[44] Schiff, N., 2008. Central thalamic contributions to arousal regulation and neurological disorders of consciousness.

Ann. N Y Acad. Sci. 1129, 105–118.

[45] Schmidt, D., MacKinnon, R., 2008. Voltage-dependent K+ channel gating and voltage sensor toxin sensitivity depend on the mechanical state of the lipid membrane. Proc. Natl. Acad. Sci. USA 105 (49), 19276–19281.

[46] Schwarz, J., Reid, G., Bostock, H., 1995. Action potentials and membrane currents in the human node of Ranvier. Pflügers Archiv European Journal of Physiology 430 (2), 283–292.

[47] Seifert, G., Huttmann, K., Binder, D., Hartmann, C., Wyczynski, A., Neusch, C., Steinhauser, C., 2009. Analysis of astroglial K+ channel expression in the developing hippocampus reveals a predominant role of the Kir4. 1 subunit. J. Neurosci. 29 (23), 7474–7488.

[48] Smit, J., Hanekom, T., Hanekom, J., 2009. Modelled temperature-dependent excitability behaviour of a single ranvier node for a human peripheral sensory nerve fibre. Biol. Cybern. 100 (1), 49–58.

[49] Smith, D., Meaney, D., Shull, W., 2003. Diffuse axonal injury in head trauma. J. Head Trauma Rehabil. 18 (4), 307.

[50] Steffensen, I., Waxman, S., Mills, L., Stys, P., 1997. Immunolocalization of the Na+-Ca2+ exchanger in mammalian myelinated axons. Brain Res. 776 (1-2), 1–9.

[51] Stys, P., Sontheimer, H., Ransom, B., Waxman, S., 1993. Noninactivating, tetrodotoxin-sensitive Na+ conductance in rat optic nerve axons. Proc. Natl. Acad. Sci. USA 90 (15), 6976.

[52] Taddese, A., Bean, B., 2002. Subthreshold sodium current from rapidly inactivating sodium channels drives spontaneous firing of tuberomammillary neurons. Neuron 33 (4), 587–600.

[53] Thomas, E., Hawkins, R., Richards, K., Xu, R., Gazina, E., Petrou, S., 2009. Heat opens axon initial segment sodium channels: a febrile seizure mechanism? Ann. Neurol. 66 (2), 219–226.

[54] Tokuno, H., Kocsis, J., Waxman, S., 2003. Noninactivating, tetrodotoxin-sensitive Na+ conductance in peripheral axons. Muscle Nerve 28 (2), 212–217.

[55] Viano, D., Casson, I., Pellman, E., Bir, C., Zhang, L., Sherman, D., Boitano, M., 2005. Concussion in professional football: Comparison with boxing head impacts-Part 10. Neurosurgery 57 (6), 1154.

[56] Wang, J., Lin, W., Morris, T., Banderali, U., Juranka, P., Morris, C., 2009. Membrane trauma and Na+ leak from Nav1. 6 channels. Am. J. of Physiol. 297 (4), C823.

[57] Wolf, J., Stys, P., Lusardi, T., Meaney, D., Smith, D., 2001. Traumatic axonal injury induces calcium influx modulated by tetrodotoxin-sensitive sodium channels. J. Neurosci. 21 (6), 1923.

[58] Yuen, T., Browne, K., Iwata, A., Smith, D., 2009. Sodium channelopathy induced by mild axonal trauma worsens outcome after a repeat injury. J. Neurosci. Res. 87 (16), 3620–3625.

Chapter 6

Subthreshold oscillations

A feature of modeled left-shifted Nav channels not presented in the articles (but still relevant to traumatic brain injuries) is the possibility of generating subthreshold oscillations which eventually lead to action potentials. Subthreshold oscillations are enhanced in Dorsal Root Ganglion (DRG, the part of a nerve which contains the cell bodies) neurons by nerve injury[104, 105], causing neuropathic pain (see Fig. 6.1). Knowing that trauma causes Nav channels to left-shift, it can easily be hypothesized that subthreshold oscillation in traumatized neurons are caused by the smeared out window conductance regions of variously left-shifted Nav channels.

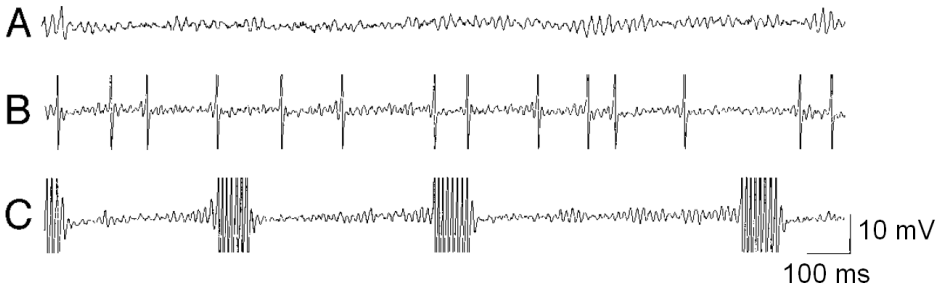

Figure 6.1 Subthreshold membrane potential oscillations in rat dorsal root ganglion neurons (A) can lead to intermittent action potential firing (B) and burst firing (C). Such membrane potential oscillations are present in $\sim 5\%$ of the neurons in the control experiment; that fraction is increased to $\sim 15\%$ by trauma (axotomy). Spikes are truncated. Liu *et al.*, J. Neurophysiol., 2000,[104] Am Physiol Soc, used with permission.

To say that subthreshold oscillations in DRG neurons are caused solely by the widening of the window conductance region because of left-shifted activity of Nav channels would however be presumptuous. Nevertheless, the fact that a widened window conductance region can lead to subthreshold oscillations reinforces the claim that left-shifted Nav channels participate in neuropathic pain.

In DRG neurons (as opposed to modeled systems) there is at least two types of sodium channels (Nav1.2 and Nav1.6), which both left-shift upon trauma (in recombinant systems); the left-shift could be a mix of graded and all-or-none shifts such that the window conductance region (and the activation thresholds) are smeared over a whole region of potentials; there is a thermal background noise, pushing and kicking on everything, possibly accentuating subthreshold oscillations and ectopic firing. Considering that expression of Nav1.3 channels is up-regulated in injured DRG neurons[110], the increased subthreshold oscillation observed might be the result not of left-shifted channel activity, but rather of changing levels of expression of different Nav channel types. Such a situation is still handled by our model, by considering that a left-shifted population could in fact be a different channel type (to be more accurate, more precise kinetics would also be required).

To reproduce the behavior in Fig. 6.1, requires at least three populations of channels in the system: one intact and two left-shifted by different amounts. The rationale being that the most left-shifted channel would have a large window conductance near the resting potential, thus depolarizing the membrane towards the window conductance region of the second shifted channels population which would further depolarize the membrane, possibly enough to reach the threshold of the intact channel population which would open thus leading to an action potential (see Fig. 6.2). Each iteration of the process which does not create an action potential is followed by a repolarization phase because the depolarization caused the channels to inactivate. Each iteration increases the amplitude of this depolarization-repolarization cycle with eventually a large enough amplitude to yield an action potential (see Fig. 6.3).

Interestingly, stimulating a system experiencing subthreshold oscillations does not generate a repetitive firing mode and any oscillations disappear. There is at most a single spike at the onset of the stimulating current (not shown). The stimulating current possibly depolarizes the system outside of the window conductance region necessary to maintain the subthreshold behavior.

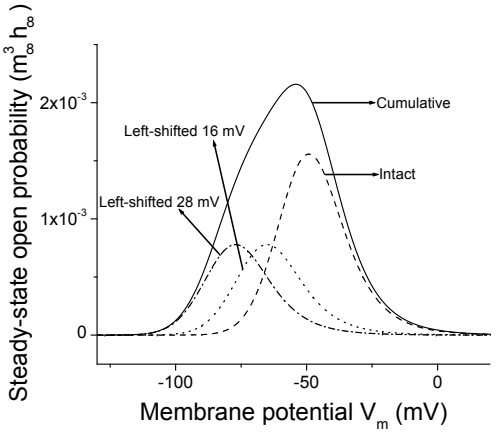

Figure 6.2 Window conductance (steady-state open probability) in the model with three populations: one intact, one left-shifted 16 mV and one left-shifted 28 mV. The intact population comprises 50% of the channels and the shifted populations 25% each. Such a configuration leads to growing subthreshold oscillations, eventually spiking to action potential.

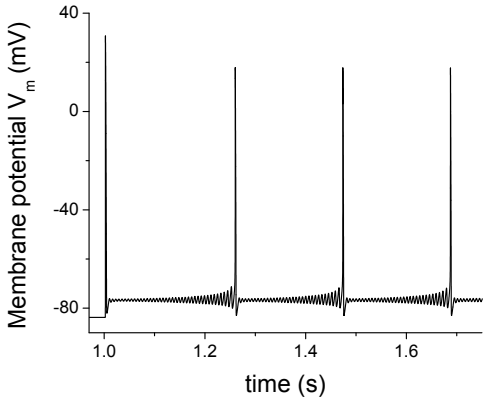

Figure 6.3 Subthreshold oscillations growing into spikes. The pattern is reminiscent of Fig. 6.1B. Parameters used: $AC_1 = 25\%$, $LS_{AC1} = 16$ mV, $AC_1 = 25\%$, $LS_{AC1} = 28$ mV.

Subthreshold oscillations have been reproduced in model systems using "late" currents, Na currents with slow inactivation[102]. Interestingly, the "late" currents were left-shifted compared to the "rapid" Na current. Adjusting the Na and K conductances allows shift between different firing modes (tonic and burst firing). These firing modes can also be generated in our model (albeit without subthreshold oscillations). Our results stress the fact that the left-shift of channels (or possibly multiple populations of channels), which can cause different spontaneous firing modes, can also contribute to the subthreshold oscillations seen

in injured DRG neurons.

To complete this study, it would be interesting to modify the model to keep track of a larger number of left-shifted channel populations. In the present model, every population of channels has its own kinetics adding a set of equations to be solved numerically. Still it is well within our computational power to write a program which would be able to handle say 20 populations of channels, each with a different left-shift. Such a solution would be cumbersome due to the large number of parameter involved (AC and LS_{AC} for each population). Still 20 populations of channels would enable the simulation of a spread of channel left-shift, which might be closer to what happens in reality.

Chapter 7

Conclusion

7.1 On membrane spandex

In the first part of this thesis, we presented our work on membrane spandex. Many studies on bilayer-protein interactions (e.g., [45, 46, 47, 19]) have been published, but an aspect that has never been considered before was studied: that not only bilayer mechanics influence protein conformation, but that the reverse could also be true.

We studied if and how a cell could possibly use proteins with large area changes between silent states to damp membrane tension excursions, or to maintain a fixed level of tension. MscL and MscS, because of their large in-plane expansion, were used as case studies. Experimental data also suggests that they possess large silent transitions: MscL silently pre-expands before opening and MscS possesses an expanded inactivated state.

To perform the study, we used a simple two-state model of a membrane spandex and explored the model's predictions computationally. The location (along an area axis) of the transition barrier controls the kinetics of the spandex. A spandex with a midpoint below that of the osmovalves and a transition barrier at a large area would optimize osmovalve activity, preventing costly accidental openings. Another spandex, with a transition barrier located halfway between the contracted and expanded state could act as a tension damper if its tension midpoint is equal to the target tension. Spandex expansion/contraction would

prevent tension fluctuations away from the target tension. We also suggested experimental approaches to detect spandex proteins.

The challenge now resides in getting experimentalists interested in testing these ideas. Some groups are already looking into the "spandex effect" (as referred to in [28]). Belyy *et al.*[28] studied the adaptation of MscL and MscS to tension: in a patch-clamp setting, when tension (through pressure) is applied, they open but over time a part of the population closes (i.e., adapts to the tension) even as the pressure level is maintained. They show that the effect is dependent on the experimental method used: when whole-cell clamp is used, no adaptation is detected. They show that the apparent adaptation effect is due to a sliding of the inner lipid bilayer leaflet which relaxes tensions. Because MscL and MscS sense tension from the inner leaflet, it does not "feel" the same tension even though the pressure level is maintained. They considered whether the spandex effect of expanding channels could be involved in the apparent adaptation. It turns out that their expression level was too low (~ 100 MscL in a 1 μm patch) to obtain any detectable effect. Hopefully they will continue to consider the question.

Romantsov *et al.*[111] used fluorescence microscopy to study the localization of various proteins in *E.coli*. They showed that cardiolipin causes MscS to segregate at the poles of *E.coli*. They note: "Aggregation of MscS at the cell poles could influence both its channel function and the impact of its structural transitions on membrane strain." They do not prove that MscS has any effect on membrane strain or tension, but they expect that it does; the idea of spandex is catching on. Indeed segregating at the pole when cardiolipin is present might mean that cardiolipin itself segregates at the poles and MscS interacts favorably with it. Does this change the kinetics of MscS? Its midpoint? Does it favor the closed to inactivated state seen in mutant forms of MscS? These questions have still to be answered. In the spandex article, we suggested that some osmovalve-capable channel could segregate at the poles whereas spandex proteins would segregate in the cylindrical region of a bacteria. According to Laplace's law, the osmovalve would be in a lower tension environment than the spandex thus lowering the probability of accidental openings. So far no segregation of MscL has been detected, however this does not rule out the possibility that MscL could be affected by its lipid environment, perhaps stabilizing the pre-expanded state, turning MscL into a spandex.

Atomic force microscopy (as used by Beyder and Sachs[38]) could be very useful in

studying membrane spandex. They used it to study *Shaker* (a voltage-gated potassium channel)-transfected HEK cells and they showed that the area expansion of the channel has an effect on electromotility, possibly due to uneven expansion of the channel (*Shaker* expanding mostly in the inner leaflet), causing the membrane to buckle. Using this method in conjunction with other potential spandex candidates might prove interesting for the study of their effect on bilayer mechanics.

With all these methods available to study membrane spandex, it would be surprising that no effect would ever be detected, but even if there is no spandex effect, this would be interesting as it would raise the question: "why?" and then the model could be refined.

The model could be improved in many ways; we will discuss a few. In our model, the bilayer-spandex interaction is limited to the areal expansion of the spandex and relaxation of bilayer tension. Effects such as the hydrophobic mismatch (the energy arising from the difference in hydrophobic height between the bilayer and protein) and local curvature around a protein could be included in the model. This would allow for a more complete and accurate description of the energetics of a membrane spandex.

The model could further be refined by considering the localization of membrane spandex in a lipid bilayer (or even spandex and say MscL), allowing the study of large scale curvature effects (say at the poles of a cylindrical bacterium) and of different tension at the poles and sides of the bacterium. Forcing MscL to remain at the poles would allow a more elaborate study of whether a spandex operating from the cylindrical sides would be more effective in preventing accidental openings of a pole-located osmovalve.

Such an improved model would allow the study of cooperative gating[50]. If for example the open and closed states of a channel do not have the same height, then there is an energetic cost to placing two channels, one open, one closed next to each other. Such an effect, through bilayer deformation, could be significant over the distance of a few channel radii. Channel transition would have an additional energetic component: e.g., opening a single channel next to closed channels would be energetically costly. Clustered channels would then tend to open all at the same time. This is in contrast of what was shown in the spandex article where spandex expansion provides a negative feedback: spandex expansion relieves tension, decreasing the probability of expanding more spandex. Cooperative gating and tension relief provide opposite feedback mechanisms; it is not clear how a system where both effects are important would behave.

This conjugate effect might perhaps shed some light on mechanosensitive channels displaying oscillatory behavior under a fixed level of tension (B. Martinac, personal communications).

This work on membrane spandex has already raised some interest from experimentalists working on mechanosensitive channels. Hopefully interest will continue to grow and the article will contribute to a change in the view of bilayer inclusions: that they can have an effect on bilayer structure and mechanics.

7.2 On Traumatized Nav channels

In the second part of this thesis, we used modeling and computer simulations to study left-shifted Nav channels and the excitability of a traumatized node of Ranvier. In the first article, Ch. 4, we studied whether any "non-inactivating" sodium currents become left-shifted with the transient current left-shift observed. In Ch. 4, we also proposed a voltage-step protocol which would allow to determine whether the left-shift of Nav channels occurs as an all-or-none or graded process. Interestingly our study revealed that an experimental measurement protocol often used could fail in the case of left-shifted channels. Persistent currents are often measured as the fraction of steady-state to peak currents for a voltage step to 0 mV (from a polarized potential). The argument behind that use is that a more "leaky" channel would have larger steady-state currents. When left-shift is present, this is not the case: steady-state currents at 0 mV would actually decrease, reflecting the left-shifted "window conductance" from which steady-state currents arise.

In Ch. 4 we suggested that Nav channels could switch mode (from an active to a relaxed mode) where the inactivation particle would be unable to bind to the pore region, thus rendering the channel "persistent". An interesting next step would be to establish a complete model of Nav channel gating from both experimental data and theory, possibly unifying all the different Na currents observed experimentally (e.g., "late", "persistent", "transient", "non-inactivating", "slow" etc.). Ideally the model would explain transient, window and persistent currents, but also the tension dependence of Nav channels on bilayer tension, possibly even explaining from a mechanistic point of view the trauma-induced left-shift

In the second paper, Ch. 5, we studied the firing regimes of an injured node of Ranvier in two scenarios: fixed and non-fixed concentrations. The results show unequivocally that left-shifted channels have profound consequences on the excitability of a node. Depending on the amount of shifted channels, and on the extent of that shift, a node can fire spontaneously or be rendered silent. Essentially, shifting Nav channels allows a switch between Hodgkins's[90] excitability classes. The model also revealed that even for small shifts, the sodium gradient would rapidly dissipate. Left-shift of Nav channels thereby provides a bridge between mechanical trauma and the increase in axonal Ca observed after trauma[63] (see Fig. 3.25). We suggest that the spontaneous firing of nodes of Ranvier could underlie neuropathic pain which arises from ectopically generated action potentials. We also suggest that large shifts of Nav channels could cause sudden loss of consciousness by rendering axons silent.

The global aim of this study is to help develop drugs that will cure such conditions as diffuse axonal injury and neuropathic pain. Nav channels are already known to mediate the axonal Ca increase which follows mechanical injury. Proving *in situ* that it is their trauma-induced left-shift that renders them "leaky", and understanding how that left-shift occurs would most likely help in designing drugs that would specifically block misbehaving Nav channels.

Trauma-induced left-shift of Nav channels and the resulting excitability changes could have wide ramifications. For example, traumatic brain injury and diffuse axonal injury[112], tooth pain[113], carpal tunnel syndrome[114] and neuropathic pain[103] could all be linked to Nav channel malfunction. We must be careful here as we do not state that all these conditions are caused by left-shifted Nav channels, rather we hypothesize that they could play a role in these conditions. Hopefully this study will help focus experimental studies on the causes of excitability changes and on the mechanism of the left-shift of Nav channels.

Aside from whether injured Nav channels are involved in these conditions, it would be interesting to test if other channels can be left-shifted by trauma. The current hypothesis is that left-shift is induced by a decrease of the energetic barrier for voltage-sensor movement, caused by a change in local bilayer mechanics/composition. It would be unlikely that Nav1.6 is the only channel normally sitting in a specialized microdomain and hence it would be unlikely that no other membrane protein would be affected by trauma. Potassium channels would be the first obvious candidate to test as they are already known to be modulated

by tension[37] and play an important role in excitability[98]. Other proteins involved in excitability and ion homeostasis could be also affected by trauma and bleb formation. For example, if the Na/K pump were to malfunction, the consequences would rapidly be catastrophic as the Na gradient would rapidly be depleted and Ca loading would ensue. Studies on trauma-modified channel and protein function is sure to prove interesting.

Modifications could be made to improve the model, and improve its biophysical predictions. For instance, calcium could be explicitly included in the model. This would require including the Na/Ca exchanger, Ca pumps, voltage-gated Ca channels and Ca buffers. The main pathway of Ca entry following axonal stretch injury could then be identified. Currently two modes of entry are regarded as possible (see Fig. 3.25). 1) The Na/Ca exchanger uses the Na and Ca gradients as the driving force to transport Na and Ca across the membrane. It normally uptakes Na and extrudes Ca, but a dissipated Na gradient might reverse the exchanger, which would then start uptaking Ca. 2) Dissipation of the Na gradient depolarizes the membrane thus opening voltage-gated Ca channels, allowing Ca ions to flow inside. Additionally, Ca dynamics would have an electrogenic contribution thus contributing (favorably or negatively) to membrane excitability and ion homeostasis. Note however that in this work we did not include Ca dynamics as it is not absolutely necessary: it is an experimental fact that a dissipated Na gradient entails a rise in internal Ca. Including Ca dynamics would also necessitate more parameters, some of which are not currently known precisely (e.g., the number of Na/Ca exchangers at nodes of Ranvier); more detailed modeling would not necessarily mean more accurate results.

The model could also be improved by a better modeling of myelin. The model we used was simple, assuming myelin to be a perfect insulator, but other more sophisticated models of myelin exist[92]. Our study of action potential transmission on a myelinated axon was limited to qualitative aspects, and a single quantitative aspect (i.e., firing frequency). A more complex model would allow a complete nonlinear dynamics study of the myelinated axon with an injured node. An aspect we didn't cover was the axon's conduction velocity. The time needed for an action potential to reach the axon terminal would be affected by the presence of a faster (or slower) firing node. For instance, localization of sounds in space relies, in part, on the timing of these sounds (see e.g., [115]) and hence on the time needed for the information to travel from the ear to the brain.

Another improvement would be to include concentration changes in interior and exterior

compartments for each node of Ranvier on an axon (possibly along with the inclusion of Ca modeling). Diffusion between the compartments (interior and exterior) would need to be included too, thus allowing to study whether a single injured node is sufficient to deplete the Na gradient in the whole axon (and raise calcium levels); or how much trauma is required? Ideally the glial cells (the cells that form the myelin sheath) would also be included in such a model as they are known to buffer the external K concentration and help maintain ion homeostasis.

Finally, levels of expression of different channels are known to change in damaged nodes of Ranvier (see e.g., [113]). It would be interesting to establish a model that would not only include currents through membrane channels and ion homeostasis, but would also include channels expression (and changing levels thereof). Such a model may seem idealistic at this point, but some feel that we are on the brink of a radical change in biological thinking and that mathematics and physics will play an important role in this change[116].

Appendix A

Reversal potential

In this annexe we derive the equation for reversal potential following Matthews[117] and Hille[30]. The reversal potential is the value of membrane potential for which the net current of ion X is zero. We start with the Nernst-Planck equation for ion fluxes which extends Fick's law for diffusing particles which are also moved by electrostatic forces:

$$J_X = zFD\left(\frac{dc_X}{dx} + \frac{Fzc_X}{RT}\frac{dV}{dx}\right), \tag{A.1}$$

where J_X is the flux (current per unit area) of ion species X, z is the valence, F is Faraday's constant, D is the diffusion constant, c_X is the concentration, R is the ideal gas constant, T is the temperature, V is the electrical potential and x is position.

By definition the net flux at the reversal potential is 0, so we have:

$$\frac{dc_X}{dx} = -\frac{Fzc_X}{RT}\frac{dV}{dx}, \tag{A.2}$$

which can be rewritten as:

$$dV = -\frac{dc_X}{c_X}\frac{RT}{zF}. \tag{A.3}$$

Integrating (from the exterior to the interior) on both sides yields:

$$V_{in} - V_{out} = -\frac{RT}{zF} \int_{[X]_{out}}^{[X]_{in}} \frac{dc_X}{c_X} = \frac{RT}{zF} \ln\left(\frac{[X]_{out}}{[X]_{in}}\right). \tag{A.4}$$

Replacing $V_{in} - V_{out} = E_X$, where E_X is the reversal potential, in the preceding equation finally yields:

$$E_X = \frac{RT}{zF} \ln\left(\frac{[X]_{out}}{[X]_{in}}\right). \tag{A.5}$$

Appendix B

Numerical Methods

All models in this work were solved using the fourth order Runge-Kutta method. In this chapter, we give a brief overview of the RK4 method.

Consider an initial conditions problem:

$$\frac{dy}{dt} = f(t, y), \quad y(t_0) = y_0. \tag{B.1}$$

For example $\frac{dy}{dt}$ could be replaced by the equation from the HH model: $\frac{dV}{dt} = -\frac{I_{tot}}{C_m}$ with the initial condition that $V_m = V_{rest}$. The RK4 method solves this initial condition problem using:

$$y_{n+1} = y_n + \tfrac{1}{6}h\left(k_1 + 2k_2 + 2k_3 + k_4\right), \tag{B.2}$$

$$t_{n+1} = t_n + h, \tag{B.3}$$

where y_{n+1} is the approximation of $y(t_{n+1})$. The coefficients k_1 to k_4 are given by:

$$k_1 = f(t_n, y_n), \tag{B.4}$$
$$k_2 = f(t_n + \tfrac{1}{2}h, y_n + \tfrac{1}{2}hk_1), \tag{B.5}$$
$$k_3 = f(t_n + \tfrac{1}{2}h, y_n + \tfrac{1}{2}hk_2), \tag{B.6}$$
$$k_4 = f(t_n + h, y_n + hk_3). \tag{B.7}$$

Essentially the RK4 method calculates four approximations of $y(t_{n+1})$: one at the beginning of the interval, two in the middle and one at the end, and then takes a weighted average of these values to be the final approximation.

The RK4 method also works for a system of equations. As an example, we present the equations for two time-dependent variables (from there, adding more variables is trivial).

The initial problem (using variables similar to those used in the HH model) is:

$$\frac{dV}{dt} = f(m, V, t), \quad V(t_0) = V_{rest}, \tag{B.8}$$
$$\frac{dm}{dt} = g(m, V, t), \quad m(t_0) = m_0. \tag{B.9}$$

The RK4 solution to this problem is:

$$V_{n+1} = V_n + \tfrac{1}{6}h\left(k_1 + 2k_2 + 2k_3 + k_4\right), \tag{B.10}$$
$$m_{n+1} = m_n + \tfrac{1}{6}h\left(l_1 + 2l_2 + 2l_3 + l_4\right), \tag{B.11}$$
$$t_{n+1} = t_n + h, \tag{B.12}$$

with the k_1 to k_4 and l_1 to l_4 parameters given by:

$$
\begin{aligned}
k_1 &= f(m_n, V_n, t_n), && \text{(B.13)}\\
l_1 &= g(m_n, V_n, t_n), && \text{(B.14)}\\
k_2 &= f(m_n + \tfrac{1}{2}hl_1, V_n + \tfrac{1}{2}hk_1, t_n + \tfrac{1}{2}h), && \text{(B.15)}\\
l_2 &= g(m_n + \tfrac{1}{2}hl_1, V_n + \tfrac{1}{2}hk_1, t_n + \tfrac{1}{2}h), && \text{(B.16)}\\
k_3 &= f(m_n + \tfrac{1}{2}hl_2, V_n + \tfrac{1}{2}hk_2, t_n + \tfrac{1}{2}h), && \text{(B.17)}\\
l_3 &= g(m_n + \tfrac{1}{2}hl_2, V_n + \tfrac{1}{2}hk_2, t_n + \tfrac{1}{2}h), && \text{(B.18)}\\
k_4 &= f(m_n + hl_3, V_n + hk_k, t_n + h), && \text{(B.19)}\\
l_4 &= g(m_n + hl_3, V_n + hk_k, t_n + h). && \text{(B.20)}
\end{aligned}
$$

This kind of algorithm was implemented in Fortran. Simulations took from seconds to days depending on the system to be solved.

Bibliography

[1] CE Morris. *How did cells get their size?*, ***Anat. Rec.*** **268**, 239–251 (2002).

[2] PA Boucher, CE Morris, B Joós. *Mechanosensitive Closed-Closed Transitions in Large Membrane Proteins: Osmoprotection and Tension Damping*, ***Biophys. J.*** **97**, 2761–2770 (2009).

[3] B Alberts, A Johnson, J Lewis, M Raff, K Roberts, P Walter. *Molecular biology of the cell*. Garland Science, New York, NY (2007).

[4] DH Boal. *Mechanics of the Cell*. Cambridge University Press, Cambridge, UK (2002).

[5] `http://en.wikipedia.org/wiki/File:Cell_membrane_detailed_diagram_4.svg`, (12 août 2010).

[6] SJ Singer, GL Nicolson. *The fluid mosaic model of the structure of cell membranes*, ***Science*** **175**, 720–731 (1972).

[7] V Bennett, AJ Baines. *Spectrin and ankyrin-based pathways: metazoan inventions for integrating cells into tissues*, ***Physiol. Rev.*** **81**, 1353 (2001).

[8] F Sachs, C Morris. *Mechanosensitive ion channels in nonspecialized cells*, ***Rev. Physiol. Bioch. P.*** **130**, 1–77 (1998).

[9] OP Hamill. *Twenty odd years of stretch-sensitive channels*, ***Pflüigers Arch. Eur. J. Physiol.*** **453**, 333–351 (2006).

[10] E Perozo. *Gating prokaryotic mechanosensitive channels*, ***Nat. Rev. Mol. Cell Biol.*** **7**, 109–119 (2006).

[11] B Corry, B Martinac. *Bacterial mechanosensitive channels: Experiment and theory*, ***BBA-Biomembranes* 1778**, 1859–1870 (2008).

[12] F Sachs. *Stretch-Activated Ion Channels: What Are They?*, ***Phyiol.* 25**, 50–56 (2010).

[13] S Sukharev, SR Durell, HR Guy. *Structural models of the MscL gating mechanism*, ***Biophys. J.* 81**, 917–936 (2001).

[14] SI Sukharev, WJ Sigurdson, C Kung, F Sachs. *Energetic and Spatial Parameters for Gating of the Bacterial Large Conductance Mechanosensitive Channel, MscL*, ***J. Gen. Physiol.* 113**, 525–540 (1999).

[15] N Levina, S Tötemeyer, NR Stokes, P Louis, MA Jones, IR Booth. *Protection of Escherichia coli cells against extreme turgor by activation of MscS and MscL mechanosensitive channels: identification of genes required for MscS activity*, ***EMBO J.* 18**, 1730–1737 (1999).

[16] IR Booth, MD Edwards, S Black, U Schumann, W Bartlett, T Rasmussen, A Rasmussen, S Miller. *Physiological Analysis of Bacterial Mechanosensitive Channels*, ***Methods Enzymol.* 428**, 47–61 (2007).

[17] IR Booth, MD Edwards, S Black, U Schumann, S Miller. *Mechanosensitive channels in bacteria: signs of closure?*, ***Nat. Rev. Microbiol.* 5**, 431–440 (2007).

[18] SI Sukharev, VS Markin. *Kinetic model of the bacterial large conductance mechanosensitive channel*, ***Biol. membrany* 18**, 440–445 (2001).

[19] VS Markin, F Sachs. *Thermodynamics of mechanosensitivity*, ***Phys. Biol.* 1**, 110–124 (2004).

[20] CS Chiang, A Anishkin, S Sukharev. *Gating of the Large Mechanosensitive Channel In Situ: Estimation of the Spatial Scale of the Transition from Channel Population Responses*, ***Biophys. J.* 86**, 2846–2861 (2004).

[21] A Anishkin, S Sukharev. *State-stabilizing Interactions in Bacterial Mechanosensitive Channel Gating and Adaptation*, ***J. Biol. Chem.* 284**, 19153 (2009).

[22] S Sukharev. *Purification of the Small Mechanosensitive Channel of Escherichia coli (MscS): the Subunit Structure, Conduction, and Gating Characteristics in Liposomes*, ***Biophys. J.* 83**, 290–298 (2002).

[23] A Anishkin, S Sukharev. *Water dynamics and dewetting transitions in the small mechanosensitive channel MscS*, ***Biophys. J.*** **86**, 2883–2895 (2004).

[24] A Anishkin, K Kamaraju, S Sukharev. *Mechanosensitive channel MscS in the open state: modeling of the transition, explicit simulations, and experimental measurements of conductance*, ***J. Gen. Physiol.*** **132**, 67 (2008).

[25] M Barclay, DC Rees, RB Bass, P Strop. *Crystal Structure of Escherichia coli MscS, a Voltage-Modulated and Mechanosensitive Channel*, ***Science*** **298**, 1582–1587 (2002).

[26] B Akitake, A Anishkin, S Sukharev. *The "dashpot" mechanism of stretch-dependent gating in MscS*, ***J. Gen. Physiol.*** **125**, 143 (2005).

[27] B Akitake, A Anishkin, N Liu, S Sukharev. *Straightening and sequential buckling of the pore-lining helices define the gating cycle of MscS*, ***Nat. Struct. Mol. Biol.*** **14**, 1141 (2007).

[28] V Belyy, K Kamaraju, B Akitake, A Anishkin, S Sukharev. *Adaptive behavior of bacterial mechanosensitive channels is coupled to membrane mechanics*, ***J. Gen. Physiol.*** **135**, 641 (2010).

[29] V Belyy, A Anishkin, K Kamaraju, N Liu, S Sukharev. *The tension-transmitting "clutch" in the mechanosensitive channel MscS*, ***Nat. Struct. Mol. Biol.*** **17**, 451–458 (2010).

[30] B Hille. *Ionic Channels of Excitable Membranes.* Sinauer Associates Inc, Sunderland, MA (2001).

[31] E Evans, V Heinrich, F Ludwig, W Rawicz. *Dynamic Tension Spectroscopy and Strength of Biomembranes*, ***Biophys. J.*** **85**, 2342–2350 (2003).

[32] CC Häse, RF Minchin, A Kloda, B Martinac. *Cross-Linking Studies and Membrane Localization and Assembly of Radiolabelled Large Mechanosensitive Ion Channel (MscL) of* Escherichia coli, ***Biochem. Biophys. Res. Commun.*** **232**, 777–782 (1997).

[33] NR Stokes, HD Murray, C Subramaniam, RL Gourse, P Louis, W Bartlett, S Miller, IR Booth. *A role for mechanosensitive channels in survival of stationary phase: regulation of channel expression by RpoS*, ***Proc. Natl. Acad. Sci. USA*** **100**, 15959 (2003).

[34] J Zheng, W Shen, DZZ He, KB Long, LD Madison, P Dallos. *Prestin is the motor protein of cochlear outer hair cells*, ***Nature*** **405**, 149–155 (2000).

[35] AJ Hudspeth. *Making an Effort to Listen: Mechanical Amplification in the Ear*, ***Neuron*** **59**, 530–545 (2008).

[36] KH Iwasa. *A two-state piezoelectric model for outer hair cell motility*, ***Biophys. J.*** **81**, 2495–2506 (2001).

[37] U Laitko, CE Morris. *Membrane Tension Accelerates Rate-limiting Voltage-dependent Activation and Slow Inactivation Steps in a Shaker Channel Abbreviation used in this paper: LS, linear substraction.*, ***J. Gen. Physiol.*** **123**, 135–154 (2004).

[38] A Beyder, F Sachs. *Electromechanical coupling in the membranes of Shaker-transfected HEK cells*, ***Proc. Natl. Acad. Sci. USA*** **106**, 6626 (2009).

[39] TD Lamb, EN Pugh. *Dark adaptation and the retinoid cycle of vision*, ***Prog. Retinal Eye Res.*** **23**, 307–380 (2004).

[40] P Sens, MS Turner. *Budded membrane microdomains as tension regulators*, ***Phys. Rev. E*** **73**, 31918 (2006).

[41] PA Boucher, B Joos, MJ Zuckermann, L Fournier. *Pore Formation in a Lipid Bilayer under a Tension Ramp: Modeling the Distribution of Rupture Tensions*, ***Biophys. J.*** **92**, 4344 (2007).

[42] B Martinac, M Buechner, AH Delcour, J Adler, C Kung. *Pressure-sensitive ion channel in Escherichia coli*, ***Proc. Natl. Acad. Sci. USA*** **84**, 2297 (1987).

[43] AF Batiza, MMC Kuo, K Yoshimura, C Kung. *Gating the bacterial mechanosensitive channel MscL in vivo*, ***Proc. Natl. Acad. Sci. USA*** **99**, 5643 (2002).

[44] E Perozo, A Kloda, DM Cortes, B Martinac. *Physical principles underlying the transduction of bilayer deformation forces during mechanosensitive channel gating*, ***Nat. Struct. Mol. Biol.*** **9**, 696–703 (2002).

[45] P Wiggins, R Phillips. *Analytic models for mechanotransduction: Gating a mechanosensitive channel*, ***Proc. Natl. Acad. Sci. USA*** **101**, 4071–4076 (2004).

[46] P Wiggins, R Phillips. *Membrane-Protein Interactions in Mechanosensitive Channels*, ***Biophys. J.*** **88**, 880–902 (2005).

[47] R Phillips, T Ursell, P Wiggins, P Sens. *Emerging roles for lipids in shaping membrane-protein function*, ***Nature*** **459**, 379–385 (2009).

[48] B Martinac, OP Hamill. *Gramicidin A channels switch between stretch activation and stretch inactivation depending on bilayer thickness*, ***Proc. Natl. Acad. Sci. USA*** **99**, 4308 (2002).

[49] C Norman, ZW Liu, P Rigby, A Raso, Y Petrov, B Martinac. *Visualisation of the mechanosensitive channel of large conductance in bacteria using confocal microscopy*, ***Eur. Biophys. J.*** **34**, 396–402 (2005).

[50] T Ursell, KC Huang, E Peterson, R Phillips. *Cooperative gating and spatial organization of membrane proteins through elastic interactions*, ***PLoS Comput. Biol.*** **3**, e81 (2007).

[51] D Reeves, T Ursell, P Sens, J Kondev, R Phillips. *Membrane mechanics as a probe of ion-channel gating mechanisms*, ***Phys. Rev. E.*** **78**, 041901 (2008).

[52] AM Powl, JM East, AG Lee. *Anionic Phospholipids Affect the Rate and Extent of Flux through the Mechanosensitive Channel of Large Conductance MscL*, ***Biochem.*** **47**, 4317–4328 (2008).

[53] PC Zhang, AM Keleshian, F Sachs. *Voltage-induced membrane movement*, ***Nature*** **413**, 428–432 (2001).

[54] J Árnadóttir, M Chalfie. *Eukaryotic Mechanosensitive Channels*, ***Ann. Rev. Microbiol.*** **63**, 79–98 (2009).

[55] JA Wang, W Lin, T Morris, U Banderali, PF Juranka, CE Morris. *Membrane trauma and Na+ leak from Nav1. 6 channels*, ***Am. J. Physiol.*** **297**, C823 (2009).

[56] WL Maxwell. *Histopathological changes at central nodes of Ranvier after stretch-injury*, ***Microscopy Res. Tech.*** **34**, 522–535 (1996).

[57] WA Catterall. *From Ionic Currents to Molecular Review Mechanisms: The Structure and Function of Voltage-Gated Sodium Channels*, ***Neuron*** **26**, 13–25 (2000).

[58] FH Yu, WA Catterall. *Overview of the voltage-gated sodium channel family*, ***Genome Biol* 4**, 207 (2003).

[59] `http://en.wikipedia.org/wiki/File:Sodium-channel.svg`, (16 juillet 2010).

[60] G Eaholtz, T Scheuer, WA Catterall. *Restoration of inactivation and block of open sodium channels by an inactivation gate peptide*, ***Neuron* 12**, 1041–1048 (1994).

[61] A Taddese, BP Bean. *Subthreshold sodium current from rapidly inactivating sodium channels drives spontaneous firing of tuberomammillary neurons*, ***Neuron* 33**, 587–600 (2002).

[62] A Chatelier, J Zhao, P Bois, M Chahine. *Biophysical characterisation of the persistent sodium current of the Na v 1.6 neuronal sodium channel: a single-channel analysis*, ***Pflügers Archiv. Eur. J. Physiol.* 460**, 77–86 (2010).

[63] JA Wolf, PK Stys, T Lusardi, D Meaney, DH Smith. *Traumatic axonal injury induces calcium influx modulated by tetrodotoxin-sensitive sodium channels*, ***J. Neurosci.* 21**, 1923 (2001).

[64] AL Hodgkin, AF Huxley. *A quantitative description of membrane current and its application to conduction and excitation in nerve*, ***J. Physiol.* 117**, 500 (1952).

[65] W Gerstner, WM Kistler. *Spiking neuron models: Single neurons, populations, plasticity*. Cambridge Univ Pr (2002).

[66] T Ivancevic, L Jain, J Pattison, A Hariz. *Nonlinear dynamics and chaos methods in neurodynamics and complex data analysis*, ***Nonlinear Dynam.* 56**, 23–44 (2009).

[67] JR Schwarz, G Reid, H Bostock. *Action potentials and membrane currents in the human node of Ranvier*, ***Pflügers Archiv. Eur. J. Physiol.* 430**, 283–292 (1995).

[68] W Nonner. *A new voltage clamp method for Ranvier nodes*, ***Pflügers Archiv. Eur. J. Physiol.* 309**, 176–192 (1969).

[69] DE Goldman. *Potential, impedance, and rectification in membranes*, ***J. Gen. Physiol.* 27**, 37 (1943).

[70] AL Hodgkin, B Katz. *The effect of sodium ions on the electrical activity of the giant axon of the squid*, ***J. Physiol.* 108**, 37 (1949).

[71] OP Hamill, A Marty, E Neher, B Sakmann, FJ Sigworth. *Improved patch-clamp techniques for high-resolution current recording from cells and cell-free membrane patches*, ***Pflügers Archiv. Eur. J. Physiol.*** **391**, 85–100 (1981).

[72] `http://en.wikipedia.org/wiki/File:Patch_clamp.svg`, (12 août 2010).

[73] `http://en.wikipedia.org/wiki/File:Patchmodes.svg`, (12 août 2010).

[74] MJ McGinn, BJ Kelley, L Akinyi, MW Oli, MC Liu, RL Hayes, KKW Wang, JT Povlishock. *Biochemical, structural, and biomarker evidence for calpain-mediated cytoskeletal change after diffuse brain injury uncomplicated by contusion*, ***J. Neuropathol. Exp. Neurol.*** **68**, 241 (2009).

[75] LL Isom. *Sodium channel β subunits: anything but auxiliary*, ***Neuroscientist*** **7**, 42 (2001).

[76] AM Rush, SD Dib-Hajj, SG Waxman. *Electrophysiological properties of two axonal sodium channels, Nav1. 2 and Nav1. 6, expressed in mouse spinal sensory neurones*, ***J. Physiol.*** **564**, 803 (2005).

[77] W Hu, C Tian, T Li, M Yang, H Hou, Y Shu. *Distinct contributions of Nav1.6 and Nav1.2 in action potential initiation and backpropagation*, ***Nature Neurosci.*** **12**, 996–1002 (2009).

[78] Y Chen, FH Yu, EM Sharp, D Beacham, T Scheuer, WA Catterall. *Functional properties and differential neuromodulation of Nav1. 6 channels*, ***Mol. Cell. Neurosci.*** **38**, 607–615 (2008).

[79] SA Burbidge, TJ Dale, AJ Powell, WRJ Whitaker, XM Xie, MA Romanos, JJ Clare. *Molecular cloning, distribution and functional analysis of the Nav 1.6 Voltage-gated sodium channel from human brain*, ***Mol. Brain Res.*** **103**, 80–90 (2002).

[80] DM Krzemien, KL Schaller, SR Levinson, JH Caldwell. *Immunolocalization of sodium channel isoform NaCh6 in the nervous system*, ***J. Comp. neurol.*** **420**, 70–83 (2000).

[81] JH Caldwell, KL Schaller, RS Lasher, E Peles, SR Levinson. *Sodium channel Nav1. 6 is localized at nodes of Ranvier, dendrites, and synapses*, ***Proc. Natl. Acad. Sci. USA*** **97**, 5616 (2000).

[82] S Cestèle, WA Catterall. *Molecular mechanisms of neurotoxin action on voltage-gated sodium channels*, ***Biochimie* 82**, 883–892 (2000).

[83] GT Charras. *A short history of blebbing*, ***J. Microsc.* 231**, 466–478 (2008).

[84] E Boucrot, T Kirchhausen. *Endosomal recycling controls plasma membrane area during mitosis*, ***Proc. Natl. Acad. Sci. USA* 104**, 7939 (2007).

[85] OT Fackler, R Grosse. *Cell motility through plasma membrane blebbing*, ***J. Cell Biol.* 181**, 879–884 (2008).

[86] M Bovellan, M Fritzsche, C Stevens, G Charras. *Death-associated protein kinase (DAPK) and signal transduction: blebbing in programmed cell death*, ***FEBS J.* 277**, 58–65 (2010).

[87] MP Sheetz, JE Sable, HG Döbereiner. *Continuous membrane-cytoskeleton adhesion requires continuous accommodation to lipid and cytoskeleton dynamics*, ***Annu. Rev. Biophys. Biomol. Struct.* 35**, 417–434 (2006).

[88] GT Charras, M Coughlin, TJ Mitchison, L Mahadevan. *Life and times of a cellular bleb*, ***Biophys. J.* 94**, 1836–1853 (2008).

[89] X Wan, JA Harris, CE Morris. *Responses of neurons to extreme osmomechanical stress*, ***J. Membr. Biol.* 145**, 21–31 (1995).

[90] AL Hodgkin. *The local electric changes associated with repetitive action in a non-medullated axon*, ***J. Physiol.* 107**, 165 (1948).

[91] JB Patlak, M Ortiz. *Slow currents through single sodium channels of the adult rat heart.*, ***J. Gen. Physiol.* 86**, 89 (1985).

[92] AG Richardson, CC McIntyre, WM Grill. *Modelling the effects of electric fields on nerve fibres: influence of the myelin sheath*, ***Med. Biol. Eng. Comput.* 38**, 438–446 (2000).

[93] RC Hogg, RJ Lewis, DJ Adams. *Ciguatoxin-induced oscillations in membrane potential and action potential firing in rat parasympathetic neurons*, ***Eur. J. Neurosci.* 16**, 242–248 (2002).

[94] HA Tokuno, JD Kocsis, SG Waxman. *Noninactivating, tetrodotoxin-sensitive Na+ conductance in peripheral axons*, ***Muscle Nerve*** **28**, 212–217 (2003).

[95] A Iwata, PK Stys, JA Wolf, XH Chen, AG Taylor, DF Meaney, DH Smith. *Traumatic axonal injury induces proteolytic cleavage of the voltage-gated sodium channels modulated by tetrodotoxin and protease inhibitors*, ***J. Neurosci.*** **24**, 4605 (2004).

[96] E Shirahata, H Iwasaki, M Takagi, C Lin, V Bennett, Y Okamura, K Hayasaka. *Ankyrin-G regulates inactivation gating of the neuronal sodium channel, Nav1. 6*, ***J. Neurophysiol.*** **96**, 1347 (2006).

[97] CA Villalba-Galea, W Sandtner, DM Starace, F Bezanilla. *S4-based voltage sensors have three major conformations*, ***Proc. Natl. Acad. Sci. USA*** **105**, 17600 (2008).

[98] SA Prescott, Y De Koninck, TJ Sejnowski. *Biophysical basis for three distinct dynamical mechanisms of action potential initiation*, ***PLoS Comput. Biol.*** **4** (2008).

[99] C Morris, H Lecar. *Voltage oscillations in the barnacle giant muscle fiber*, ***Biophys. J.*** **35**, 193–213 (1981).

[100] A Ochab-Marcinek, G Schmid, I Goychuk, P Hänggi. *Noise-assisted spike propagation in myelinated neurons*, ***Phys. Rev. E*** **79**, 11904 (2009).

[101] EA Thomas, RJ Hawkins, KL Richards, R Xu, EV Gazina, S Petrou. *Heat opens axon initial segment sodium channels: a febrile seizure mechanism?*, ***Ann. Neurol.*** **66**, 219–226 (2009).

[102] Y Kovalsky, R Amir, M Devor. *Simulation in Sensory Neurons Reveals a Key Role for Delayed Na+ Current in Subthreshold Oscillations and Ectopic Discharge: Implications for Neuropathic Pain*, ***J. Neurophysiol.*** **102**, 1430 (2009).

[103] M Devor. *Ectopic discharge in $A\beta$ afferents as a source of neuropathic pain*, ***Exp. Brain Res.*** **196**, 115–128 (2009).

[104] CN Liu, M Michaelis, R Amir, M Devor. *Spinal nerve injury enhances subthreshold membrane potential oscillations in DRG neurons: relation to neuropathic pain*, ***J. Neurophysiol.*** **84**, 205 (2000).

[105] R Amir, M Michaelis, M Devor. *Burst discharge in primary sensory neurons: triggered by subthreshold oscillations, maintained by depolarizing afterpotentials*, ***J. Neurosci.*** **22**, 1187 (2002).

[106] Y Kovalsky, R Amir, M Devor. *Subthreshold oscillations facilitate neuropathic spike discharge by overcoming membrane accommodation*, ***Exp. Neurol.*** **210**, 194–206 (2008).

[107] A Lorincz, Z Nusser. *Molecular identity of dendritic voltage-gated sodium channels*, ***Science*** **328**, 906 (2010).

[108] SI Börjesson, T Parkkari, S Hammarström, F Elinder. *Electrostatic Tuning of Cellular Excitability*, ***Biophysical journal*** **98**, 396–403 (2010).

[109] A Hasenstaub, S Otte, E Callaway, TJ Sejnowski. *Metabolic cost as a unifying principle governing neuronal biophysics*, ***Proc. Natl. Acad. Sci.*** **107**, 12329 (2010).

[110] JA Lindia, MG Kohler, WJ Martin, C Abbadie. *Relationship between sodium channel NaV1. 3 expression and neuropathic pain behavior in rats*, ***Pain*** **117**, 145–153 (2005).

[111] T Romantsov, AR Battle, JL Hendel, B Martinac, JM Wood. *Protein Localization in Escherichia coli Cells: Comparison of the Cytoplasmic Membrane Proteins ProP, LacY, ProW, AqpZ, MscS, and MscL*, ***J. Bacteriol.*** **192**, 912 (2010).

[112] DH Smith, DF Meaney, WH Shull. *Diffuse axonal injury in head trauma*, ***J. Head Trauma Rehabil.*** **18**, 307 (2003).

[113] S Luo, GM Perry, SR Levinson, MA Henry. *Pulpitis Increases the Proportion of Atypical Nodes of Ranvier in Human Dental Pulp Axons without a Change in Nav1. 6 Sodium Channel Expression*, ***Neurosci.*** **169**, 1881–1887 (2010).

[114] S Kuwabara, S Misawa, N Tamura, M Nakata, K Kanai, S Sawai, K Ogawara, T Hattori. *Latent addition in human motor and sensory axons: different site-dependent changes across the carpal tunnel related to persistent Na+ currents*, ***Clin. Neurophysiol.*** **117**, 810–814 (2006).

[115] B Grothe, M Pecka, D McAlpine. *Mechanisms of sound localization in mammals*, ***Physiol. Rev.*** **90**, 983 (2010).

[116] D Noble. *Biophysics and systems biology*, ***Phil. Trans. R. Soc. A*** **368**, 1125 (2010).

[117] GG Matthews. *Cellular physiology of nerve and muscle*. Wiley-Blackwell (2003).